S
University of Stavanger

Faculty of Science and Technology

MASTER'S THESIS

Study program/ Specialization: Petroleum Engineering/ Natural Gas Technology	Spring semester, 2019 Restricted access
Writer: OBINNA EGWU ELERI	*Elerina* …………………………………… (Writer's signature)
Faculty supervisor: Prof. Zhixin Yu External supervisor(s): Dr. Fengliu Lou	
Thesis title: Non-Destructive Activation of Pine Wood (*Picea Abies*)	
Credits (ECTS): 30	
Key words: Activated carbon Supercapacitor Non-Destructive Activation Pine Wood Characterization Chemical Activation High Surface area Porosity	Pages: 106 Stavanger, 15/06/2019

ACKNOWLEDGMENT

Abstract

This study investigates a novel technique of non-destructive activation(NDA) of Pine wood (*Picea Abies*) via the aid of chemical activation in the presence of a metal additive. Two additives (Cu and Al) were considered in the process with their ratios varied at selected amounts from 0.25,0.5, 1 and 2 to the wood char. Activation temperatures of 750 ^{o}C and 850 ^{o}C were utilized in combination with KOH impregnation ratios of 2 and 4 for the various additive ratios. The effect of increase in temperature, impregnation ratio and additive ratio were compared in relation to changes in the specific surface area as a measure of level of activation. Blank samples without additives at the two temperature levels and impregnation ratios were also synthesized and compared to the non-destructively activated carbon. Nitrogen adsorption, X-ray diffraction, Scanning Electron Microscopy/ EDS characterizations were carried out on the various activated carbons produced. An impregnation ratio of 4, in combination with activation temperature of 850 ^{o}C was found to be the optimum condition for high surface area. Cu additive was more successful in the NDA with additive intensity of (Char:Cu:KOH) 1:1:4 at 850 ^{o}C and 1:0.5;4 at 750 ^{o}C considered as the optimum intensity for high specific surface area. In general, activated carbon with very high specific surface areas up to 3350 m^2/g were obtained. Electrodes and coin cells were fabricated with some of the samples and compared to those fabricated with commercial activated carbon YP80F. Ohmic resistance, self-discharge and specific capacitance were measured for the Blank, NDA with Al and commercial activated carbon and compared. The blank samples exhibited highest specific capacitance of 156F/g @ 0.056 mA/cm^2 and 161 F/g @ 2.83 mA/cm^2 but the NDA with Al had the lowest ohmic resistance of 0.13 Ωcm^2. The blank experiment and NDA sample with Al had better properties in terms of higher specific capacitance and lower self-discharge rates than the commercial activated carbon compared YP80F with similar loading.

TABLE OF CONTENTS

LIST OF FIGURES

LIST OF TABLES

CHAPTER 1

1.0 BACKGROUND

1.1 INTRODUCTION

The world today is facing a constant increase in the amount of energy being consumed[1, 2]. This has prompted the research into new and alternative energy sources with the focus shifted away from conventional fossil fuels[2, 3]. The humongous increase in energy consumption has been attributed to advances in technology, electric vehicles, electronic devices and the ever-increasing human population[1, 3]. An evidence of this is the report by Nocera (2009) that the global energy demand is expected to double by 2050 and triple towards the year 2100[4]. Researchers have looked towards replacing the conventional energy resources derived from coal and petroleum derivatives with clean natural and replenishable options[5]. These options include solar, wind, geothermal and biomass energy[5, 6].

Elements attributed to the rise in greenhouse gas emissions and the increase in global warming has led to the shift towards utilization of clean energy sources to meet energy requirements in the world today[5, 7]. The advent of industrialization encouraged the use of coal initially as the chief energy source at that time due to its abundance and limited technological requirements to tap into the potential[8]. The consequences of utilization of coal as the chief energy source became abundant with concerns growing over the rise in Sea levels, melting of glaciers and the effects on the arctic circle, increase in average temperature of the earth and quality of air in specific industrialized nations. The need to diversify the energy source brought forth the gold rush era sequential to the discovery of crude oil and energy benefits from petroleum[9]. Harnessing these resources also contributed to the detrimental effects on the environment via environmental pollution and increase in carbon dioxide emissions chiefly and other greenhouse gasses. In as much as petroleum products utilization was a cleaner alternative compared to coal, the concern increased due to significant emissions being released into the atmosphere. Major decisions such as those made by the European union to reduce the greenhouse gas emissions by 60% by 2030, highlighted the turning point in the search for cleaner energy sources. A comparative study of emissions from typical supply ships vying the North Sea showed that their

Carbon and Nitrogen Oxide emissions are similar to those generated by about 6000 and 70000 cars respectively for the two oxides[10, 11]. Electrification was proposed as a solution to reduce the energy consumption and greenhouse gas emissions while striving to achieve the Norwegian target of climate neutrality in the year 2030[12]. The shift from conventional propulsion systems burning fuels to electrically powered system can be achieved in ships, cars and truck but the significant challenge lies in the availability of adequate energy storage systems specifically to store energy in form of electricity as opposed to chemical energy in fossil fuels. Other options explored included tapping into the energy potential of natural resources such as water via hydro power to generate electricity, geothermal energy for heating, Solar energy from the sun in hotter climates for heating and electricity generation, wind power for electricity generation with the general term Renewable energy resources given to all these as a collective name[13, 14].

Renewable energy resources especially those other than Hydro, pose a new challenge due to their erratic nature and intermittency. Periods existed where the sun wasn't out, wind intensity and speed was low and dry seasons with reduced volume of water in dams. Thus the push for methods to store the available energy in peak periods so as to utilize it when needed in erratic periods of energy supply[14] summarized as creating adequate energy storage systems is necessary. This need has been proposed to be tackled via researches into the fields of electrochemistry, simply explained as a means of converting energy stored in form of chemicals into electrical energy. Several types of energy storage systems arose which include but are not limited to batteries (secondary, primary and lithium ion), electrochemical cells, flywheels, hydroelectric dams etc. These batteries come in various sizes and shapes with the lithium ion batteries showing remarkable properties especially their ability to store large amounts of energy[15]. Despite the advantage of having high energy densities, drawbacks exist in their ability to rapidly discharge stored energy due to the latency associated with chemical reactions to transfer the chemical energy into electrical energy. This problem can be solved via the utilization of super-capacitors which store energy directly on the plates and whose discharge rate is a function of conductive capabilities of the capacitor plates[16]. Other solutions were the hybridization of a capacitor and a lithium ion battery which resulted in a hybrid with improved energy dissipation abilities without the challenges of latency associated with chemical reaction[6]. This was made possible via the substitution of the lithium ion cathode for activated Carbon and the anode for graphene to improve the energy density, although several other proposed combinations have been also been reported[6].

Various techniques and materials have been proposed for use to synthesize electrode materials for supercapacitors with key considerations in their electrical conductivities, availability of starting materials, cost and toxicity. Examples such as activated carbon, graphite, carbon nanotubes, fullerenes and graphene have been considered. The technical complexities and expenses associated with the production of carbon nanotubes, fullerenes and graphene have discouraged their industrial application[17]. This has left activated carbon as the more favorable option considered due to its relative abundance, availability of wide range of precursors, high purity and relatively environmentally friendly nature[17]. In addition, The high specific surface area of activated carbon gives it the ability to store larger amount of charges in the double layer compared to other carbon materials[18].

The challenge lies in finding a suitable combination of an appropriate precursor, activation method that would produce activated carbon with outstanding properties such as high surface area, appropriate pore size for electrolyte transport, good electrical conductivities and electrochemical stability. Forest residues of up to about 1.6 million tons have been produced as waste alone in Norway[19]. Inadequate disposal and handling creates issues such as forest fires, environmental concerns and greenhouse emissions[20]. Conversion into biofuels were considered as good options for disposal but economic viability arose as challenges citing the low price of biofuels as the key contributor. A suitable option was the conversion of this biomass to activated carbon for high value supercapacitors which would also realize the targets set by the forest innovation and wood industry in Vestlandet.

Supercapacitors have the potential to be used to achieve the aim of electrification and hybridization of the maritime and other forms of transportation previously involving the utilization of hydrocarbon fuels in their propulsion systems. A good example of utilization as pure electric propulsion has been seen in France, the ferry (Ar Vag Tredan)[21]. Other forms include their use as complementary storage options in combination with Li-ion batteries, combustion engines in instances requiring short term high power and additional advantage of lifetime extension.

Despite the good positive attributes, the application of super capacitors is plagued by their low specific energy and high price per unit energy. Methods which have been suggested to improve this do so at the detriment of the specific power and cyclic stability thus the focus lies on improving the specific energy of super capacitors without detrimental effects on their cyclic stability and specific power. One suggested method of achieving this would be the reduction of the defect level in synthesized activated carbon which would be applied in the fabrication of

supercapacitors. The supercapacitors operating voltage window would be widened by the use of modified activated carbon with reduced defect during their assembly [10]. A first step towards achieving this would be the investigation of the potentials of nondestructive activation of a wood precursor with the aim of producing activated carbon with reduced defect and improved properties via this technique.

1.2   AIM

Investigation of nondestructive activation of a wood precursor for the production of activated carbon with reduced defect and high surface area.

1.3   OBJECTIVES

This aim would be achieved via the following objectives,

- Development of a nondestructive activation method to reduce the defect level of activated carbon produced
- Selection of activation additive for non-destructive activation
- Synthesis of activated carbon via nondestructive activation aided by KOH
- Investigation of effect of temperature, impregnation ratio and additive ratio on surface area of synthesized activated carbon via this technique
- Removal of additives present as impurities in the activated carbon
- Characterization of activated carbon produced via the above-mentioned methods via Nitrogen Adsorption, X-ray diffraction , Scanning Electron Microscopy/EDS and ash content determination.
- Fabrication of supercapacitors (Coin cells) with the modified activated carbon
- Testing of supercapacitors to determine their Specific capacitance, Self-discharge rates and Ohmic resistance.

1.4   PROBLEM STATEMENT

Supercapacitors are distinguished by their ability to exhibit higher specific power and improved cyclic stability compared to the widely utilized Li-ion batteries and fuel cells. Nevertheless,

they have been known to suffer due to their low specific energy which has resulted to higher prices in relation to unit energy and consequently hinderance in their widespread application. Several methods exists which have been aimed at improving their specific energy, but these methods do so at the expense of the specific power /cyclic stability of the supercapacitor. A suitable method would be investigated in this study to overcome this challenge via the development of activated carbon with reduced defect level which upon utilization would widen the operating voltage window of the supercapacitor and sequentially increase the specific energy. Chemical and physical activation methods do so with significant damage to the structure of the synthesized activated carbon. This etching method produces defects on the carbon and thus active sites are produced which accelerates the decomposition of the electrolyte and thereby narrowing the operating voltage window. A nondestructive activation method is sort which would reduce the defect level of the activated carbon.

1.5   JUSTIFICATION

The Vestlandet region has been reported to produce large amount of forest residues with results reaching 1.6 million tons as wastes in Norway alone. This large amount of wastes has led to environmental concerns and fear due to possible outbreaks of forest fires and greenhouse gas emissions. Conversion of the biomass into biofuels have been considered but drawbacks exists due to the low price of biofuels resulting to detrimental effects on its economic viability. Conversion into activated carbon presents a suitable high value product which can be obtained from the biomass. This would also present an opportunity to key into the agenda of forest innovation and the wood industry in Vestlandet with focus on the optimization of bioenergy from the forest industry sector in Rogaland and Vestlandet.

In addition to the above, the high activity of maritime transport in Vestlandet presents an opportunity for utilization of the developed supercapacitors as energy storage systems in maritime transport. Maritime transport in Vestlandet accounts for about 30% of total sea throughput in Norway. This shows that a large market for high-power supercapacitors used in Maritime vessel electrification exists in this region. The developed supercapacitors with enhanced specific energy will thereafter contribute greatly to the realization of the goal of electrification for sustainable maritime transport in Rogaland and Vestlandet.

1.6   RESEARCH QUESTIONS

The following research questions would be answered in the course of this study,

1. Which activation additive is the best for nondestructive activation?
2. What is the best intensity of nondestructive activation?
3. What is the best condition to achieve a high specific surface area and optimized pore size distribution?

CHAPTER 2

2.0   LITERATURE REVIEW

2.1   BATTERIES AND CAPACITORS

Batteries refers to a term used in describing galvanic cells. They could be coupled in the single cell configuration or multiple cell configuration where larger emfs are required and the emf is an additive function[22].

The similar configuration and constituents of a battery and capacitor often brings about confusion in distinguishing between the two. Batteries and capacitors both have a couple of electrodes (Anode and Cathode), an electrolyte, current collectors in addition to separators. Batteries generate electricity from redox reactions taking place at the electrodes. The voltage of each cell is calculated by the difference in potential between the two electrodes used. It is therefore very optimal to use electrodes with potentials which are widely positioned on the potential scale. The electrolyte performs the function of replacement of ions which have been lost from the electrodes and a medium for ion transport between the two. Current flows in form of electrons from the anode conducted via external circuitry to the cathode. The reactions between the electrolyte and the anodes produce electrons in other words an oxidation reaction take place. Reduction reaction takes place on the cathode as ions migrate from the electrolyte and are deposited on the cathode. These phenomena are broadly explained by the term redox reactions. The exhaustion of constituents of the electrolytes or degradation of the electrodes uses up all the chemical energy in the batteries and thus cannot be able to produce electricity. The battery or electrochemical cell is said to have been used up or dead. In other to continue using them, they would need to either replace the electrode with new ones, refill the electrolyte or pass electric current via chargers into the system. Based on this, there are several types of batteries; the primary cell, secondary cell and lithium ion.

2.1.1   Primary Cell

The primary cell batteries refer to a single galvanized cell in which when fully discharged, the chemical reactions cannot be reinitiated by introduction of an external current via the electrodes

in order to regenerate the active ingredients. A basic example is the lechanche cell shown in the Figure 2.1
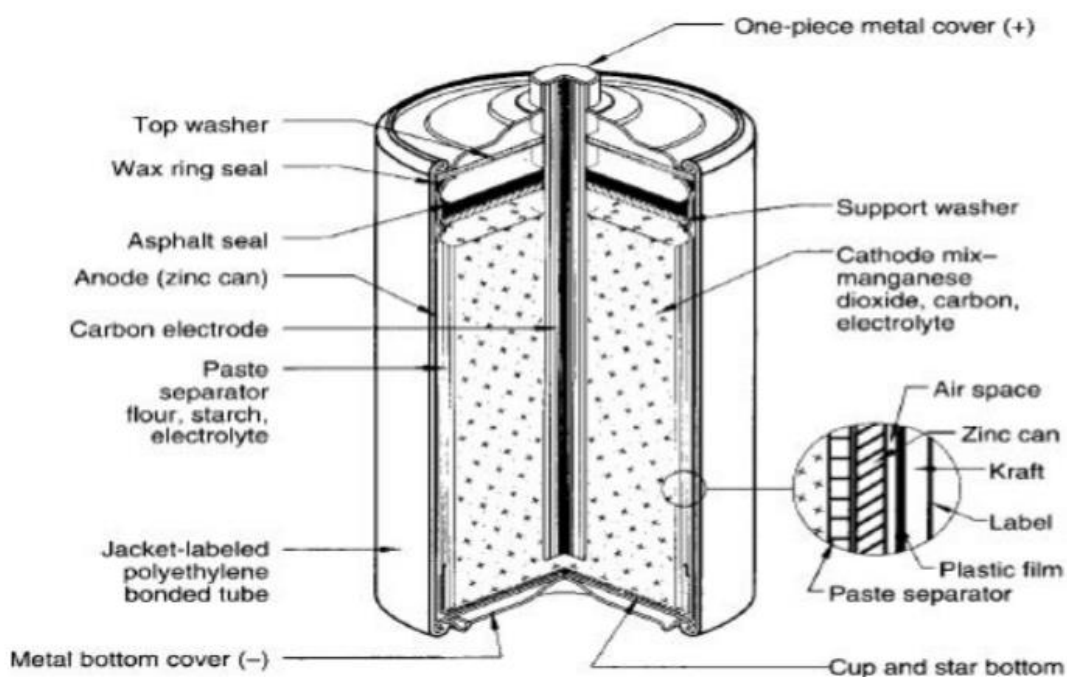
Figure 2. 1 Components of a leclanche cell

The Leclanche cell consists of a zinc anode, a cathode mixture containing manganese dioxide and carbon, $NH_4Cl/ZnCl_2$ electrolyte as well as modified containing vessels and separators.

Primary cell batteries have the advantage of being very portable, providing a light weight, cheap, easy to use and safe energy supply option to power low current demanding items (small electronic devices). Several primary cell units could be added together to increase the supplied emf to the loaded device.

2.1.2   Secondary Cell Batteries

These are batteries in which an externally supplied current can be used to regenerate the chemical energy stored in the batteries. They are also called rechargeable batteries. The process of flow of electrons is reversed while the battery charges. The cathode takes the place of the anode and vice versa in similar manner occurring during electrolysis. The positive electrode becomes the anode and the negative electron becomes the cathode. Charge and discharge cycle of secondary batteries can also be repeated more than a thousand times. This process is only stopped when there is excessive growth of insulation layers of products from the chemical reactions which have highly resistant properties.

2.2 CAPACITORS AND SUPERCAPACITORS

Supercapacitors are an upgrade from the ordinary capacitors. They make use of the double layer in the electric field to store their energy while also utilizing high surface area electrodes which increases their capacitance [23]. Supercapacitors present an opportunity to combine the advantages of electrochemical batteries, with the ability to store high energy and their drawbacks of low power values and capacitors which deliver rapidly high power in seconds[23]. A sketch of the Ragone plot for various energy storage and conversion devices shows how super capacitors tend to bridge the gap between capacitors and batteries.
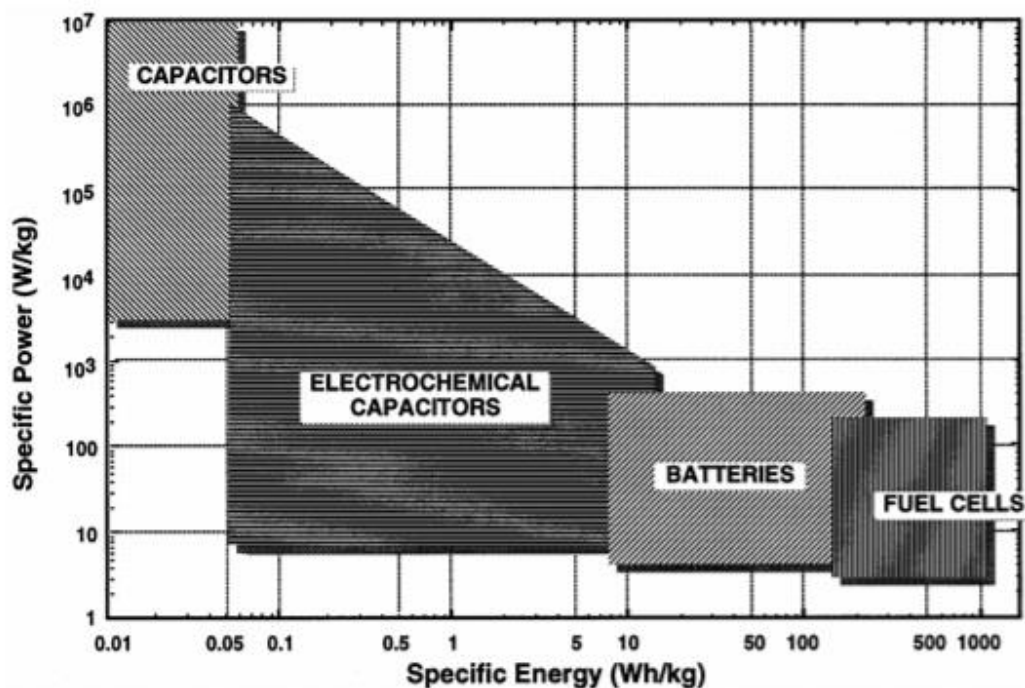
Figure 2. 2 Ragone plot[23, 24]

The specific power output of supercapacitors lie in the range of 0.5-5 kW/kg with energy densities in the range of 0.5-10 Wh/kg[25]. Applications of the supercapacitors could be seen in computers, electric vehicles, power electronics and areas where environmentally friendly, high energy density, limited maintenance life time o3,peration and rapid charge and discharge rates are required[26].

2.2.1 Classification of Super Capacitors

Super capacitors can be classified according to the nature of the electrode material used, the composition of the electrolyte and the variations in the cell design.

9

2.2.1.1 Nature of the electrode

The nature of the electrodes refers to the active agents used in the construction of the electrodes. This could either be Carbon based, Polymer based, or Metal oxide based[25].

1. **Carbon based**

   The existence of several allotropes of carbon in addition to properties such as high surface area, availability, low cost and well documented electrode application potential has led to the frequent use of carbon in the construction of electrodes for super capacitors[23]. Examples of carbon in porous forms which have been used include Activated carbon, Carbon Nanotubes[27], Graphene[28], Carbide derived carbons[24] etc. the use of these porous carbons as electrodes has been greatly influenced by properties such as their electrical conductivities, pore size, specific surface area, pore volume which affect their electrochemical performance. Activated carbon, which is the most commonly used, can have surface areas within the range of 2000-2500 m^2/g. In the construction of electrodes for supercapacitors, the specific surface area of the active material plays a significant role in achieving high capacitance values[25]. The optimization of certain parameters in the production of activated carbon can further increase the surface area, micro-texture which would aid the penetration of the electrolyte into internal surface of the electrode as well as other desired properties. Yan et al[6] investigated the postulation that increasing specific surface area increases the specific capacitance. Reports from the investigation showed that not all micropores of the produced activated carbon with large specific surface area can be accessed by the electrolytes to from the electrochemical double layer. Lagelot et al. and Chmiola et al investigated the relationship between porosity and specific capacitance of carbon materials[29, 30]. Conclusions were made that obtaining an optimal pore size is the key to obtaining large capacitance values compared to obtaining high specific surface area with optimal values in the range of 0.8-1.0nm. When the activated carbon is produced, they are typically mixed with a binder and an additional conductor (graphite or Aluminium) to enhance the mechanical and electrical properties of the electrode during fabrication. Precursors such as coal, seeds, biomass, wastepaper, nuts, varieties of wood have all been used in addition to a combination of physical, chemical activating procedures. In general, carbon based electrodes produce supercapacitors with very high power capabilities derived from the fast adsorption and desorption of ions (following their high porous) but they are plagued by low specific energy[31].

2. Polymer based

Polymers have been used in fused form to construct electrodes via cathodic deposition and coprecipitation[26]. Conducting polymers when used as electrodes, undergo redox reactions as their charge storage mechanism. This takes place in the bulk of the material which is in contrast with those of the carbon electrodes occurring at the surface of the material. The conducting polymers by virtue of this, have advantages in terms of increased specific energy/energy stored and reduced self-discharge[31]. Nevertheless, significant disadvantages could also be noted upon observation of their specific power which has been attributed to the sluggish ion transport during diffusion within the bulk of the electrode[32]. Kandasamy et al reported that low cost in term of prices, good permeation and electrochemical properties, high surface area, environmental stability, low density, and high specific capacitance are some of the gains obtained from the use of Polyaniline[33]. Another disadvantage can be encountered in form of their brittle nature/ strength and structure-wise deficiencies leading to challenges, especially when considering long term stability. Improved properties have been reported upon combination with graphene. Yan et al reported that the pseudo capacitance properties of conducting polymers arises from the redox reactions in addition to the conjugated pie double bonds in polymer networks. Polyaniline and Polypropylene when used in supercapacitors, resulted in specific capacitances of 150-190 F/g and 80-100 F/g in aqueous and non-aqueous electrolytes respectively[6]. The poor conductivities of these materials have limited its commercial application as the values of the capacitance obtained is below the commercially expected demands in order for it to meet practical expectations. The structure wise deficiencies, swelling, shrinking and degradation of electrodes brings up challenges in terms of cyclic stability. Options to improve this challenge could be via the enhancement of the backbone and structure of the polymers through hybridization with various materials. These materials could either be metals, carbon, and metal oxides. Yan et al. produced graphene/PANI composite while utilizing in situ polymerization to produce supercapacitors with specific capacitance of 1046 F/g with an energy density of 39Wh/kg and power density of 70kW/kg[6]. The enhanced capacitive properties obtained was attributed to the synergistic effect between graphene and PANI.

3. Metal Oxide based

The existence of series of redox reactions attributed to the ability to attain various valence configuration stand out as one of the striking factors in the use of metal oxides

as electrodes[33]. They have been reported to possess high specific capacitance as well as low resistance[23]. These attributes explained the very high specific powers obtained from the use of metal oxide electrodes. Despite the positives, the expensive nature of transition and rare earth metals used discouraged the utilization of this material for electrode construction purposes. Limitations also arose from their restrictions to only aqueous electrolyte which significantly affects the nominal cell voltage obtainable from the use of metal oxides. Prominent examples include RuO_2 and IrO_2 electrodes[34]. Metals diluted in Nitrides have been suggested as options to reduce the material cost while also maintaining the positive properties of such metals[35].

2.2.1.2 Electrolyte

An electrolyte is a substance that can dissociate and form ions in solution, giving it the perfect ability to conduct electricity. They could exist as either strong electrolytes or weak electrolytes based on complete dissociation or partial dissociation during ion formation in solution[36].Supercapacitors can be classified based on the electrolytes used. The most common divisions are the organic and aqueous electrolytes.

1. **Organic electrolytes**

   Organic electrolytes have the advantages of higher achievable voltage from their utilization. They allow for cell voltages greater than 2V, this is possible due to their limited water content. Water content is detrimental to the achievable voltage of the capacitor. Special purification techniques and coating of carbon electrodes have been employed by some companies to take care of this problem. Some examples of Organic electrolytes include Tetraethylammonium tetrafluoroborate ($TEABF_4$) in acetonitrile or propylene carbonate. Organic electrolytes generally have better conductivities than aqueous electrolytes. In addition, they enable the supercapacitor to function at higher powers and larger operating voltage window in the range of 2.5-3.0V[37]. Other examples of organic electrolytes include sulfones, carbonates and adiponitrile which have been used due to their excellent tolerance for high voltages in super capacitors but are plagued by their lower conductivities and higher viscosities[18].

2. **Aqueous electrolyte**

   Aqueous electrolytes have been reported to pose several advantages compared to no aqueous electrolytes. Brousse et al used K_2SO_4 as a mild aqueous electrolyte for the synthesis of an electrochemical capacitor[38]. The authors stated that the environmental

challenges associated with non-aqueous electrolytes, toxicity and flammable nature of the solvents used necessitated the use of an aqueous electrolyte despite the apparent decrease in the voltage range. The decrease in the voltage range can be compensated by using high capacitance materials such as RuO_2 (about 863 F/g over a 1V potential range while using 1M aqueous H_2SO_4 [39]) and MnO_2[40]. Other examples of aqueous electrolytes include H_2SO_4, NaCl, KOH, Na_2SO_4 [38]. Aqueous electrolytes have also been reported to have specific capacitance which are higher than those of nonaqueous base. Guo et al[41] while using a rice husk precursor activated with NaOH produced supercapacitors using a 3M KCl electrolyte and obtained maximum capacitance of 210F/g measured at 0.2mA/g. Wu et al[42] activated Fir wood using steam and produced supercapacitors with capacitance of 140F/g measured at 25mV/s while using a 0.5M H_2SO_4 solution. Subramanian et al[43] activated banana fibres using $ZnCl_2$ and produced supercapacitors with capacitance of 74 F/g measured at 500mA/g while using Na_2SO_4 electrolyte.

2.2.2 Application of Super Capacitors

The improvement in the properties of supercapacitors has granted them the potential to be utilized in different ways. Some of these applications are discussed below.

2.2.2.1   *Electric vehicles*

The push for clean energy and emission control has led to the increase in the manufacturing and utilization of electric vehicles. These vehicles with their battery power, have several limitations in terms of their low energy density, long charging time and low cyclic ratio. The utilization of super capacitors solves some of these problem despite the fact that the supercapacitors are also plagued with some disadvantages (Cost and low energy densities have been one of the major challenges. This could be solved via the combination of the positives of the super capacitor and batteries[44]. During acceleration and driving in difficult terrains, high power is needed from the batteries and this could be supplied by the super capacitors. They in turn could be charged during the braking and thus energy can be conserved in the process[23].

2.2.2.2   *Extension of battery life*

Many electrical and battery powered applications today have variations in their operating conditions. Deviations in their conditions occur during the switch from an average state to a stage requiring high performance. This switch corresponds to period where the current drawn is at an average steady low rate and periods of high performance where the current drawn is of

high powered and fast pulses. Using a battery to deliver high powered current intermittently would drain the life of the battery since they do not have the ability to maintain long charge and discharge cycle. A super capacitor could be used to take care of this applications and thus in combination with the batteries, help in extending the life of the batteries[23].

2.2.2.3   *Renewable energy storage options*

The extend cyclic abilities of the super capacitor grants them the power to be effectively used as energy storage options for Electricity from Solar energy via photovoltaic cells. Using batteries as storage options for this, presents challenges due to the continuous charge and discharge process. Thus, batteries would have to be periodically changed which would result in extra costs. Super capacitors can be continually charged and discharge for more than 10,000 cycles and need not to be replaced until a very long time[23].

2.2.2.4   *Energy efficiency*

Supercapacitors have the ability to operate in a wider range of temperature conditions compared to batteries[23]. They also lose little amount of energy during their charging process compared to about 30% lost by batteries. Remote locations with extreme cold temperatures require units which help in keeping the Batteries at room temperature. This adds to the energy cost in the whole process of storing energy. The use of hybrid supercapacitors with increase energy density can help in mitigating this challenge. Although extreme cases requiring high energy densities results in extra cost when using super capacitors, this is expected to decrease as more advancement in the design and availability of materials for construction of hybrid/high energy density super capacitors.

2.3   IMPROVING THE PROPERTIES OF SUPER CAPACITORS

The focus of this research is to improve the specific energy of the super capacitor. This can be done by modifying the properties of the activated carbon which serves as the cathode. The property could be fine-tuned by improving the surface area (2000 - 3000 m^2/g), pore size/pore size distribution and surface properties. Efficient optimization carried out on these properties would increase the specific capacity of the activated carbon (pore size optimization) from commercial standards of 114F/g to 156F/g and above. Other methods are discussed in subsequent sections

2.3.1 Removal of Oxygen Functional Group

Removal of oxygen functional group helps in expanding the voltage window and reducing incidences of self-discharge[45]. Activated carbon which contains oxygen has the disadvantage of being unstable, reduced conductive properties, high self-discharge rate, poor wettability and hydrophilic nature[45, 46]. A heat treatment process is required which would ensure the complete removal of oxygen functional group. Another solution which would reduce the self-discharge rate is by the employment of heteroatom doping whereby Fluorine is added to the activated carbon.

2.3.2 Utilization of 3D Collector

The activated carbon produced serves as the active agent in the electrode design. The AC is mixed with the polymer binder, slurry and solvent and then coated on a current collector before being left to dry. The conductivity of the electrodes can be improved by using a 3D current collector (Al fibre array current collector). This also helps in improving the activated carbon loading thus an increase in the specific energy on cell level. The operating voltage window and specific energy can also be improved by tuning the initial electrode potential.

2.3.3 Hybrid Capacitors

Hybrid capacitors tend to combine the advantages of supercapacitors and batteries in order to further increase the specific energy. The cathode being used is the activated carbon while the anode used is Silicon. The anode could also be lithinated with silicon to further improve the properties in addition to the electrolyte 1M LiPF6. the silicon anode is prepared from silicon Nano powders which are then rolled into the electrodes. Lithiation of the anode helps in reducing the potential of the anode and thus an indirect increase in the voltage window. The utilization of the pseudocapacitive properties of nanomaterials in the form of polymers, oxides, nitrides and nanostructured lithium electrodes could serve as a means of bridging the gap between batteries and super capacitors in terms of energy densities[47].

2.3.4 Composite Electrodes

Based on studies on the relationship between the activation and electrical conductivity of porous substances, several authors reported that the electrical conductivities of activated carbon is improved via the process of annealing at high temperature under inert atmospheres[48-51]. This doesn't not affect the electro-adsorptive properties they have. Most often, employment of highly

porous substances is critical in order to ensure utilization at maximum capacity, but this effect is detrimental to the electrical conductivity due to the extreme porosities exhibited by these materials. A possible solution to this would be the application of composite electrodes constituting of the active material in combination with additives likes graphene sheets, carbon nanotubes, carbon black, graphite, that would help improve the electrical conductivity of the electrode. The incorporation of these materials especially carbon nanotubes and graphene sheets help improve the electrical and mechanical properties, impact high surface area and aspect ratios which are characteristic properties of these additives in addition to their excellent electrical conductivities and electrochemical stabilities[51].

2.3.5   Other Methods

In addition to the other methods mentioned, the energy density of the supercapacitor can also be improved by the introduction of faradic reactions in the form of pseudo capacitance. This can be done in the form of introduction of redox active groups via addition of other functional groups at the surface or in-situ integration of metal oxides[37]. The utilization of electrolytes with high conductivities for example Tetraethylammonium tetrafluoroborate (TEABF$_4$) in acetonitrile or propylene carbonate helps in the minimization of resistive loses and ensure that the capacitors have the ability to operate at high power.

2.4   A REVIEW ON ACTIVATED CARBON PRODUCTION

Activated carbon is coined from the term referring to carbon in which the structural properties in particular, the porosity has been modified in order to impact special kind of characteristics in relation to its intended use or industrial application. The modification of the pores of the activated carbon could come in form of enlargement of the pores, creation of pores in nonporous carbonation, narrowing of pore diameters in other selected materials[52]. This could be carried out by either the physical, chemical or combination of both the physical and chemical means of activation[53].

The production of activated carbon is a process which cannot be possible without several components namely; The Carbon precursor, activating agent, activating procedure. This would all be discussed in the following sections.

2.4.1 The Carbon Precursor

Raw materials used in the preparation of activated carbon are classified as carbon precursors. A variety of lignocellulosic materials consisting mostly of coconut shells as wells as different kinds of woods have been predominantly used to produce a large number of activated carbons with figures estimated to be greater than 300,000 tons each year[54]. Selecting the appropriate precursor is crucial for activated carbon production. This can be limited to the cost of the precursor, obtainability, purity and purification process needed for the end product/method of synthesis and intended application of the produced activated carbon[55].

The use of coconut shells arose from the large amount of waste products from the coconut oil and other coconut processing industries. Activated carbon produced from coconut have been reported to be more durable and attrition resistant compared to carbons made from other materials. They also possess higher density, purity and exist in a dust free form[56].

Olives have also been used in the production of activated carbon. They belong to the group of most widely cultivated plants in the world. They are grown predominantly in the middle eastern and Mediterranean regions which accounts for 99% of the world olive fruit production[57, 58]. The regions derive economic benefits, cultural significance as well as environmental benefits from the cultivation of this fruit crop[58]. Good adsorptive properties especially relating to environmental safety in addition to hardness are some of the remarkable properties derived from utilization of activated carbon from Olive stones.

Extracts from the leaves of the tea plant also known as Camellia sinensis[59] have been used to produce activated carbon. The production of activated carbon from the extracted residue is a method of utilizing the discarded waste to produce a compound of economic value while also providing a suitable means of waste utilization and disposal from the tea industry. High carbon to ash ratio, pores which were well developed and results from structural analysis showing cracks and channels in the synthesized activated carbons were some of the results obtained[60].

Wood tar and coal tar have been used to produce activated carbon although the process has been plagued by the cost of acquisition of the precursors and thus rendered the process inefficient[61]. Results obtained from the use of Eucalyptus and wattle wood to synthesis ACs showed the existence of a microporous structure accounting for about 80% of the total pore volume[62]. Softwood and hard wood fibers upon activation, produced fibrous-like short hollow activated carbons consisting of micropores and a combination of micro,meso and macro

pores for the soft and hard woods respectively. Reports showed that they also possessed high aspect ratios and remarkable adsorption capacity[63].

2.4.2   Activation Technique

Activation of an organic precursor serves as a means of improving its properties and maximizing its potential for use in adsorption and other applications[17]. The process of activation selectively removes carbon atoms from the structures of organic matter thus maximizing their potential after carbonization. Carbonization is usually taken as the first step towards activation whereby inorganic substances are removed from the activated carbon. In this process, the material becomes more porous with the existing micro porosity widened or transformed into mesoporous forms. The diameter and nature of the pores play very important roles in determining what kind of molecules that could be adsorbed by the activated carbon. Molecules with larger pore size diameters can only be adsorbed if the porosity of the specific adsorbate is opened up to be able to contain these molecules. Activation can either be carried out via the physical means or the chemical means.

2.4.2.1 Physical Activation

The process of physical activation takes place in two steps. Carbonation which occurs as the first step removes the other volatile substances except the carbon from the precursor at low temperatures. The second step involves the activation of the carbonized precursor at higher temperatures. Inert gases such as Nitrogen, carbon monoxide, Steam, and Argon are usually used to prevent burning of the carbon and uncontrolled oxidation during the activation process. Of these gases, Nitrogen gas has been frequently used due to its lower economic cost, availability and ease of use. The activation is usually carried out in temperatures from the range of 700-1100 C under an atmosphere of an inert gas which prevents the formation of oxides of carbon during the process[64]. Subsequently, a variety of pores of different sizes are created and they are influenced by the activation temperature, time and inert gas flow rate[65].

2.4.2.2 Chemical Activation

In chemical activation, a chemical agent usually with desiccating abilities is used to impregnate the carbon precursor prior or subsequent to carbonization. The impregnated carbon precursor is then subjected to heat treatment under an inert atmosphere. The development of the pores begins after a series of processes which include degradation and dehydration, with the chemical agent playing the role of reducing the need for higher activation temperatures due to their interactions with the carbon precursor[65].Benefits accrued from using chemical activation include reduced

18

energy requirements arising from the lower activation temperature when compared to the physical activation process. Chemical activation also combines carbonization and activation in one step which also lowers the heat requirements. Several researchers have reported other advantages which include reduced activation time, addition of specific functional group, higher yields and larger surface area of the produced activated carbon[17, 66]. Despite these advantages, downsides include environmental concerns over the reagents used during the activation process, toxicity of the chemicals and recovery of the chemicals after treatment of the carbon precursor.

A variety of precursors need to be precarbonized before chemical treatment due to their composition and the nature of activating reagent used[67]. The precarbonization step ensures that external surface of the char is easily accessible by the reagent molecules and the rich carbon structure of the char produced ensures that more activation is possible. Other advantages of precarbonization reported include the modification of the textural properties, preliminary pore development, increased formation of mesopores and micropores via the combination of the above-mentioned advantages[68-70].

Factors which affect the success of chemical activation include; the nature of the chemical agent, complete mixing of the activation agent and the carbon precursor and activation temperature. In light of this, several activating agents have been considered, Phosphoric acid[57, 65], Potassium hydroxide[52, 65], Zinc Chloride[52] and Sodium hydroxide [52, 65]which would be discussed in the succeeding section.

1. **Zinc Chloride**

    Hernandez-Montoya et al [52]reported that when Zinc chloride was used to activate lignocellulosic materials, activated carbons with very good porosity was obtain in high yields. Material degradation as well as alteration of the carbon skeleton occurred in various forms during the impregnation and carbonization step respectively. Well-developed pores were created as a result of dehydration, degradation via charring and aromatization of the carbon skeleton[71]. For this type of activation of the carbon precursor, Zinc chloride is first used to impregnate the precursor for a given contact time. The solution is then evaporated, and carbonization is carried out in an inert atmosphere. The obtained activated carbon is then washed thoroughly to extract the Zinc Chloride. The porosity of the produced activated carbon is affected by the carbonization temperature and the impregnation ratio/amount of Zinc Chloride used in the process. Caturla et al and Hu et al [71, 72]Reported that using high impregnation ratios of 2-2.5

in addition to high temperatures around 800 °C yielded activated carbons with very large surface area (2000- 2400 m^2/g) while those prepared using similar ratios of chemical agent to precursor and lower activation temperatures of 500 °C yielded lower specific surface areas (750- 1200 m^2/g). Despite the fact that well developed porosities could be obtained while using Zinc Chloride, the toxicity and environmental concerns associated with the use of Zinc compounds has hindered its effective application**.**

2. **Potassium and Sodium Hydroxide (Alkalis)**

KOH and NaOH have been used to synthesize activated carbons with high surface area. Two basic methods have been employed namely; homogenous solid to solid reactions where by the solid Alkali pellets are mixed directly with the carbon precursor and Heterogenous Solid to liquid reactions where the concentrated Alkali is impregnated on the carbon precursor[52]. The mixing step and impregnation is then followed by thermal treatment under Nitrogen to generate the porosity. Mopoung et al used KOH during the chemical activation of Tamarind seeds to produced activated carbon[66]. Results showed that a decrease in yield of activated carbons produced occurred with corresponding increase in activation temperature and impregnation ratio. They also reported that chemical activation using NaOH led to increased functional groups identified at the surface of the activated carbon confirmed via FTIR analysis. The utilization of KOH results in highly microporous activated carbons with desirable properties than those of other chemical reagents like ZnCl2, H3PO4. In addition, introduction of -OH functional group on the surface of the activated carbon occurs as well as enhancement of the high specific surface area. Li et al obtained activated carbons with surface area of 2763 m^2/g while using KOH in the activation of kraft lignin[73]. Similar high surface area of 2696 m^2/g was obtained by Muniandy et al during the activation of rice husk to produce activated carbon[69].

3. **Phosphoric acid**

The use of Phosphoric acid for the chemical activation of carbon precursors has increased from figures two decades ago[52]. This increase has been reported as due to the following positive attributes observed during the utilization of phosphoric acid

- Phosphoric acid performs the role of a template during the formation of activated carbon. The volume occupied by the acid upon impregnation of the precursor is similar to the micropore volume of activated carbon formed[74].

- Phosphoric acid plays the role of a catalyst in the dehydration, cross linking reactions, bond cleavage and hydrolysis during the preparation of activated carbon[52].

Several researchers have reported the concentration of Phosphoric acid used in chemical activation to be greater than 50% (w/w) while employing activation temperature within the range of 350-600 ^{o}C. the impregnation ratio has great influence on the specific surface area of the produced activated carbon. Hernadez et al [52]reported that large surface areas within the range of 1785-1802 m^2/g were obtained while using large impregnation ratios and lower values of about 356 m^2/g was obtained upon the usage of smaller impregnation ratios. The figure below shows a distribution of specific surface area of the activated carbon produced from different precursors while using chemical activation. The columns highlighted in black were activated using high phosphoric acid impregnation ratios. Kouotou et al reported that excess of phosphoric acid being used during impregnation would inhibit the formation of tars and play the role of a dehydrating agent[75]. These tar inhibition as well as other liquids, would reduce the possibility of blockage of the pores of the carbon. Thus, movement of volatiles would not be hindered during their release from the carbon sequential to activation.

2.4.2.3 Combination of Physical and Chemical Activation

It has been reported that the merits of the two methods can be combined in form of a combination of physical and chemical activation to obtain improved properties of the synthesized activated carbon (porosity, surface functional groups, surface area)[76]. Different ratios have been employed from 1-4[76, 77] in combination with steam or carbon dioxide as a second step activation. This specific kind of studies were aimed at reducing the amount of chemical agent used and determination of effects and possible outcomes upon consideration of large-scale manufacturing. A possible experimental alternative involving two methods is outlined as follows which would aid the reduction in the costs associated with the large use of chemical agents. The first method involves the employment of 1:1 impregnation ratio (Wood precursor to Phosphoric acid) followed by steam activation. After impregnation, the sample is introduced into the reactor and activated at temperatures between 600 to 1000 ^{o}C[30, 76-78] for a duration of 15 to 120 mins in the presence of steam. The second method involves a precarbonization step where the activated carbon is initially impregnated with the chemical agent (Phosphoric acid in this study) and desired impregnation ratio. The impregnated sample

is then transferred to a furnace programed using a desired temperature between 350 and 600 °C [79-81] and for a duration of 1 hour. After this process, steam is then used in the second step to carry out the activation at temperatures between 600-850 °C. The flow rate of steam has often been reported to be within the range of 100 ml/min to 2 Liters/min ([76, 78-81] and activation time varied from 15 mins to 120 mins[76, 79-81].

2.5 CHARACTERIZATION OF ACTIVATED CARBON

After the synthesis of activated carbon, it is always necessary to find out the inherent characteristics of the material. This is broadly termed as characterization of activated carbon. Several characterization techniques would be employed to determine the surface area, pore size, crystal size, functional groups and conductivity of the activated carbon. The following section explains the different characterization techniques that would be employed in this process

2.5.1 Nitrogen Adsorption

A very popular method of characterizing the surface area and pore size of porous materials is the gas adsorption. Physical and chemical adsorption are the two prominent types of adsorption with the physical adsorption being the most suitable approach for surface measurements due to its lower heat of adsorption and the nonoccurrence of violent and disruptive changes to the surface as measurement takes place. Multilayers of adsorbate cover the surface which takes place in steps from monolayer to multilayer otherwise known as capillary condensation. The process does not require activation energy and thus the equilibrium is rapidly achieved. The analysis of the data obtained during measurement would give valuable information such as volume of pores, size and their respective distributions.

The Brunauer – Emmett- Teller (BET) theory is a suitable and widely applied method used in the determination of surface area of porous materials. Adsorption isotherms are obtained from the plots of Quantity adsorbed against the relative pressure.

There are six different adsorption isotherms which can be obtained according to the International Union of Pure and applied chemistry (IUPAC) classification. The type 1 is related to adsorbents with extremely small pores, type 2 and 4 refers to nonporous adsorbents or adsorbents with relatively large pores, types 3 and 5 are special cases which arise in certain conditions where the adsorptive molecules have greater affinity for one another than they do for the solid, type 6 is a rare isotherm which indicates a nonporous solid with almost completely

uniform surface[82]. Commonly encountered isotherms are types 1, 2 and 4. The figure below shows the different isotherms from type 1 to VI and Hysteresis loops H1 to H4..
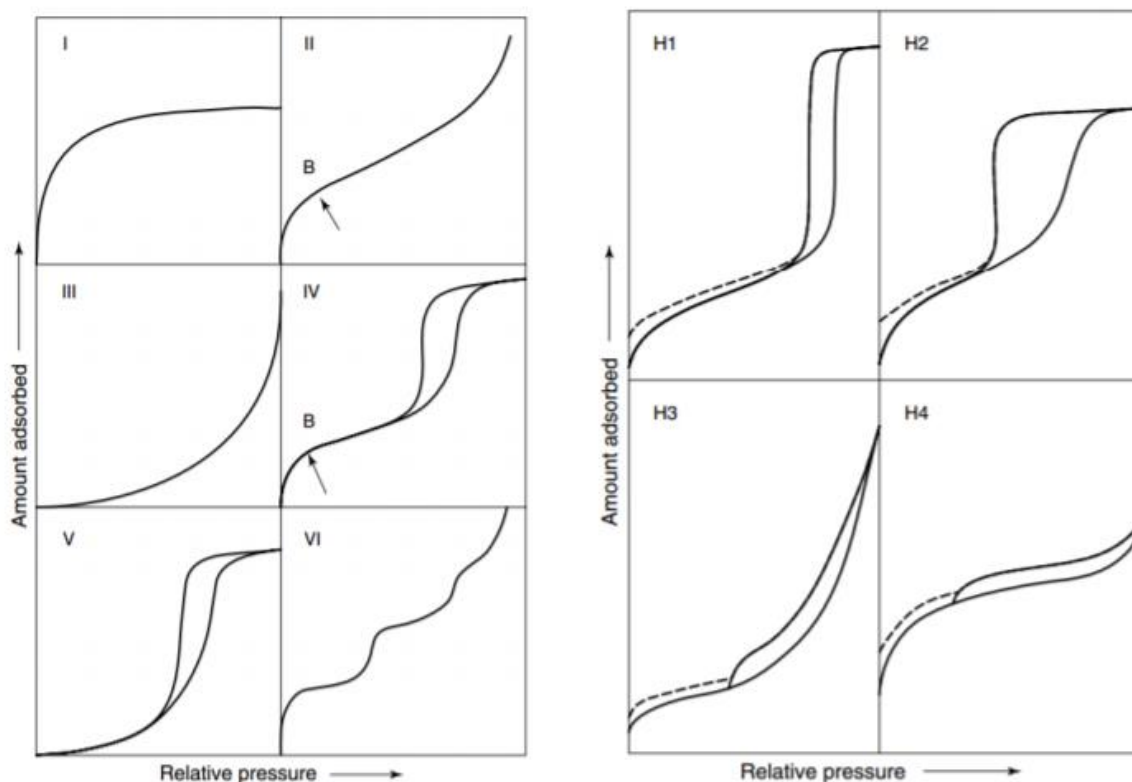
Figure 2. 3 (a and b)Types of Adsorption isotherms and Hysteresis loops[83]

Type 4 isotherms are common for mesoporous materials and they usually possess a characteristic hysteresis loop. The hysteresis loops exhibit wide varieties of shapes with each shape corresponding to specific pore structures. Type H1 is commonly associated with porous materials comprising compacted and agglomerated uniform spheres arranged in regular arrays and narrow pore size distribution. Type H2 porous adsorbents are typically very difficult to interpret[83].

The Barret-Joyer-Halenda (BJH) Desorption analysis result is used in the determination of the mesopore volume, t-plot method for the micropore volume and DFT method for the pore size distribution which are very much useful especially for classification of mesoporous and microporous material content of various samples. Information related to this is obtained from computation in the gas desorption isotherms and modification of the kelvin equation. The relationship between the volume of the capillary condensate and corresponding relative pressure is established indirectly by relating the vapour pressure depression to capillary radius[84].

23

2.5.2   X-Ray Diffraction

The X-ray diffraction method is a means of obtaining information about the atomic structures present in crystalline materials. Each material has a unique set of diffraction pattern (specific position, peaks and intensities) and the content of each sample is analyzed by comparing it with a database of materials to identify the distinctive phases present[85].

The operation begins by beaming X-rays towards the sample leading to a reflection and scattering of the waves by the sample. The wavelength of the electromagnetic radiation is related to the angle of incidence, distance between the crystal lattice plane of atoms by the Bragg's law given below[86, 87].

$$\lambda = 2 \times d \times sin\theta$$

The crystallite size can also be estimated using the Scherrer equation[88]

$$d = \frac{K\lambda}{B \cos \theta}$$

K refers to the numerical factor also known as the crystallite shape factor, B represents the full width at half maximum of the XRD peak. All calculations are done in Radians.

The X-rays impinged on the sample are generated by a cathode ray tube with a beam of electrons aimed at a metallic target (most commonly copper). The recording is made in form of diffraction intensities vs the diffraction angle. Powder X-ray diffraction method is most common diffraction method as it involves using a fixed wavelength[89]. Different possible orientations of the sample is obtained by scanning in random directions through a range of 2theta angles. A metallic target is needed with copper being one of the most utilized. This is in addition to a supplied wavelength of 1.5418 A of CuKa radiation. The angles recorded for this experiment ranges from 10-90 degrees.

Several valuable information could also be obtained from the conduction of Powdered X-ray diffraction technique. These include, phase transition study, polymorph study, variable temperature and humidity study. General information about the specimen size and shape can be obtained from the positions of the diffraction pattern while the intensity relates to examination of atomic positions of the sample. The different peak position would be compared with the XRD fingerprint database to define the sample in terms of geometry of the lattice, internal and external crystal dimensions as well as internal symmetry. Another vital information of the specimen could be obtained by considering the relative intensities of the diffracted beams and

also the integrated intensities referring to the area under the curve of intensity vs 2theta. The intensity is affected by factors such as regularity of the lattice, periodicity and order of atoms, addition of atoms and crystal orientation which occurs close to the Bragg's angle[87].

2.5.3   Scanning Electron Microscopy

The scanning electron microscope is used to obtaining information about the particle size and morphology of samples. It produces images about the surface by scanning with a focused beam of electrons. An interaction exists between the electrons and atoms in the sample which produces a variety of signals with relevant information about the surface topography and constituents of the sample.

2.6   SUPER CAPACITOR TEST CELLS

A good way to study the performance of single electrode is the use of a 3-electrode electrolytic cell. This cell configuration consists of a working electrode, counter electrode and a reference electrode[90]. The electrolyte solution as discussed in preceding sections can exist as either aqueous or nonaqueous electrolyte. The aqueous electrolyte depending on the ph content could also be acidic, neutral or alkaline. Acidic aqueous solutions make use of titanium, carbon or platinum as counter electrodes and silver or silver chloride as reference electrodes. Similar configuration is used for the neutral aqueous solution with an additional option of Nickel for use as a collector and counter electrode. Alkaline solutions make use of mercury or its oxide form as the reference electrode.

Different compositions exist for the nonaqueous electrolyte depending on the constituents of the electrolytes. Most commercially available non-aqueous electrolyte capacitors makes use of Aluminum foil. This usage is somewhat limited to cases with narrow potential range. Tests involving higher potential range make use of Platinum metals although their use is limited to instances where the nonaqueous solution doesn't contain Lithium ions. Lithium ion electrolyte containing supercapacitors make use of nickel or copper as the current collector. Carbon is widely used as a counter electrode due to its tolerance for different electrolyte compositions. Choosing the appropriate electrode composition is a function of the material stability in relation to the cell, cost, and its availability.

The working electrode is fabricated via a mixture of the active material (activated carbon), Conductive agent (acetylene black) and a Binder (PTFE). This mixture is rolled into a film or

compressed using a compression molding press. Afterwards, it is then pressed onto a collector mesh or foil. Measurements are the taken to note the mass of the active materials present in the electrodes in addition to the volume. The electric double layer formation occurs on the electrodes either by cation adsorption or by anion adsorption. The negative electrode is that which the electric double layer is formed by cation adsorption while the positive electrode is that which is formed by anion adsorption. Although in this study, coin cells consisting of two similar electrodes would be used in evaluating the performance of supercapacitors.

2.7 EVALUATING THE ELECTROCHEMICAL PERFORMANCE OF SUPER CAPACITORS

The electrochemical activity of a super capacitor is measured as a function of its electrode performance. Most supercapacitors consists of 3 electrode cells with evaluations done based on their Cyclic voltammetry, electrochemical impedance spectroscopy and galvanostatic chronopotentiometry[90]. On a cell basis, the evaluation is done using a 2-electrode configuration. This is very important in the assessment of its cycle life, power density and energy density. The set up consists of two working electrodes placed on the opposite sides of a separator. Measurements are then taken to note and control the potential difference. The capacitance measurement is based on the sum of the active materials in the electrodes. The value obtained for a single electrode in a dual electrode cell is different from those obtained in a triple electrode cell. Inconsistencies in the value of measurements taken for a single electrode in a two configuration and three configuration system arise from variances in the size of cation and anion as well as various potential changes occurring in the positive and negative electrodes while measurements are being taken.

2.8 REDUCING THE DEFECT IN ACTIVATED CARBON FOR SUPER CAPACITORS ASSEMBLY

Activated carbon has been extensively utilized as an electrode material due to the large surface area it possesses especially in comparison to other carbonaceous materials[91]. Despite this large surface area, possession of a rough structure has led to reportedly reduced conductivities which has necessitated the use of additives to decrease the internal resistance[92]. Possession of irregular structures in combination with unwanted surface functional groups meant that the activated carbon was always prone to long-term degradation[27]. These impurities especially in form of metals and other uncontrolled functional groups had detrimental effects on the

26

supercapacitors specifically via their scrounging reactions causing limitations in their lifetime and specific surface area with adverse effects on the capacitance. A method of reducing the defect is via the nondestructive activation comprising the introduction of a suitable additive during the activation process.

2.8.1 Proposed Mechanism of Nondestructive Activation

The process of activation of carbon precursors via KOH takes place in an oxidative manner[93]. The reaction is in form of a redox equation following the combination of the potassium hydroxide with the carbon atoms. The carbon atoms are oxidized into carbon oxides, carbonates and other carbon and potassium impurities[94]. An etching process occurs which leads to the generation of the pores by the oxidative effect the potassium hydroxide has on the carbon thereby converting these oxidized carbon atoms into carbonates. Potassium compounds which are formed also intercalate into the carbon framework and their removal is sequential to the washing step highlighting one of the importance of the washing step. The rapid break down of the KOH into Potassium metal which intercalates into the carbon frame works brings about Exfoliation activation (upon their removal while washing) and this type of activation reduces the defects formed in the activated carbon. Upon higher temperatures, the potassium carbonates could also decompose into CO_2 at temperatures greater than 700 ^{o}C. This as a consequence brings about more activation of the carbon via gasification of the carbon atoms[95]. A suitable additive which would be introduced in the process would help enhance the decomposition of potassium hydroxide into potassium metal and thus promote exfoliation activation.

The washing step would have to be optimized to ensure the removal of the additives introduced due to possible negative effects such as faradic reaction which could occur when the activated carbon comes in contact with the electrolyte their hindering electrochemical performance. The additive could be responsible for blockage of the pores due to complexes formed and if not removed properly via the washing step, would lead to reduced porosity and available surface area. Aluminum and Copper would be investigated in this process. A deviation from the normal trend encountered such as increase of surface area at lower temperatures or negatives in positive trends would indicate the optimum additive intensity.

2.9 COIN CELLS FABRICATION AND ELECTROCHEMICAL TESTING

After obtaining the synthesized activated carbon, the next step is the conversion into either coin cells or pouch cells. Due to the small nature of finished products, coin cell assembly is the preferable choice at this point due to minimal requirements during the assembly process in terms of amount of activated carbon, process and time. The coin cells electrodes can be produced via the coating method or the rolling method. The rolling method is used in cases where small masses are used to produce the coil cells.

2.9.1 Procedure (Electrode Preparation)

2.9.1.1 Mixing (Dough preparation)

A measured amount of activated carbon is placed in a crucible and mixed with a corresponding solution of PTFE in the ratio 92% (Activated carbon) to 8% (PTFE). Ethanol is used in aiding the dispersion of the mixture until a paste like form is obtained (PTFE forms a fiber with Ethanol when mixed together with the activated carbon). The polymer binder ensures that the active materials are fused together and gives the electrode the ability to stick to the current collector[96]. 3ml of Ethanol is typically added to 1g of activated carbon. If the weight of the activated carbon is less than 1g, a few drops of ethanol is used and the consistency is checked until a dough like form is achieved. The slurry/paste is then rolled with the aid of a roller at 80 °C.

2.9.1.2 Rolling

The rolling process starts at 1000 µm which is the typical aperture space between the two rollers when using small amounts of activated carbon less than 1g. The dough like mixture of (AC, PTFE and Ethanol) is then passed in between the two rollers of the MSK-HRP-04 Hot Rolling press (taking care to position it in the middle). The aperture size is then reduced by an interval of 100 µm on each different crossing, with the thickness of the dough reduced smaller as the aperture size reduces. Beyond 400 µm, the reduction takes place by an interval of 50 µm and beyond 200 µm the interval reduces to 25 µm. at this stage great care is taken due to the very thin nature of the dough. At 100 µm, the thickness of the dough is measured to estimate the closeness to the required loading when the disc is cut as the thickness is related to the mass of the disc formed eventually. This loading is calculated by mass of the disc divided by the area of the disc. The loading is measured in mg/cm^2. It is of utmost importance to ensure that during

each reduction interval, the rough and inconsistent edges are trimmed until the final rectangular straight edged shape with the required thickness is obtained.

2.9.1.3 Lamination

When the required loading has been obtained and the thickness noted, the active material is placed on top of a current collector (made of Aluminum or Copper coated with carbon). Aluminum is typically used when constructing coin cells in which the active material is activated carbon. The thickness of the foil is 15 µm and the electrode is (80-85) µm. The lamination takes place with the aid of the roller and the temperature is increased to 160 °C. The electrode and current collector is then passed through the roller to reduce the thickness to a size less than 100 µm. This is passed in between the rollers 3 times making sure to alternate the different sides going in through the middle of the rollers to ensure that a consistent thickness is obtained.

2.9.1.4 Disc cutting

After the lamination stage, the disc size is cut according to the required diameter of the coin cells and loading which had been noted. This is done by a disc cutter.

2.9.1.5 Vacuum Drying

The cut disc is then placed in a vacuum oven. The oven is pressurized with a gas mixture of hydrogen and argon. The temperature is set to 140 °C and the drying takes place for 24 hours. The dried discs are then transferred into the glove box for the coin cell assembly.

2.9.2 Coin Cell Assembly

Upon completion of the drying process, the discs are then transferred into the glove box in addition to other parts of the coin cell. These parts include; the base, the gasket, spacer, separator, cap and spring. The separator is typically made of cellulose (TF4030). The electrolyte used is $TEABF_4$. The coin cell assembly begins by matching the discs in two pairs according to their weight variation and noting each weight. Care is taken to ensure that the corresponding weights of the two selected discs match each other as close as possible. Typically, five coin cells consisting of 2 discs each are assembled and tested so as to ensure repeatability of results. After the matching process has been completed, the base of the coin cell is selected and 10ml of electrolyte solution is transferred to it. An electrode disc is then placed on it and centred with the active side facing up. 50 ml of electrolyte solution is then added on top of the electrode. The separator is placed afterwards and then the gasket. 50ml of electrolyte solution is then placed on the separator, followed by the other electrode with the active side facing down. The

spacer is then placed on top of the electrode followed by the spring and then the cap. The setup is then transferred to a crimper which then seals it up and the coin cell is considered as assembled and ready for testing.

2.9.3   Coin Cell Testing

The procedure for coin cell testing is described in chapter 3. It involves a series of charge and discharge cycles as well as rest periods. The behavior of the coin cells are observed while also noting the voltages after each cycle of charge and discharge at specified current and voltage. Appropriate formulas are then used in the calculation of the specific capacitance and self-discharge after 72 hours.

2.10   COMMON ISSUES PERTAINING TO SUPERCAPACITORS

2.10.1 Self-Discharge

Self-discharge phenomena can be discussed in retrospect in terms of relative importance with respect to the application of the supercapacitors and its characteristic use[97]. The importance is seen is aspects where the supercapacitors are coupled with batteries used in electronic gadgets where charge frequency and cycle are of great importance. It is seen as less critical in aspects of regenerative breaking common in electric vehicles. Self-discharge can be explained as a term used in the characterization of processes associated with the physical and chemical nature leading to decrease in voltage of supercapacitors when stored in their charged state. Self-discharge issues are more prominent in supercapacitors than batteries[98, 99], thus highlighting one of the key factors responsible for the interest in this phenomenon. The critical nature of the decrease in the relatively smaller energy possessed by the supercapacitors in comparison to the batteries buttress this point further by highlighting the fact that over 75% of the voltage in the supercapacitor is delivered in the first half of the voltage window[97, 100]. This also shows that the usability of the supercapacitor is hampered by the self-discharge once the voltage drops to half of the initial supplied charging voltage. Frequent recharging or application of trickle charging with a small constant current would always be needed to keep the capacitor fully operational[97].

2.10.2 Internal Resistance

The internal resistance of the supercapacitor is one factor responsible for the limitation of its specific power. A large portion of the energy of a supercapacitor is lost as a result of the internal resistance and the effective series resistance[101]. This is prominent in high power operations with severe reductions of efficiency being documented. The conductivity of the activated carbon in combination with the electrolyte conductivity plays a great role in ensuring efficient supercapacitors especially at higher temperatures. The capacitance and life cycle are governed by the influence of this factors. A study of the resistance variations with temperature is necessary to obtained optimized conditions required in high powered operations that would not be prone to internal heating. Several studies related to this have been carried out by Gualous et al[101].

CHAPTER 3

3.0   EXPERIMENTAL

This chapter describes the experiments to be carried out, equipment to be used, reagents and raw materials employed to achieve the desired objectives of the research.

3.1   MATERIALS

This section outlines the materials and other reagents used during the experiment

3.1.1   Activated Carbon Precursor

Saw dust obtained from Pine wood (*Picea Abies*) used in wood processing industries was used as a precursor for this process.

Pine wood falls under the family of lignocellulosic materials. They consist Lignin, Cellulose and other combinations of carbon hydrogen and oxygen in form of volatiles which can be driven of sequential to heating.

3.1.2   Reagents

The table below shows a list of the reagents and other chemicals used during the experiment.

S/N	Name	Description	Source
1	Distilled water	Distilled water	Phoenix trading AS
2	Coin cell accessories	Beyonder's Specification	Beyonder AS
3	Hydrochloric acid	S.G = 1.18 (~37%), MW=36.46	Fisher Scientific UK
4	Nitrogen gas	99.999% purity	Praxair Norge AS
5	Potassium Hydroxide	S.G= 2.04, MW = 56.1	Fischer Scientific
6	Aluminum	Finely ground Aluminum foil	Aluminum foil sourced commercially
7	Copper	Powder, < 75 µm, 99%	Sigma Aldrich

Table 3. 1 List of Reagents and Chemicals used

3.2 EQUIPMENT

A brief description of some of the equipment used is given below.

3.2.1 Splitting Tube Furnace

The Splitting tube furnace is the equipment in which the activation process and other heating required reactions are carried out. The OTF-1200X is used in this study with the maximum operating temperature of 1000 ºC and heating rate of 10 ºC/min. Samples are placed carefully in a quartz boat and loaded in the furnace. The inert gas supply is used to purge the air left in the tube and temperature profile programmed to required heating rate. The operating procedure is set as required and the setup is turned off upon completion of the temperature profile . Inert gas supply is turned off when the temperature drops below 120 ºC and sample is removed upon cooling. An illustration of the setup is shown in Figure 3.1
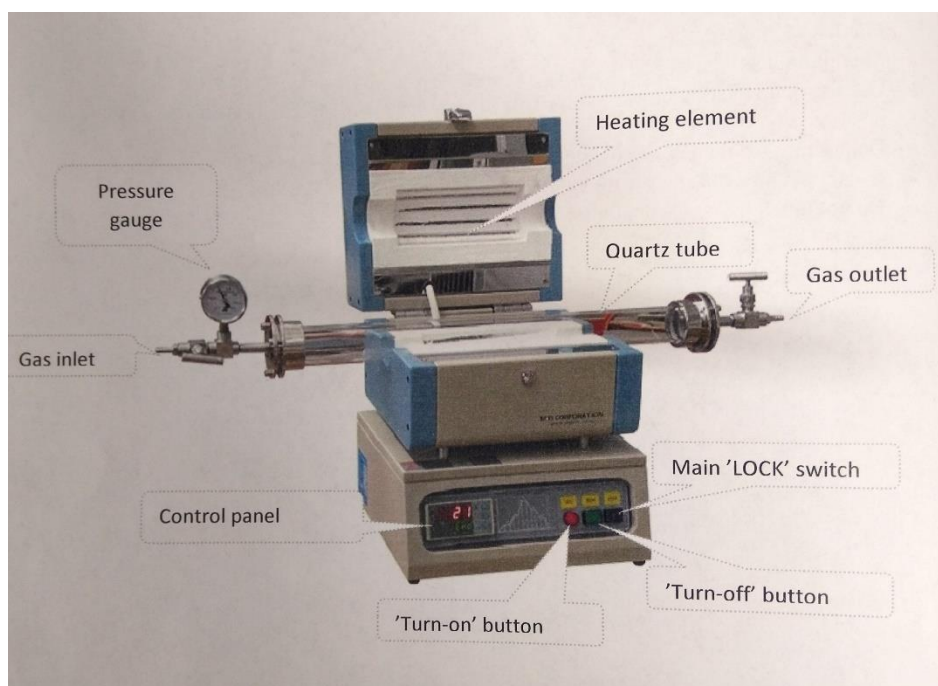
Figure 3. 1 Splitting Tube Furnace

3.2.2 Vacuum Filtration Set Up

Vacuum filtration is used in the washing process after the activation has been carried out in the furnace and stirring on the magnetic stirrer and hot plate. The fine particle nature of the activated carbon makes it extremely difficult to obtain the washed samples without the aid of vacuum filtration. Faster separation rate of the solid activated carbon particles from the washing agent

are attained upon the use of the technique in comparison to normal gravity filtration. A pressure gradient provides this force needed for the removal of the liquid through the funnel. This is provided by the vacuum pump attached to the arm of the flab bottom flask as shown Figure 3.2

Figure 3. 2 Vacuum filtration setup

3.2.3   Hot Rolling Press

The hot rolling press is the equipment used in the rolling/ pressing of fiber mixture of active materials and binder into the electrode and also the lamination process with the current collector.

3.3   EXPERIMENTAL SET-UP

The experimental plan consists of an investigation of different ratios and conditions for non-destructive activation of the Carbon Precursor. Chemical activation as explained in the preceding chapters would be carried out via the aid of KOH impregnation and addition of finely ground Aluminium in different ratios and configurations.

3.3.1 Carbonization

25g of Saw dust is transferred into quartz boat and placed in the furnace for carbonization. The process is carried out under inert conditions in the presence of Nitrogen gas which is used in purging the furnace for 20 mins at 500 sccm, and then during operation the flowrate is reduced to 80 sccm. The furnace is programmed to a temperature of 600 $^{\circ}$C to be held for 1hr using a heating rate of 10 $^{\circ}$C/min and similar cooling rate.

3.3.2 Activation

1g of produced char, Aluminum/ Copper, KOH pellet according to the desired ratios as listed in the experimental plan is mixed together with the aid of a mortal to crush the KOH pellets until a well dispersed mixture is obtained. The mixture is then placed in a quartz boat and transferred to the furnace. Nitrogen gas at flowrate of 500 sccm is used in purging the furnace initially for 20 mins and then reduced to 80 sccm upon commencement of heating. The furnace is then programed at the desired temperature (750-850 $^{\circ}$C), for 2 h at a heating and cooling rate of 10 $^{\circ}$C/min. The mass obtained after activation is measured, recorded and labelled according to the date produced, type of activation (NDA for nondestructive activation) and temperature for easy identification and tracking from experimental logbook.

3.3.3 Washing

After the samples have been cooled and removed from the furnace, the sample is weighed and placed in a beaker with a hot solution of 250 ml of 1M or 2M KOH depending on the amount of Aluminium additive present in the samples (Ratios of 2M were for values higher than 1g). The mixture is then placed on a heating plate and washed with the aid of a magnetic stirrer, stirring at 400 rpm, and hot plate temperature of 120 $^{\circ}$C for 2hours. After this step, the mixture is then rinsed off with the aid of vacuum filtration and 2 litres of distilled water. The next washing step is carried out immediately by washing with 500 ml of 1M HCl solution, stirred at 400 rpm and heating plate at 120 $^{\circ}$C for 2 hours. The sample is then rinsed off via vacuum filtration with 2 Litres of distilled water, dried, measured and labelled accordingly.

3.4   EXPERIMENT PLAN

Experimental runs in the following format

S/N	Sample ID	Description (Ac:Al:KOH) ratio	Activation Temperature (°C)	Time (h)
1	1801NDA850	1:2:2	850	2
2	0312NDA750	1:2:2	750	2
3	2811NDA750	1:2:4	750	2
4	2911NDA850	1:2:4	850	2
5	1303NDA750A	1:0.25:4	750	2
6	1303NDA750B	1:0.5:4	750	2
7	1103 NDA850A	1:0.5:4	850	2
8	1103 NDA850B	1:0.25:4	850	2
9	1504NDA850B	1:1:4	850	2
10	1104NDA750B	1:1:4	750	2
11	1504NDA850A	1:1:2	750	2
12	1104NDA750A	1:1:2	850	2

Table 3. 2 Experimental runs and configuration with Al additive

S/N	Sample ID	Description (Ac: KOH) ratio	Activation Temperature (°C)	Time (h)
1	2203BL850A	1:2	850	2
2	1004BL750A	1:2	750	2
3	2203BL850B	1:4	850	2
4	1004BL750B	1:4	750	2

Table 3. 3 Experimental runs and configuration for the blank experiments

S/N	Sample ID	Description (Ac:Cu:KOH) ratio	Activation Temperature (ºC)	Time (h)
1	2404NDA850A	1:0.5:4	850	2
2	2404NDA850B	1:0.25:4	850	2
3	2504NDA750A	1:0.5:4	750	2
4	2504NDA750B	1:0.25:4	750	2
5	0905NDA850A	1:1:4	850	2
6	0905NDA850B	1:1:2	850	2
7	1505NDA750A	1:1:4	750	2
8	1505NDA750B	1:1:2	750	2
9	2005NDA750A	1:2:2	750	2
10	2005NDA750B	1:2:4	750	2
11	2105NDA850A	1:2:4	850	2
12	2105NDA850B	1:2:2	850	2

Table 3. 4 Experimental runs and configuration with Cu additive

3.5   CHARACTERIZATION

The samples were characterized to determine the surface area, pore size, crystal size, crystallinity and surface properties. These characterizations were carried out with the aid of Scanning electron microscope (SEM), Nitrogen Adsorption and X-ray Diffraction (XRD).

3.5.1   Scanning Electron Microscopy (SEM)

The sample already in powdered form is transferred to the sample mount with the aid of a sticky conducting tape. The conducting tape helped to keep the samples in place while also preventing it from adhering to the sensitive optics columns of the SEM equipment (Zeiss Supra 35VP). In addition, the conducting tape also ensured that the electrical conductivity to the sample mount holder was attained which would prevent the distortion of electron beams, sequential to charging and consequently, production of misconstrued images.

3.5.2 X-ray Diffraction

The sample to be analysed was carefully transferred into the sample holder (quartz sample holder) with a name tag and corresponding identity as noted on the sample. Care was taken to ensure that the orientation of the sample was not affected during sample preparation step. The sample was then loaded on the Bruker XRD equipment and corresponding name tags correctly inputted on the computer before commencement of the analysis. After the analysis, the sample was then taken out and sample holders cleaned. X-ray diffraction analyses of the samples were performed using the Bruker AXS micro-diffractometer D8 advance. A CuK-α was used as the radiation source. The patterns were recorded with a 2theta range from $10 - 90$ and a step interval of 1 degree/min.

3.5.3 Nitrogen Adsorption

The first step in the BET analysis consisted of the degassing step, where the sample was heated to high temperatures 120 ^{o}C under vacuum overnight and then the weight measured and noted. The sample was then loaded into the Tristar II 3020 micrometrics surface analyser. The adsorption was carried out with the use of Nitrogen and constrained by the equipment being capable of measuring just 3 different samples simultaneously and independently. The required information about the samples is then entered in the software taking note of the corrected mass after degassing, sample ID and conditions. The sample holder was then attached properly on the equipment and liquid Nitrogen filled to the appropriate levels in the containing vessels before commencement of the analysis.

3.6   ELECTRODE FABRICATION AND COIN CELL ASSEMBLY

This process takes place as described in chapter 2 section 2.10. The best samples of activated carbon (with respect to the surface area) selected from both the blank experiments and non-destructively activated (with Aluminium additive and Copper additive) were used in fabrication of the coin cells and tested. Table 3.6 shows the different samples prepared and their constituent which were assembled for analysis and testing. Care was taken to ensure that the activated samples were free of oxygen and moisture before electrode fabrication by calcining at 1000 ^{o}C for 1hour before utilization. 8 wt % of PTFE (Polytetrafluoroethylene) was used as a binder in the milling process during the formation of the electrodes. This was in addition to 92 wt%

activated carbon. Carbon Black was not added during the electrode preparation so as to effectively determine the characteristics of the activated carbon alone.

SAMPLE ID	Description	PTFE Binder	Mass ratio of AC:PTFE	Solvent	Temperature ºC	Initial Gap of Hot rolling press	Final Gap of hot rolling press
1103NDA850B	NDA	PTFE 10%	92:0.8	Ethanol	80	1000	75
2203BL850B	Blank	PTFE 10%	92:0.8	Ethanol	80	1100	75
1103NDA850BHT	NDA+HT	PTFE 10%	92:0.8	Ethanol	80	2200	100
YP80F20190410	Commercial AC	PTFE 10%	92:0.8	Ethanol	80	1200	75

Table 3. 5 Electrode preparation parameters

For the coin cell assembly, 2 discs of electrodes made up of activated carbon bonded with the (carbon coated aluminium foil) was used in combination with TF4030(19 mmØ) separator. The electrolyte used was $TEABF_4$ in PC (Tetraethylammonium tetrafluoroborate in PC) and a constant volume of 110(µl). the parameters for the different components are shown in Table 3.6

| SAMPLE | Cell No | DISC | | Foil Mass mg | AC Mass 1, mg | AC Mass 2, mg | Separator | Electrolyte | Electrolyte Volume (µl) |
		Mass 1, mg	Mass 2, mg						
2401NDA750	1	30.9	31.60	9.2	19.964	20.608	TF4030 (19 mmØ)	S1	110
	2	31.7	31.5	9.2	20.7	20.516			110
1103NDA850B	1	17.4	17.5	9.2	7.544	7.636	TF4030 (19 mmØ)	TEABF4 in PC	110
	2	17.6	17.4	9.2	7.728	7.544			110
	3	17	17.4	9.2	7.176	7.544			110
	4	17.4	17.8	9.2	7.544	7.912			110
2203BL850	1	16.5	16.8	9.2	6.716	6.992	TF4030 (19 mmØ)	TEABF4 in PC	110
	2	17	16.8	9.2	7.176	6.992			110
	3	16.6	16.7	9.2	6.808	6.9			110
	4	16.6	16.5	9.2	6.808	6.716			110
Commercial AC	1	17.5	17.4	9.2	7.636	7.544	TF4030 (19 mmØ)	TEABF4 in PC	110
	2	17.1	17.1	9.2	7.268	7.268			110
	3	17.4	17.6	9.2	7.544	7.728			110
	4	17.2	17.1	9.2	7.36	7.268			110

Table 3. 6 Coin cell assembly parameters

3.7   ELECTROCHEMICAL TESTING OF COIN CELLS

Different set of tests are carried out on the coin cells to determine the electrochemical properties of the assembled coin cells. These properties include the specific capacitance, self-discharge, ohmic resistance and voltage window.

3.7.1   Specific Capacitance

After the fabrication of the coin cells, the cells are left to rest for 720 min before the sequence of steps highlighted below are carried out on it. The battery analyser is used during this process.

a) The cell is charged to 2.5V and discharged to 1.5V at 0.1mA in 5 cycles

b) The cell is charged to 2.5V and discharged to 1.5V at 0.2mA in 5cycles

c) The cell is charged to 2.5V and discharged to 1.5V at 0.5mA in 5 cycles

d) The cell is charged to 2.5 V and discharged to 1.5V at 1mA in 5 cycles

e) The cell is charged to 2.5V and discharged to 1.5V at 5mA in 5 cycles

The initial discharge voltage at 0.1mA for the fifth cycle is obtained from the equipment as well as the discharge time at 0.1mA and computed into the equation below to compute the specific capacitance at 0.1mA in F/g. the mass of the activated carbon electrode used in the coin cell fabrication is also taken into consideration.

Specific capacitance at 0.1mA = $(0.1*t_{id})/(M_{ac})/ (V_{id} - 1.25) *4$

Where

t_d = Discharge time of the 5th cycle at 0.1mA

V_{id} = Initial Discharge Voltage of the 5th cycle at 0.1mA

The calculation is repeated to obtain the specific capacitance at 5mA using the values obtained from the 5th cycle at 5mA and the formula below

Specific capacitance at 0.1mA = $(5*t_{id})/(M_{ac})/ (V_{id} - 1.25) *4$

3.7.2 Self-Discharge

The self-discharge test takes place in succession after the tests for the specific capacitance. The cell is charged to 2.5 V at 1mA and held for 120 min at 2.5V. it is then left to rest for 4320min(72h). the voltage left after 72 hours is recorded and substituted in the formula below to obtain the self-discharge rate after 72 hours.

Self-discharge rate % = $((2.5 - \text{Voltage left after 72 h})/ 2.5) *100$

3.7.3 Ohmic Resistance

The ohmic resistance of the prepared electrodes were carried out using a constant current of (0.1A) effectively maintained by a source of constant current. A digital multimeter was used in recording the observed voltage drop with a resolution of 0.01mV. it was ensured that the cut

stripes of electrodes were arranged in such a manner that the overlap area was about 1.5 cm². This is explained in the figure below
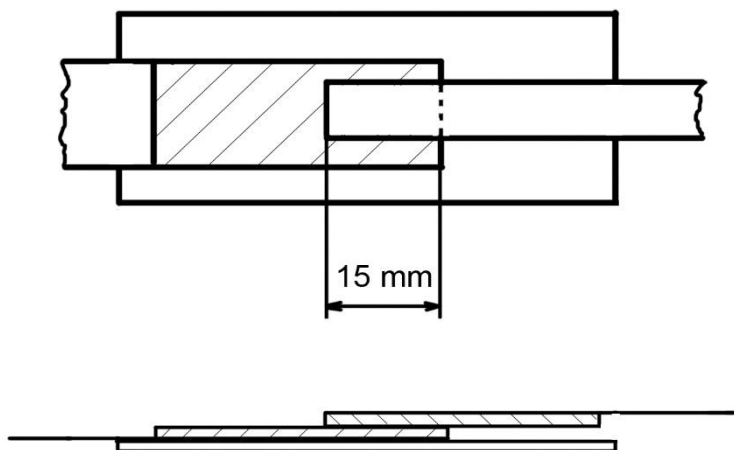
The following equation was used in the calculation of the specific value of the total ohmic resistance of the electrode (Ohm.cm²)

$$R = \frac{U}{I} \times 1{,}5 \text{ см}^2$$

The value obtained is an indication of the ohmic resistance of the active material layer in addition to the contact resistance between the current collector and active material layer.

Where

U = Voltage

R = Ohmic resistance

I = Current

CHAPTER 4

4.0   RESULTS AND DISCUSSION

This section shows the results obtained during the experiment and their discussion. Three different factors were investigated in this study. They include temperature at two levels 750 $^{\circ}$C and 850 $^{\circ}$C, impregnation ratio of activated carbon to KOH using 1:2 and 1:4, amount of additive added Al and Cu (using ratios of 0.25,0.5,1 and 2). These were all combined together while keeping the activation time of 2h constant. 3 different categories of experiments were obtained namely; NDA (Non-destructively activated) samples with Al, NDA samples with Cu and the blank experiments without any of the additive.

4.1   YIELD

The char utilized in the experiment was obtained by burning saw dust in the furnace at 600 $^{\circ}$C. The yield of char from the carbonization process is illustrated in Table 4.1.

S/N	Conditions	Samples mass before	Samples mass after	Yield
1	600 $^{\circ}$C for 1hour	20g	4.941	24.7%
2	600 $^{\circ}$C for 1hour	30g	6.5	21.7%
3	600 $^{\circ}$C for 1hour	30g	7.625	25.4%
4	600 $^{\circ}$C for 1hour	20g	5.3	26.5%

Table 4. 1 Yield obtained during Carbonization

The yields obtained during carbonization was seen to range from 21-26 wt% with an average value of 24% obtained. This was in correspondence with the work of Marsh et al.[102] who reported that the typical values of carbonization are within the range of 20 -30 wt%. This is explained by the smaller ratios of carbon about 45-46 wt% present in lignocellulosic materials which upon carbonization leads to the subsequent loss of parts of the oxygen present in addition to hydrogen leaving in the form of CO_x compounds.

The synthesized char was further activated with KOH under the presence of the different additives. The yield obtained after washing while using Al and Cu is shown in Table 4.2 and 4.3.

S/N	Sample ID	Conditions	(Char:Al:KOH) ratio	Yield %
1	1303NDA750A	750°C for 120 min	1:0.25:4	59
2	1103NDA850B	850°C for 120 min	1:0.25:4	46
3	1103NDA850A	850°C for 120 min	1:0.5:4	46
4	1303NDA750B	750°C for 120 min	1:0.5:4	60
5	1104NDA750A	750°C for 120 min	1:1:2	65
6	1104NDA750B	750°C for 120 min	1:1:4	60
7	1504NDA850A	850°C for 120 min	1:1:2	40
8	1504NDA850B	850°C for 120 min	1:1:4	35
9	1801NDA850	850°C for 120 min	1:2:2	42
10	0312NDA750	750°C for 120 min	1:2:2	58
11	2811NDA750	750°C for 120 min	1:2:4	43
12	2911NDA850	850°C for 120 min	1:2:4	47

Table 4. 2 Yield obtained for NDA samples with Al

S/N	Sample ID	(Char:Cu:KOH) ratio	Conditions	Yield
1	2404NDA850A	1:0.5:4	850°C for 120 min	46
2	2404NDA850B	1:0.25:4	850°C for 120 min	52
3	2504NDA750A	1:0.5:4	750°C for 120 min	32
4	2504NDA750B	1:0.25:4	750°C for 120 min	48
5	0905NDA850A	1:1:4	850°C for 120 min	47
6	0905NDA850B	1:1:2	850°C for 120 min	59
7	1505NDA750A	1:1:4	750°C for 120 min	60
8	1505NDA750B	1:1:2	750°C for 120 min	69
9	2005NDA750A	1:2:2	750°C for 120 min	42
10	2005NDA750B	1:2:4	750°C for 120 min	38
11	2105NDA850A	1:2:4	850°C for 120 min	49
12	2105NDA850B	1:2:2	850°C for 120 min	55

Table 4. 3 Yield obtained for NDA samples with Cu

The yield of activated carbon obtained is strongly affected by the activation temperature[95]. In this study, there existed a variance in the temperatures considered while using a high temperature of 850 °C and a lower temperature of 750 °C. The yield was seen to be lower when using 850 °C compared to 750 °C. Teng et al[95] also made similar findings while preparing

activated carbon from coal using KOH. Factors such as amount of KOH added also contributed to decreasing the yield as well. Using ratios of 2 and 4 showed that the more KOH added, the more activation occurred in the wood precursor. The degree of activation increased upon usage of higher impregnation ratios and this in turn was evident as shown in the decrease in the yield in Table 4.4.

S/N	Sample ID	Conditions	(Char: KOH)	Yield
1	2203BL850A	850°C for 120 min	1:2	58
2	2203BL850B	850°C for 120 min	1:4	43
3	1004BL750A	750°C for 120 min	1:2	51
4	1004BL750B	750°C for 120 min	1.4	37

Table 4. 4 Yield of blank experiments

The yield obtained during the experiment is given in Table 4.2. Higher temperatures and higher activation time results into lower yield since the samples are subjected to more heat action which leads to gasification reactions occurring sequential to the development of porosity in the activated carbon. The yield has been reported to be lower for more activated carbons[103, 104]. The influence of the additive can also be seen from the higher yields obtained using the either Cu or Al as compared to the Blank experiments. This can be explained by considering the blank samples as being extensively activated via the etching and the additive playing a role in reducing the nature of defect in the activated carbon. An evidence of the defect could be the loss of more carbon atoms from the structure which is related to a lower yield when comparing the NDA and blank samples. The origin of the defect could also be traced to the effect of extensive chemical etching by the KOH in the blank samples, but the NDA samples are majorly activated via the exfoliation step (Promoted by the rapid breakdown of KOH into Potassium) with significant porosity generation and loss of carbon atoms following a lower degree of gasification.

4.2   ASH CONTENT

The ash content of the sample was carried out to determine the mineral oxide content of the sample. In addition, a confirmation would be made on the removal of the additives (Al or Cu) following the washing step before the different characterizations were carried out. The first set of samples produced with an Aluminium ratio of 2 had very high ash content of over 20%. This result necessitated the improvement of the washing step as explained in Chapter 3 by increase in the concentration of KOH used which was effective in removing the Al additive. Similar

trend was observed in samples non-destructively activated with Copper additive. The high values of ash content at the initial phased was corrected by increasing the concentration of the acid HCl in the washing step which was more efficient in removing the Cu additive. The ash content for the rewashed samples were in the range of 0-5% with most of the samples having little or nothing left in the quartz boat upon completion of the heating profile. The establishment of this fact added to one of the precautions taken to prevent parasitic faradic reactions in the cathode and anode due to the presence of metal impurities commonly identified in activated carbon from saw dust. These parasitic reactions if not controlled would increase the self-discharge of the assembled coin cells.

4.3 NITROGEN ADSORPTION ANALYSIS

The results from the Nitrogen adsorption analysis for the blank samples and samples with the aluminium and Copper additive are given in Table 4.5, 4.6 and 4.7. The specific surface area(BET SSA) was determined by BET, micropore area, micropore volume and external surface area were determined by the t-plot method, the mesopore volume was estimated from the cumulative volume of pores within 2-50nm from the BJH desorption pore distribution, the macropore volume was calculated by subtracting the sum of the micropore and mesopore volumes from the single point adsorption total pore volume[105] and DFT used in obtaining the pore size distribution.

Sample ID	Description	BET SSA	Micropore area (m²/g)	External Surface area (m²/g)	Micropore vol (cm³/g)
2203BL850A	850°C for 120 min (1:2) blank	2336	924	1412	0.225605
2203BL850B	850°C for 120 min (1:4) blank	3083	1255	1828	0.134798
1004BL750A	750°C for 120 min (1:2) blank	2040	856	1184	0.250854
1004BL750B	750°C for 120 min (1:4) blank	2775	932	1844	0.126425

Table 4. 5 Result of Nitrogen adsorption analysis for the Blank experiment

Sample ID	Description	BET SSA	Micropore area (m²/g)	External Surface area (m²/g)	Micropore vol (cm³/g)
1103NDA850A	850°C for 120 min (0.5:1):4	2789	941	1847	0.152753
1103NDA850B	850°C for 120 min (0.25:1):4	2924	1070	1853	0.140903
1303NDA750A	750°C for 120 min (0.25:1):4	2692	1016	1677	0.170636
1303NDA750B	750°C for 120 min (0.5:1):4	2415	832	1584	0.170265
1801NDA850	850°C for 120 min (1:2):2	661	480	181	0.205914
0312NDA750	750°C for 120 min (1:2):2	866	603	263	0.256043
2811NDA750	750°C for 120 min (1:2):4	856	630	227	0.269789
2911NDA850	850°C for 120 min (1:2):4	1237	509	728	0.134374
1104NDA750A	750°C for 120 min (1:1)2	818	565	253	0.236584
1104NDA750B	750°C for 120 min (1:1) 4	1299	796	503	0.326691
1504NDA850B	850°C for 120 min (1:1)4	1564	723	841	0.215786

Table 4. 6 Results of Nitrogen adsorption analysis for NDA with Al samples

Sample ID	Description	BET Ssa m²/g	Micropore area (m²/g)	External Surface area (m²/g)	Micropore vol (cm³/g)
2404NDA850A	850°C for 120 min (0.5:1):4	2925	1034	1890	0.099189
0905NDA850A	850°C for 120 min (1:1)4	3204	1143	2061	0.096223
0905NDA850B	850°C for 120 min (1:1)2	2056	937	1120	0.329782
1505NDA750A	750°C for 120 min (1:1)4	2523	846	1678	0.19779
2404NDA850B	850°C for 120 min (0.25:1):4	2954	957	1997	0.086881
2504NDA750A	750°C for 120 min (0.5:1):4	3350	1046	2304	0.090828
2504NDA750B	750°C for 120 min (0.25:1):4	2636	817	1818	0.144525
1505NDA750B	750°C for 120 min (1:1):2	1724	722	1001	0.2023

2005NDA750A	750°C for 120 min (2:1):2	1050	400	650	0.067561
2005NDA750B	750°C for 120 min (2:1):4	1936	645	1291	0.106453
2105NDA850A	850°C for 120 min (2:1):4	2295	838	1457	0.104993
2105NDA850B	850°C for 120 min (2:1):2	1888	842	1045	0.270133

Table 4. 7 Result of Nitrogen adsorption experiment for NDA with Cu samples

From the results obtained, sample 1103NDA850B which was highlighted in red had the highest BET surface area of **2923 m^2/g** of the entire samples activated with the addition of Aluminium. This was achieved using a condition of (0.25:1:4) Aluminium: Char: KOH. The Blank experiments without the additive had higher surface areas of **3082 m^2/g** using the same conditions of 4:1 in terms of KOH to Char. (Insert with reference influence of surface area of AC on conductive properties and specific capacitance). Figure 4.1 shows the adsorption isotherm for selected samples with surface areas above 2000 m^2/g. They all exhibited characteristics of type 1 isotherms. This meant that they possessed extremely small pores mostly classified under the microporous nature. A hysteresis loop was observed in the Blank samples 2203BL850B which had the highest surface area of 3082 m^2/g. This hysteresis loop suggested that the sample had certain amount of mesopores in addition to an upper size restriction[82].

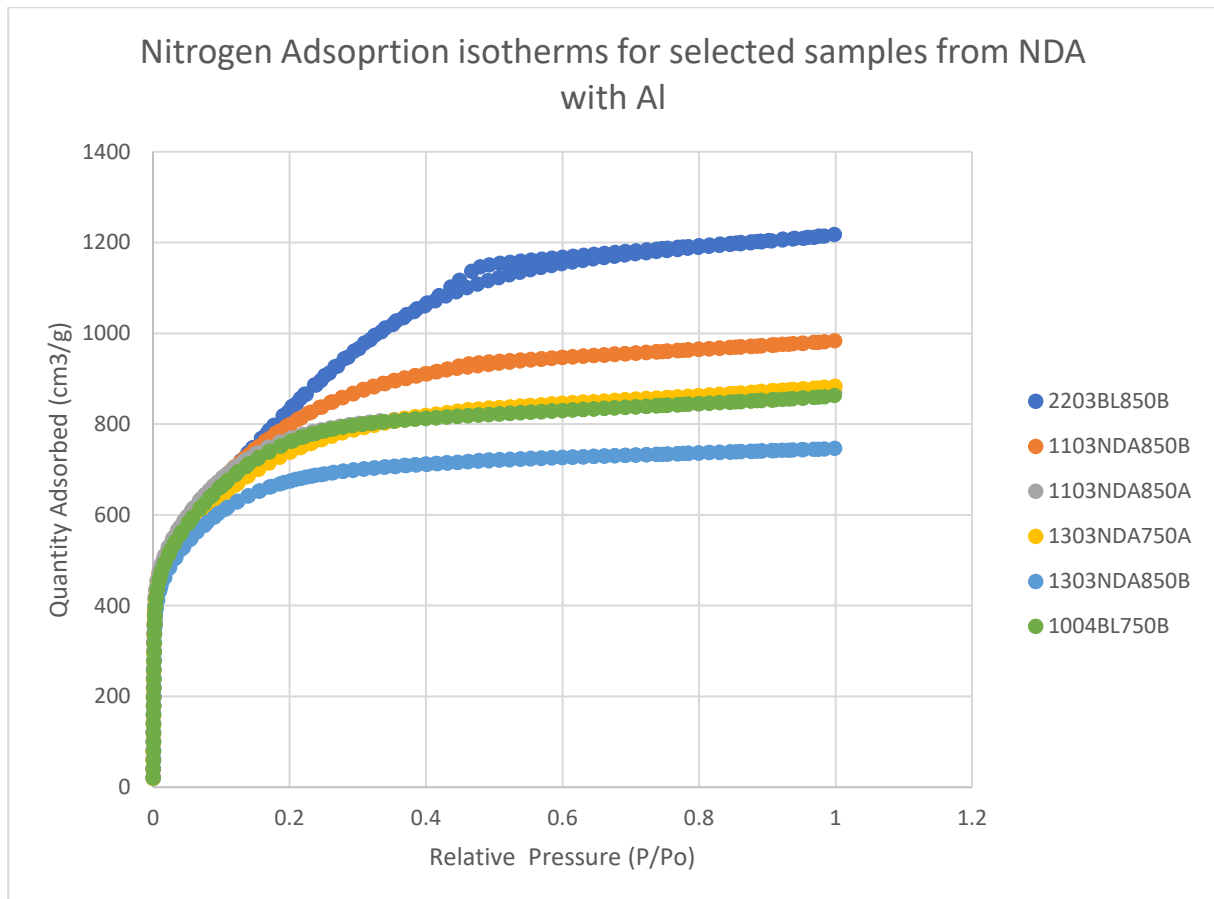*Figure 4. 1 Adsorption isotherms for Selected samples from NDA with Al and the best Blank sample*

The second phase of the study constituted the repetition of the Non-destructive activation process by the introduction of a new additive, Copper. Nitrogen adsorption characterization was carried out on the prepared samples with the adsorption isotherms shown in Figure 4.2 in comparison to the Blank sample 2203BL850B.
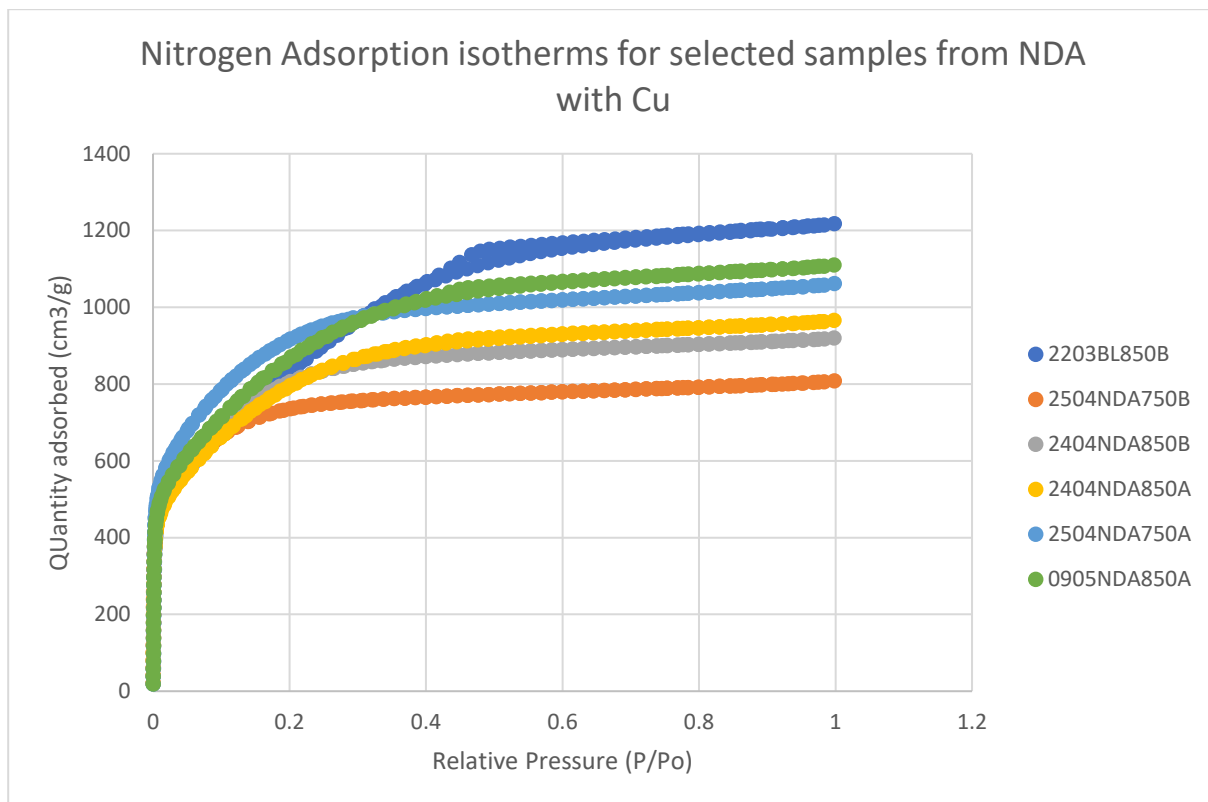
Figure 4. 2 Nitrogen Adsorption Isotherm for Selected samples from NDA with Cu and the best blank sample

The samples with the displayed adsorption isotherms were samples which had surface areas above 2500 m²/g. They all corresponded to the type 1 adsorption isotherm, thus highlighting the microporous nature they consist of. The results for the various surface areas as well as average pore volume and diameter are shown in Table 4.8.

S/N	Sample ID	Conditions (Char:Cu:KOH) ratio	BET Ssa (m²/g)	Total pore volume (cm³/g)	Avg Pore diameter (nm)
1	2504NDA750B	750°C for 120 min (1:0.25:4)	2636	1.25	1.898
2	2404NDA850B	850°C for 120 min (1:0.25:4)	2954	1.424	1.928
3	2404NDA850A	850°C for 120 min (1:0.5:4)	2925	1.495	2.044
4	2504NDA750A	750°C for 120 min (1:0.5:4)	3350	1.643	1.961

5	1505NDA750B	750°C for 120 min (1:1:2)	1724	0.845	1.95996
6	1505NDA750A	750°C for 120 min (1:1:4)	2524	1.203	1.90618
7	0905NDA850B	850°C for 120 min (1:1:2)	2056	0.995	1.93567
8	0905NDA850A	850°C for 120 min (1:1:4)	3204	1.718	2.14551
9	2105NDA850B	850°C for 120 min (1:2:2)	1888	0.912	1.932
10	2005NDA750A	750°C for 120 min (1:2:2)	1050	0.575	2.192
11	2005NDA750B	750°C for 120 min (1:2:4)	1936	0.951	1.964
12	2105NDA850A	850°C for 120 min (1:2:4)	2295	1.271	2.215

Table 4. 8 Pore volumes of Cu NDA samples

The results from the Non-destructive activation of the char using copper additive and KOH via chemical impregnation displayed several high values in terms of specific surface area (BET). The highest value obtained was from sample 2504NDA750A of about **3350 m^2/g** with an experimental condition of 750 °C for 120 min (1:0.5:4). A significant number of experimental runs had surface areas above **2500 m^2/g**. These runs were those with impregnation ratios of 0.25,0.5, 1 at 750 °C and 850 °C with the exception of sample 1505NDA750B which had 1724 m^2/g and was produced with conditions of 750 °C for 120 min (1:1:2). These high values obtained portrayed the more active nature of the copper which enhanced the activation of the carbon and opening of pores. The high surface areas could also be attributed to the washing step in which 2M HCl solution was used in washing the samples after activation to remove completely traces of copper from the activated carbon before conduction of the BET analysis.

This step proved quite tasking especially during the washing of samples with additive ratios of 2. As the 2M HCl was not effective in washing completely the Copper from the sample. In samples with lower impregnation ratios, the first washing step which was carried out with KOH oxidizes the copper and coverts some parts of it into Black Copper oxide. The second washing step which is done with the HCl converts the Copper oxide and remaining Copper in excess of

the acid into Copper Chloride indicated by the bluish filtrate in the vacuum filtration flask. This was as observed upon the first rinse of the acid following the 2 hours washing by stirring on a magnetic stirrer. Ash content tests as reported in the previous section as well as XRD analysis were conducted on the samples before conduction of the Nitrogen adsorption analysis to ensure that the results from the analysis were solely from the activated carbon and not influenced by the Cu or Al additive. This was also done to prevent the decomposition of the electrolyte which is often caused by presence of metals such as copper as reported from previous experiences by laboratory colleagues during coin cell fabrication and testing.

4.3.1 Pore Size Distribution

Despite the high surface areas possessed by some samples, it is not enough to predict the specific capacitance alone on the basis of large surface area. The pore size distribution, porosity, micropore and mesopore content are some of the factors affecting the specific capacitance especially in relation to the ion adsorption process[106].

The pore size distributions of the activated carbon were obtained using the DFT plot and would be categorized according to the blank samples Figure 4.3, NDA with Al samples Figure 4.4 and NDA with Cu samples Figure 4.5
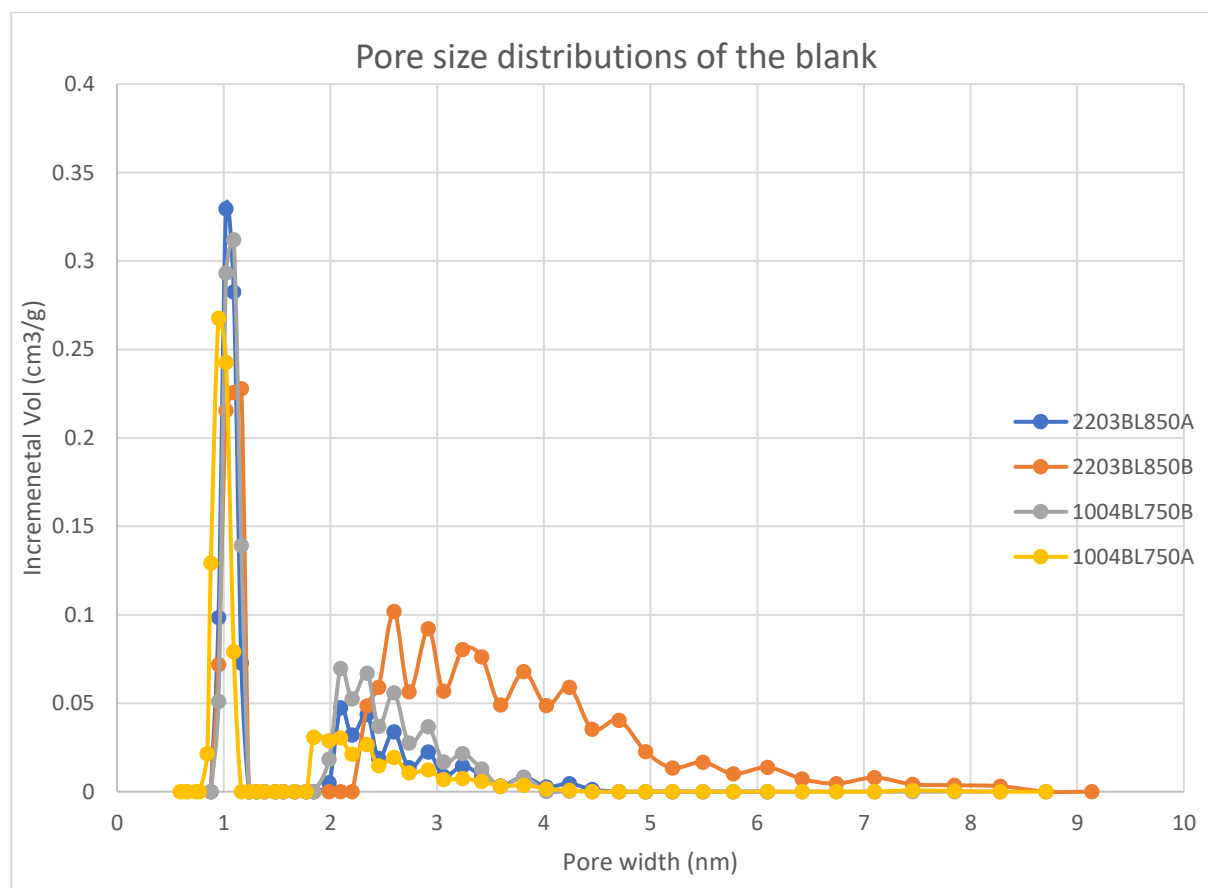
Figure 4. 3 Pore size distributions of the blank samples

Samples 2203BL850B was the standout performer of the blank samples having narrow micro porosity and sufficient mesopores. Similar findings have also been obtained by the works of Wu et al[106] who reported that the high mesopore proportion of wood activated carbon is specially suitable for the application in electrochemical capacitors. This high proportion of mesopores are often tagged as being responsible for the electrochemically accessible surface area[107]. The narrow micropore size distribution in the range of 0.8-1.1 nm has also been effectively categorized as being suitable for ion transport which effectively matches the solvation radii of the electrolytes[29, 30]. It has been reported in literature that optimum performance in supercapacitors is achieved when there is an equal match between the electrolyte ion and average micropore size of the activated carbon[3, 29].
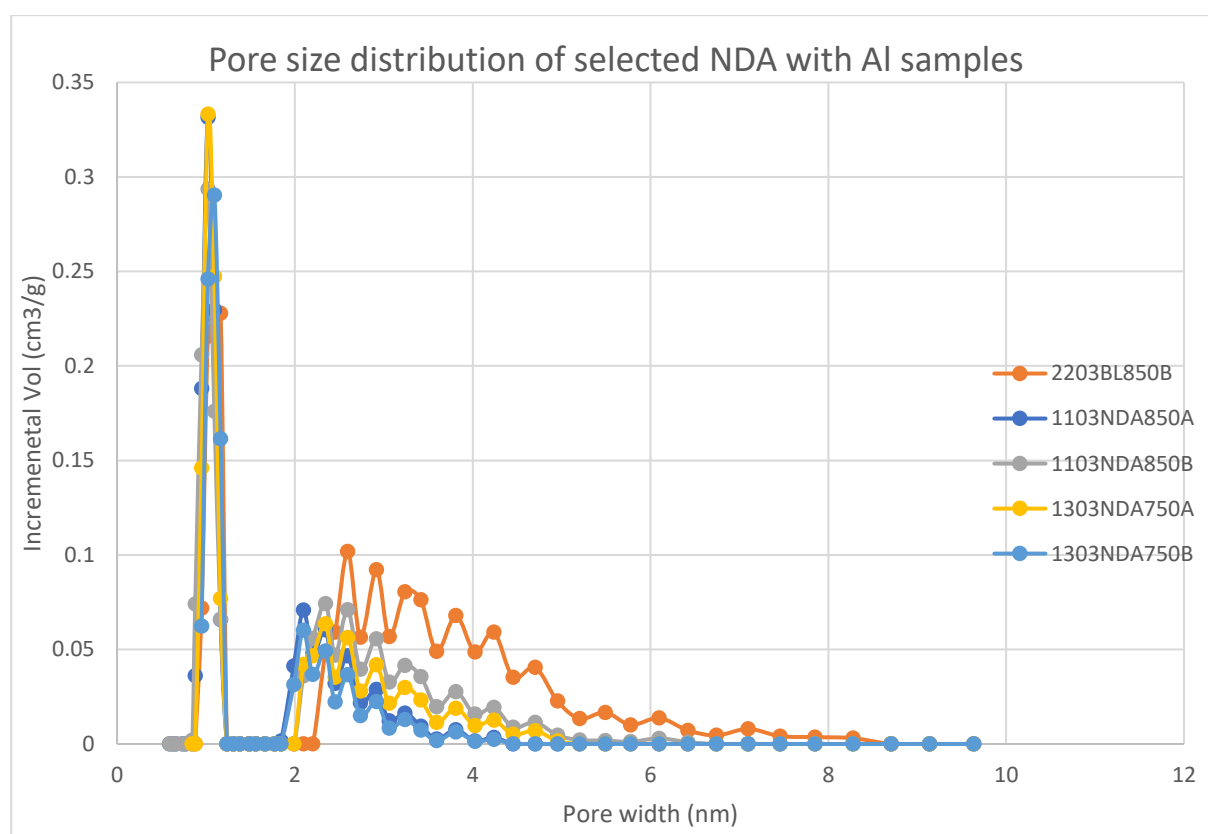
Figure 4. 4 Pore size distribution of NDA with Al samples

Comparing the pore size distribution of the blank sample with those of the NDA with Al samples show that smaller proportions of mesopore content was obtained in the NDA with Al samples. This can also be related to the superior performance exhibited by samples 2203NDA850B (Blank) as compared to samples 1103NDA850B (NDA Al). Analysing the pore size distributions of the NDA with Cu samples, it can be seen that even though they had

attendant higher surface areas, most of the samples had very low mesopore percentage and micropore area. An example is sample 0905NDA850B with specific surface area by BET of 2056 m^2/g with very low mesopore content as identified on Figure 4.5. This would clearly not be suitable for use in fabrication of high specific capacitance electrochemical cells due to incomplete utilization of the surface area as evidenced by the pore size distribution[99, 106, 107].
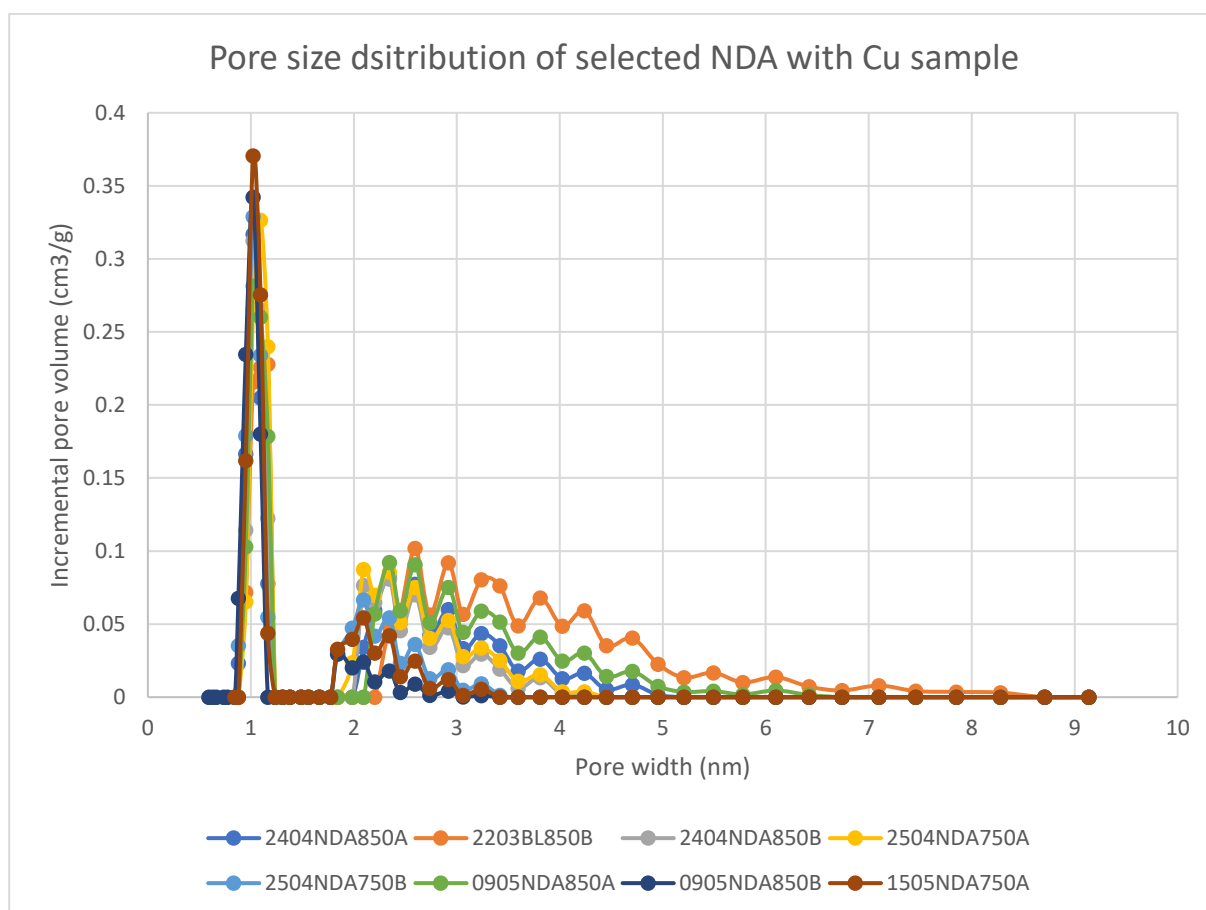
Figure 4. 5 Pore size distribution of Selected NDA with Cu samples

From the various pore size distributions obtained , it is clear that higher activation temperature of 850 ºC was suitable for more percentage of mesopore content in the activated carbon samples which is in agreement with literature on factors affecting pore size distribution of activated carbon[106, 108].

4.3.2 Effect of Additive Ratio on Pore Volume

Most often than not, a high BET specific surface area results in high micropore volume with a directly proportional relationship existing[25] but results from the NDA of the two samples showed a negative trend to this. The samples with the highest specific surface area did not have

the highest micropore volumes noted. From Table 4.8 - 4.10, the highest micropore volumes obtained were from samples using higher additive ratios of 1 and 2 with the highest values noted for additive ratios of 1 in both the Cu and Al NDA samples. The micropore volume of samples activated at 750 ^{o}C were higher than those activated at 850 ^{o}C. This corresponded to the works of Kalpana et al[109] who recorded similar findings while comparing the effect of activation temperature on micropore volume. Ssa refers to the specific surface area by BET in m^2/g, V_{micro} refers to the micropore volume using the t-plot method, $V_{meso\ des}$ refers to the volume of mesopores (cumulative between 2- 50 nm) estimated from the BJH desorption, V_{tot} refers to the sum of (V_{micro} + $V_{meso\ des}$), $V_{meso\ ad}$ refers to the volume of mesopores (Cumulative between 2 -50 nm) estimated from the BJH adsorption, $V_{stpore\ vol}$ refers to the single point adsorption total pore volume of pores, D_{micro} refers to the micropore size distribution from DFT in nm. The units of the volumes are all in cm^3/g.

Sample ID	Char:Al:KOH ratio	Ssa BET	V_{micro}	$V_{meso\ des}$	V_{tot}	$V_{meso\ ad}$	$V_{stpore\ vol}$	D_{micro}
1303NDA750A	1:0.25:4	2692	0.171	0.168	0.339	0.743	1.366	0.879 - 1.165
1303NDA750B	1:0.5:4	2415	0.170	0.084	0.254	0.471	1.156	0.951 - 1.165
1104NDA750B	1:1:4	1299	0.327	0.049	0.376	0.116	0.646	0.879 - 1.094
2811NDA750	1:2:4	866	0.270	0.035	0.305	0.075	0.439	0.879 - 1.094

Table 4. 9 Effect of increasing additive intensity on pore volume at 750 ^{o}C (Al)

Sample ID	Char:Al:KOH ratio	S_{BET}	V_{micro}	$V_{meso des}$	V_{tot}	$V_{meso ad}$	$V_{stpore vol}$	D_{micro}
1103NDA850B	1:0.25:2	2924	0.141	0.217	0.357	0.992	1.522	0.844 - 1.165
1103NDA850A	1:0.5:4	2789	0.153	0.116	0.269	0.564	1.344	0.879 - 1.165
1504NDA850B	1:1:04	1564	0.216	0.112	0.327	0.386	0.827	0.951 - 1.165
2911NDA850	1:2:04	1237	0.134	0.091	0.226	0.255	0.685	0.844 - 1.094

Table 4. 10 Effect of increasing additive intensity on pore volume at 850 ^{o}C (Al)

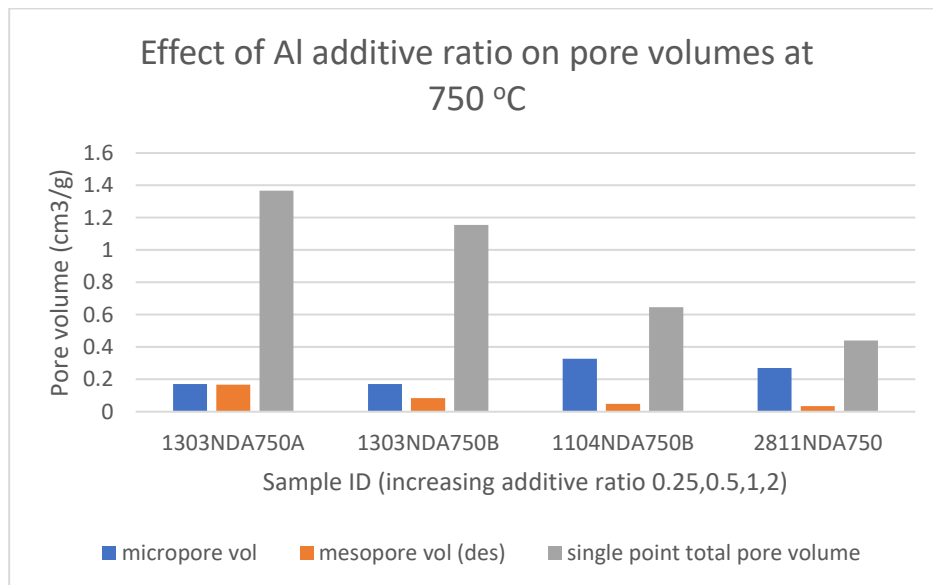Table 4.9 Effect of increasing additive intensity on pore volume at 850 ^{o}C (Al)

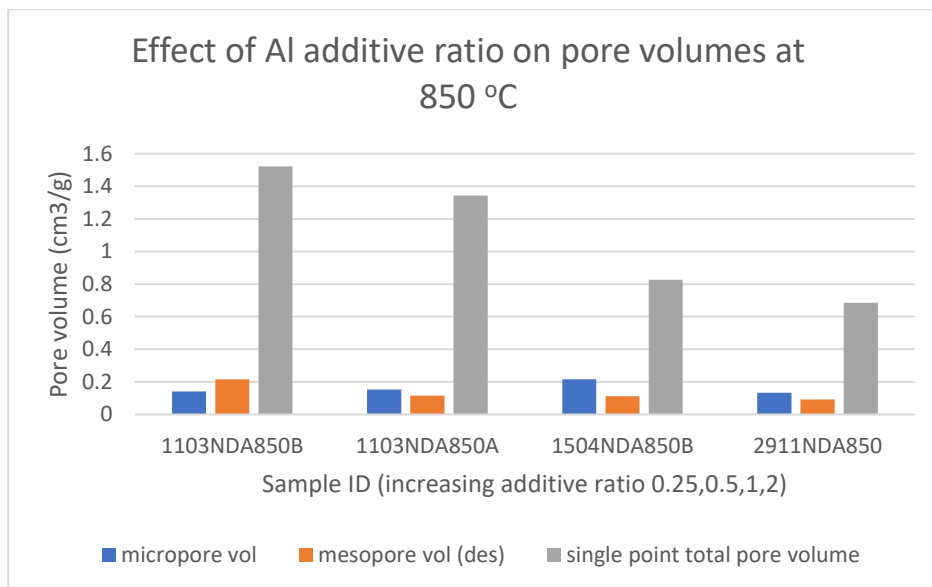*Figure 4. 6 Effect of Al additive ratio on pore volumes at 750 ^{o}C*

Figure 4. 7 Effect of Al additive ratio on pore volumes at 850 ºC

From Figure 4.6 and 4.7 , The micropore volume is also seen to increase as the additive ratio increases until a ratio of 1 where it peaks and then begins to decrease. The mesopore volumes are on a steady decrease with increasing additive ratio and the single point total pore volume decreases as Al additive ratio increases. These observations are similar while comparing the two temperature levels of 750 ºC and 850 ºC. Increasing the additive ratio brings about an increase in the micropores via the extensive activation following increase in the additive intensity. The additive is responsible for the promotion of exfoliation activation via decomposition of KOH into Potassium and gasification following the breakdown of Potassium carbonates. This favours the attack on the carbon structure leading to the formation of new pores and widening of existing pores (mesopores). As the new pores keep on forming with increasing additive intensity, the micropore volumes increase until a certain point where extensive gasification would result into the breaking of already widening pore walls and destruction of pore structures leading to both a reduction in surface area, micropore, mesopore and single point total pore volume.

The mesopore volumes and single point total pore volumes increase with increase in temperature from 750 to 850 ºC due to carbonization effects related to increased temperature while a decrease in the micropore volume is observed. An explanation to this would also be related to the breakdown of pore walls which increases as the activation temperature increases.

The pore volumes for selected samples with increasing additive ratio from the NDA with Cu are shown in Table 4.11 and 4.12

Sample ID	Char:Cu:KOH ratio	S_{BET}	V_{micro}	$V_{meso\,des}$	V_{tot}	$V_{meso\,ad}$	$V_{stpore\,vol}$	D_{micro}
2504NDA750B	1:0.25:4	2636	0.145	0.081	0.226	0.462	1.250	0.879 - 1.165
2504NDA750A	1:0.5:4	3350	0.091	0.147	0.238	0.957	1.643	0.951 - 1.165
1505NDA750A	1:1:4	2524	0.198	0.085	0.282	0.364	1.203	0.951 - 1.165
2005NDA750B	1:2:4	1936	0.106	0.076	0.1823	0.431	0.951	0.879 - 1.165

Table 4. 11 Effect of increasing additive intensity on pore volume at 750 ºC (Cu)

Sample ID	Char:Cu:KOH ratio	S_{BET}	V_{micro}	$V_{meso\,des}$	V_{tot}	$V_{meso\,ad}$	$V_{stpore\,vol}$	D_{micro}
2404NDA850B	1:0.25:4	2954	0.087	0.116	0.202	0.831	1.424	0.951 - 1.165
2404NDA850A	1:0.5:4	2925	0.099	0.183	0.282	1.006	1.495	0.879 - 1.165
0905NDA850A	1:1:4	3203	0.096	0.281	0.377	1.304	1.718	0.951 - 1.165
2105NDA850A	1:2:4	2295	0.105	0.228	0.333	0.966	1.271	0.879 - 1.165

Table 4. 12 Effect of increasing additive intensity on pore volume at 850 ºC (Cu)
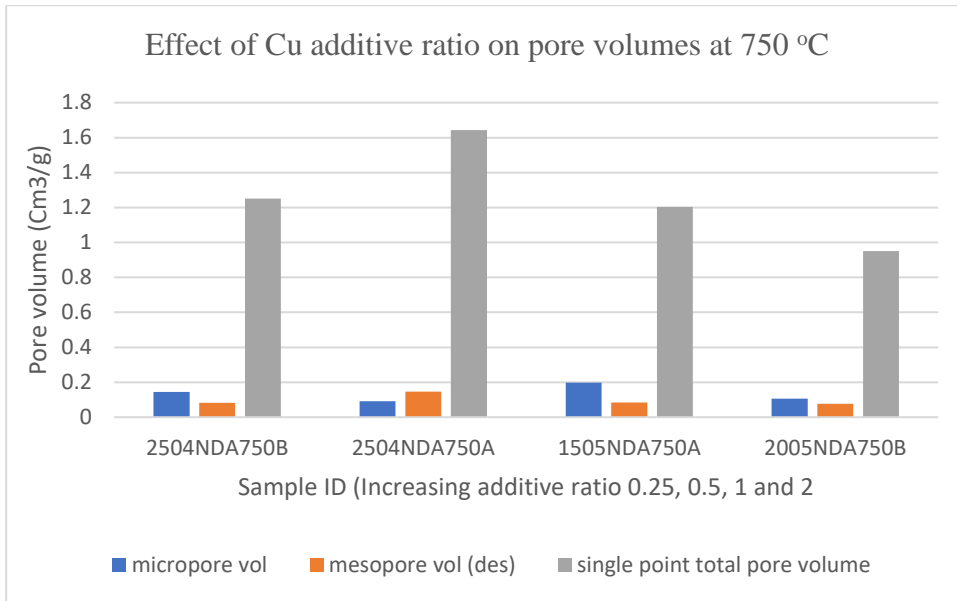
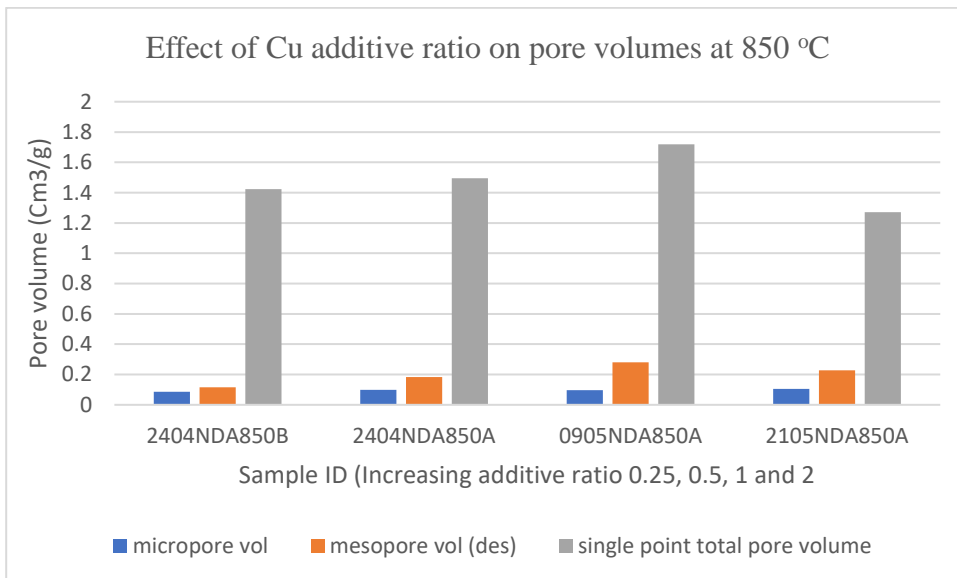*Figure 4. 8 Effect of (Cu) additive intensity on pore volumes at 750 °C*

Figure 4. 9 Effect of (Cu) additive intensity on pore volumes at 850 °C

The plots of pore volumes for samples with increasing amount of Cu additive is shown in Figure 4.8 and 4.8. From the figure, the extensive influence of the copper additive is visible in the nature and effect of the pore volumes. The single point total pore volumes and mesopore volumes are seen to increase with the additive ratio until the optimum point is reached where a decrease sets in beyond this. It is evident that the optimum point of the Al additive should have been investigated further by reducing the additive ratios beyond 0.25 in order to obtain similar patterns displayed by the samples with the Cu additive. As explained earlier, the additive was influential in the activation of the carbon via widening of existing pores as the intensity increased. This was achieved up to the optimum point with the highest mesopore volume and

single point total volume. Beyond this point, the pore structures broke down due to further increase in the additive ratio which promoted extensive exfoliation and removal of carbon atoms via the gasification process[95]. Breakdown in the pores structures resulted to decrease in single point total pore volume and mesopores. Similar observations were made for the two levels of activation at 750 ºC and 850 ºC with the difference being the optimum point at additive ratios of 0.5 and 1 for 750 ºC and 850 ºC respectively.

A significant correlation exists between the BET Ssa, External surface area and Micropore area. They all seemed to increase according as shown in Table 4.5 and 4.6 for both the NDA with Cu and Al samples.

Following the series of experiments conducted, the following sections discuss the influence of varied parameters such as temperature, impregnation ratio and additive ratio to the surface area. The relation to the specific surface area was considered only because of the similar trend which could be observed with the other factors mentioned in the previous paragraph. This would quantify the activation levels in terms of the area and porosity generated. The specific surface area of the activated carbon is responsible for the storage of energy. This occurs through the 'reversible ion adsorption on the carbon at the interface between the carbon and electrolyte'[29].

4.3.3   Effect of Increase in Temperature on Specific Surface Area

For the NDA with Al samples

In the course of the study, two different temperature levels were investigated at selected Char:Al/Cu:KOH ratios. They are presented in Table 4.12a-d. the first set of discussions would be focussed on the samples non-destructively activated with Aluminium. Identical samples with similar Ac:Al:KOH ratio but at the different temperature levels are compared to see the effect of temperature on the specific surface area in the presence of this particular additive. This would establish a trend given the amount of additive used and the temperature ratio for future optimization studies with the aim of selecting optimal conditions in terms of high surface area

Char:Al:KOH ratio	Sample ID	Temperature °C	BET Specific surface area (m²/g)
1:0.25:4	1303NDA750A	750	2692
	1103NDA850B	850	2924

Char:Al:KOH ratio	Sample ID	Temperature °C	BET Specific surface area (m²/g)
1:0.5:4	1303NDA750B	750	2415
	1103NDA850A	850	2789

Char:Al:KOH ratio	Sample ID	Temperature °C	BET Specific surface area (m²/g)
1:1:4	1104NDA750B	750	1299
	1504NDA850A	850	1564

Char:Al:KOH ratio	Sample ID	Temperature °C	BET Specific surface area (m²/g)
1:2:4	2811NDA750	750	866
	2911NDA850	850	1237

Table 4. 13 (a-d) Effect of increase in temperature on specific surface area at different additive concentrations (Al)
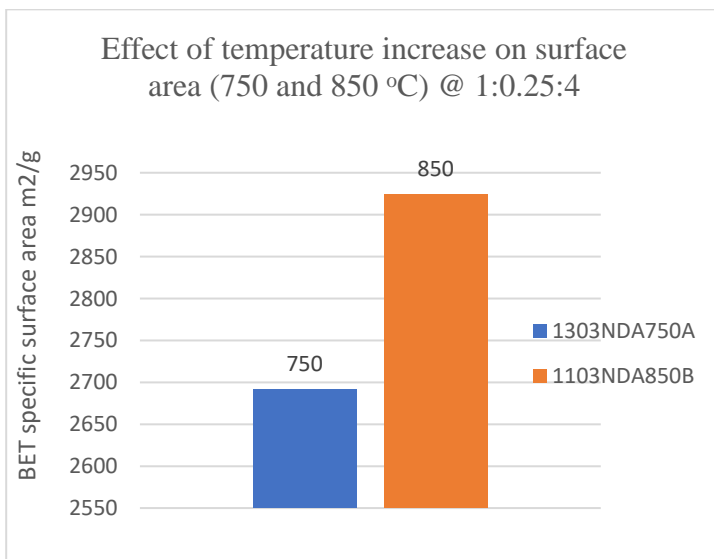

Figure 4. 10 Effect of temperature increase at 1:0.25:4 (Al)

Considering samples 1303NDA750A and 1103NDA850B with identical ratios of Ac:Al:KOH (1:0.25:4) but at different temperature levels of 750 and 850 °C respectively, the specific surface area is seen to increase from 2692 m²/g to 2923 m²/g as the temperature increased.
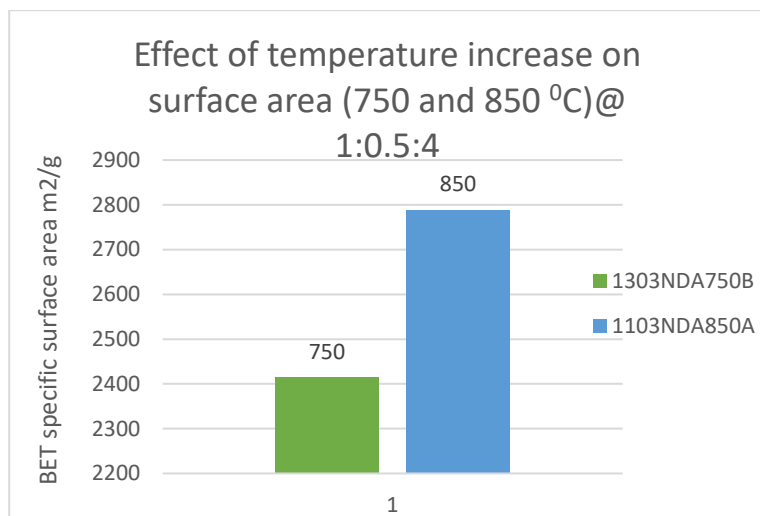
Figure 4. 11 Effect of temperature increase at 1:0.5:4 (Al)

Samples 1303NDA750B and 1103NDA850A consist of similar ratios of 1:0.5:4 but at different temperature levels also had similar trends of increase in specific surface area from 2415 m²/g to 2789 m²/g as the temperature increase from 750 to 850 °C.

Figure 4. 12 Effect of temperature increase at 1:1:4 (Al)

Samples 1104NDA750B and 1504NDA850A with similar ratios of 1:1:4 and temperature levels of 750 and 850 °C concurred with the pattern of increase in specific surface area as the temperature increased. The specific surface area increased from 1299 m²/g to 1564 m²/g.
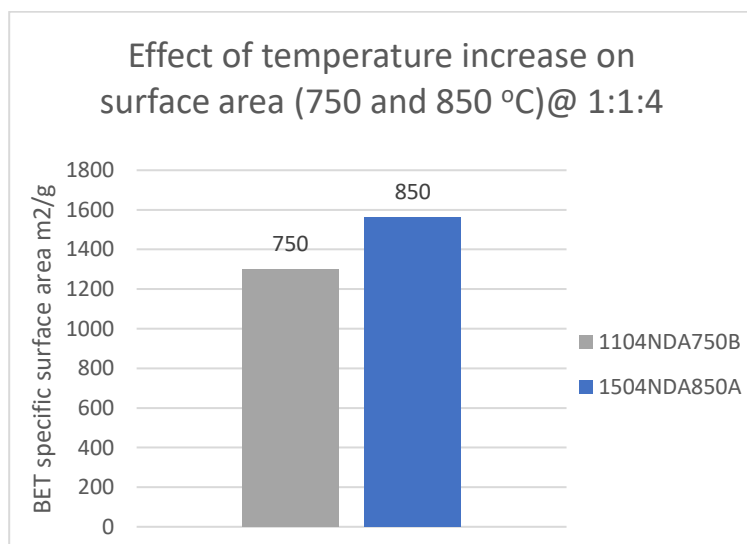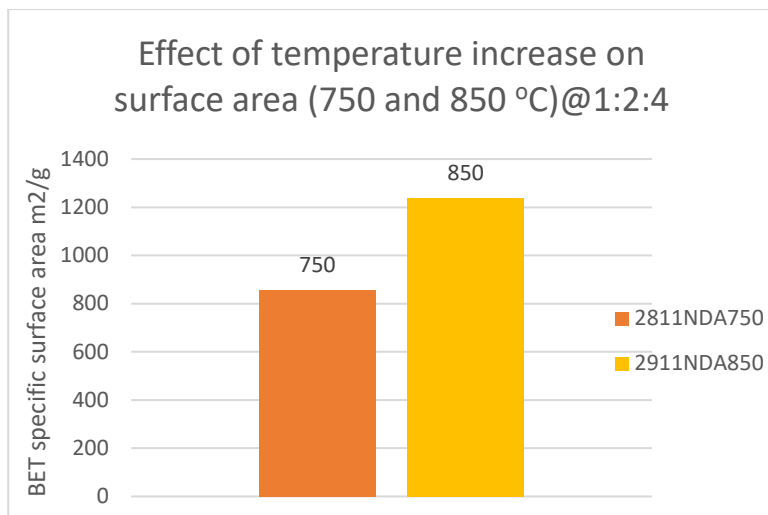
Figure 4. 13 Effect of temperature increase at 1:2:4 (Al)

Samples 2811NDA750 and 2911NDA850 were produced with identical ratios of 1:2:4 but different temperature levels of 750 ℃ and 850 ℃ also recorded an increase in the specific surface area from 856 m^2/g to 1237 m^2/g respectively.

The graphs and charts show that there exists a significant trend of higher surface areas as the temperature increases from 750 ℃ to 850 ℃. 850 ℃ is the ideal temperature at any condition to achieve a high surface area. This is as observed from the different ratios studied 1:0.25:4, 1:0.5:4, 1:1:4 and 1:2:4. Irrespective of the additive ratios, the difference in specific surface area fell in the range of about 300 m^2/g when comparing the two temperature levels at 750 ℃ and 850 ℃ for the different additive ratios considered. It can be concluded that the gaseous portions of the wood char and oxygen containing compounds were significantly burnt off more extensively as the activation temperature increased from 750 ℃ to 850 ℃. The increased release of volatiles present with increasing temperature can also be attributed to improved surface area[95].

For the NDA with the copper samples

In similar form as the experiment for the NDA with Al samples, two different temperature levels were also considered and studied to investigate the effect of increase in temperature on the specific surface area.

Char:Cu:KOH ratio	Sample ID	Temperature °C	BET Specific surface area (m²/g)
1:0.25:4	2504NDA750B	750	2636
	2404NDA850B	850	2954

Char:Cu:KOH ratio	Sample ID	Temperature °C	BET Specific surface area (m²/g)
1:0.5:4	2504NDA750A	750	3350
	2404NDA850A	850	2925

Char:Cu:KOH ratio	Sample ID	Temperature °C	BET Specific surface area (m²/g)
1:1:4	1505NDA750A	750	2524
	0905NDA850A	850	3204

Char:Cu:KOH ratio	Sample ID	Temperature °C	BET Specific surface area (m²/g)
1:2:4	2005NDA750B	750	1936
	2105NDA850A	850	2295

Table 4. 14 (a-d) Effect of increase in temperature on specific surface area at different additive concentrations (Cu)
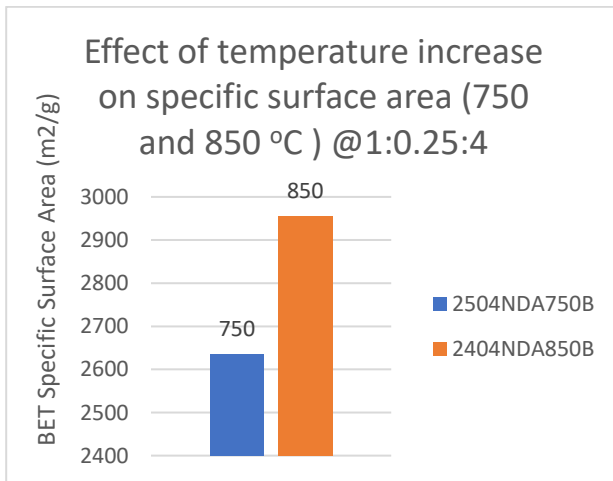
Figure 4. 14 Effect of temperature increase at 1:0.25:4 (Cu)

Samples 2504NDA750B and 2404NDA850B were produced at identical ratios of 1:0.25:4 using Copper as the additive but different temperature levels of 750 ºC and 850 ºC. The specific surface area was seen to increase from 2636 m^2/g to 2953 m^2/g as the temperature increased. This value was closely related to the figures obtained at the same ratio while using the Al additive.
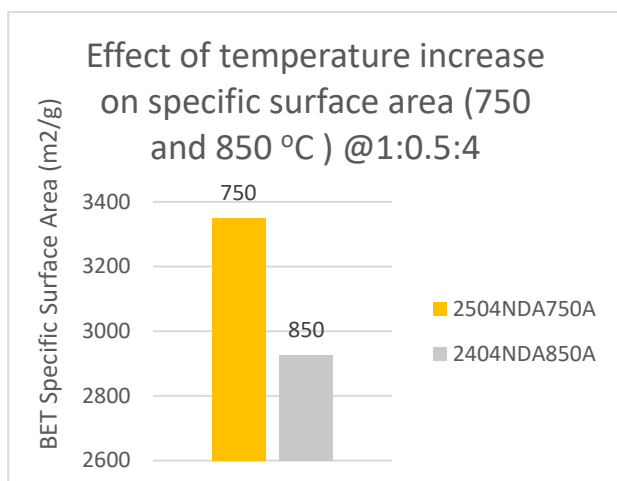
Figure 4. 15 Effect of temperature increase at 1:0.5:4 (Cu)

Samples 2504NDA750A and Samples 2404NDA850A were produced at 750 ºC and 850 ºC respectively at similar additive ratio. The surface area was seen to decrease from 3350 m^2/g to 2924 m^2/g as the temperature increased from 750 ºC to 850 ºC. This marked a difference in the trend being observed seeing that the additive concentration of 0.5 was responsible for catalysing the decomposition of the KOH into the potassium metal and thereby bringing about more activation/ removal of oxygen containing compounds at 750 ºC compared to 850 ºC.

Figure 4. 16 Effect of temperature increase at 1:1:4

Figure 4.16   Effect of temperature increase at 1:1:4

Samples 1505NDA750A and 0905NDA850A produced at 1:1:4 had specific surface areas of 2523 m^2/g and 3203 m^2/g. This conformed with the trend of increasing surface area with increase in temperature.

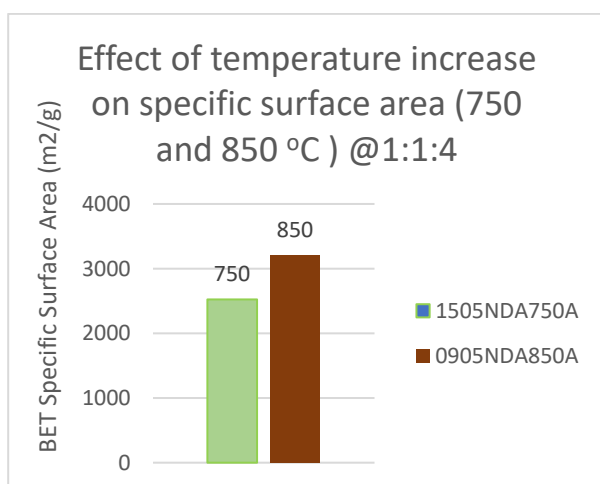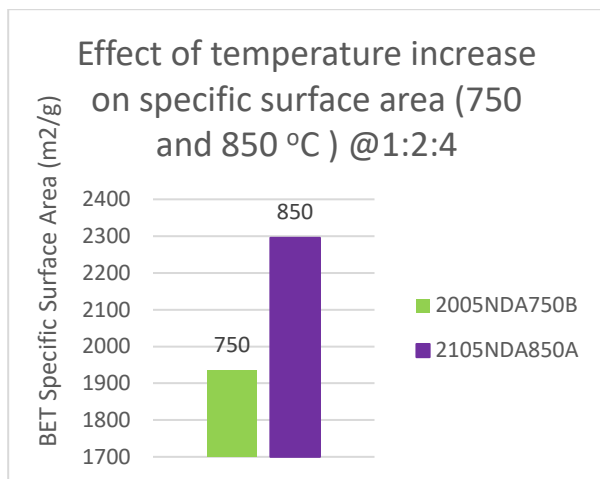*Figure 4. 17 Effect of temperature increase at 1:2:4*

Samples 2005NDA750B and 2105NDA850A having identical ratios of 1:2:4 but at different temperatures resulted in a specific surface area of 1936 and 2295 m^2/g respectively. The surface area was seen to increase with increase in temperature

The samples produced using the Copper additive at the different ratios exhibited an increasing trend of specific surface area with increase in temperature. The only exception was at 1:0.5:4 which showed an opposite trend of 750 ^{o}C being significantly higher than 850 ^{o}C. This highlighted a point at which the catalytic effect of the additive kicked in thus highlighting the optimum intensity at this ratio. The enhancement of the decomposition of Potassium containing compounds (Potassium Carbonates and Oxides intercalated in the framework) into Potassium metal which sublimates or partakes in various interactions which surface functional on the carbon atom takes place at this particular intensity. This unstable sublimated potassium metal compounds form catalytic active sites leading to increased gasification of the carbon and subsequently higher surface areas than normal[110, 111].

4.3.4   Effect of Increase in KOH Impregnation Ratio on Specific Surface Area

The impregnation ratio of KOH was kept constant at two different levels (Char:KOH) of 1:2 and 1:4. A mix between the levels varied for both the additive added and the ratio in the blank samples are presented in Table 4.4a-d. Samples with identical conditions of temperature and amount of additive added but with different amounts of KOH ratio were compared to study the effect of the various impregnation ratios on the surface area.

Temperature °C	Sample ID	Char:Al:KOH ratio	BET Specific surface area (m²/g)
750	1104NDA750A	1:1:2	818
	1104NDA750B	1:1:4	1299

Temperature °C	Sample ID	Char:Al:KOH ratio	BET Specific surface area (m²/g)
850	1801NDA850	1:1:2	661
	2911NDA850	1:1:4	1237

Temperature °C	Sample ID	Char:Al:KOH ratio	BET Specific surface area (m²/g)
750	1004BL750A	1:2	2040
	1004BL750B	1:4	2775

Temperature °C	Sample ID	Char:KOH ratio	BET Specific surface area (m²/g)
850	2203BL850A	1:2	2336
	2203BL850B	1:4	3083

Table 4. 15 (a-d) Effect of increase of impregnation ratio at different temperatures (Al) and Blank experiments
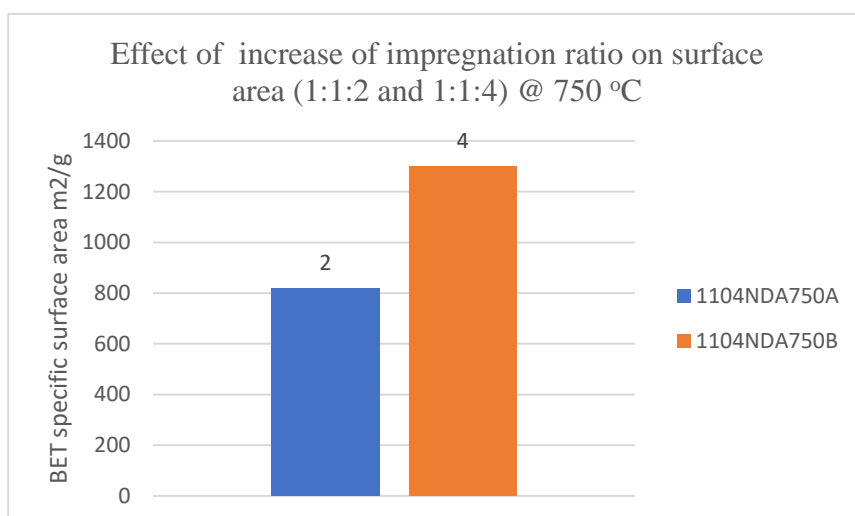
Figure 4. 18 Effect of increase of impregnation ratio at 750 ºC (Al)

Considering the case of samples 1104NDA750A and 1104NDA750B produced at similar temperatures but different impregnation ratios of 1.1:2 and 1.1:4, the surface area was seen to increase from 818 m²/g to 1299 m²/g as the impregnation ratio of KOH increase from 2 to 4.
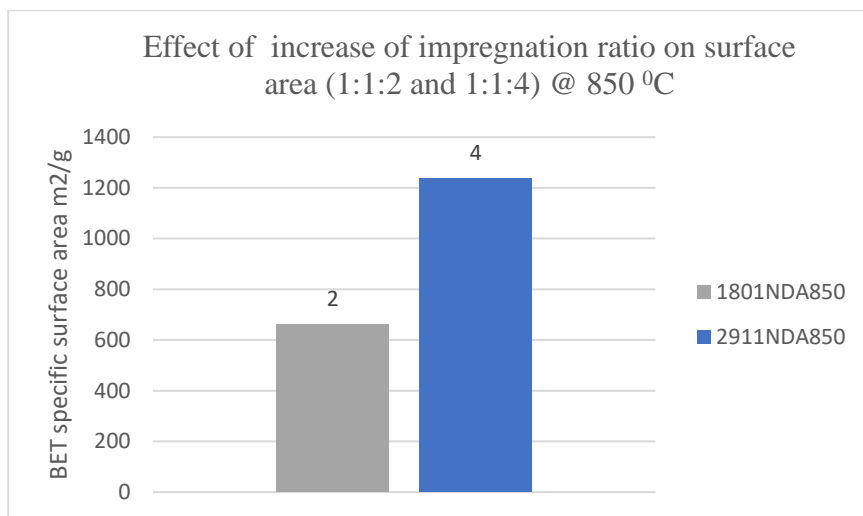
Figure 4. 19 Effect of increase of impregnation ratio at 850 °C (Al)

Figure 4.19 shows the increase in surface area with increase in impregnation ratio observed in samples 1801NDA850 and 2911NDA850 with impregnation ratios of 1:1:2 and 1:1:4. The surface area increased from 661 m²/g to 1237 m²/g as the impregnation ratio of KOH increased from 2 to 4.
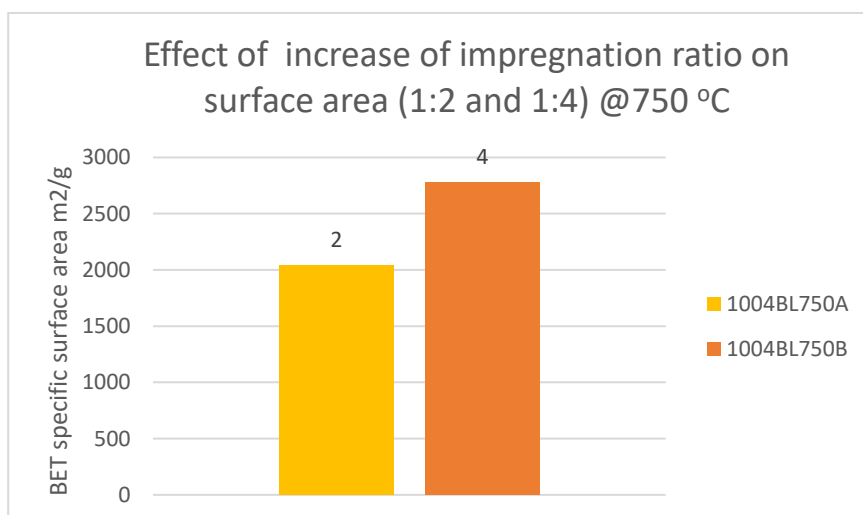
Figure 4. 20 Effect of increase of impregnation ratio at 750 °C (Blank)

Samples 1004Bl750A and 1004BL750B which were blank experiments produced with impregnation ratios of 2 and 4 without any additive, showed an increased in specific surface area with increase in impregnation ratio. The specific surface area increased from 2040 m²/g to 2775 m²/g.
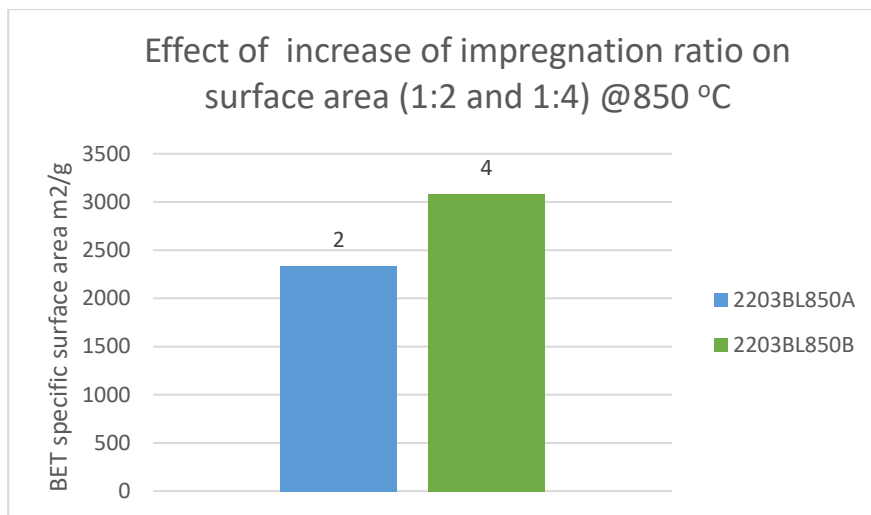
Figure 4. 21 Effect of increase of impregnation ratio at 850 °C (Blank)

Samples 2203BL850A and 2203BL850B are blank experiments produced at 850 ºC with impregnation ratios of 2 and 4. The surface area increased from 2336 m²/g to 3083 m²/g as the impregnation ration increased from 2 to 4.

The Blank experiment and selected ratios of NDA samples with Al all display and increase in specific surface area with increase in impregnation ratio of KOH. The KOH was responsible for chemical activation of the wood char via oxidation. The attack on some portions of the carbon thereby converting into carbon oxides creates the porous nature and the large surface area. Increase on the amount of KOH used via the impregnation ratio would increase this effect and is thus confirmed by the findings above. The Al additive did not influence this trend occurring as similar trend was observed in the blank experiment and reported also in literature. An impregnation ratio of 4 was observed to be the condition suitable for higher surface areas during activation irrespective of the amount of additive added.

For the NDA with Cu samples

Temperature °C	Sample ID	AC:Al:KOH ratio	BET Specific surface area (m²/g)
850	0905NDA850B	1:1:2	2056
	0905NDA850A	1:1:4	3204

Temperature °C	Sample ID	AC:Al:KOH ratio	BET Specific surface area (m²/g)
750	1505NDA750B	1:1:2	1724

	1505NDA750A	1:1:4	2524

Temperature °C	Sample ID	AC:Al:KOH ratio	BET Specific surface area (m²/g)
850	2105NDA750B	1:2:2	1888
	2105NDA750A	1:2:4	2295

Temperature °C	Sample ID	AC:KOH ratio	BET Specific surface area (m²/g)
750	2005NDA750A	1:2:2	2336
	2005NDA750B	1:2:4	3083

Table 4. 16 Effect of increase in impregnation ratio at different temperatures (Cu)
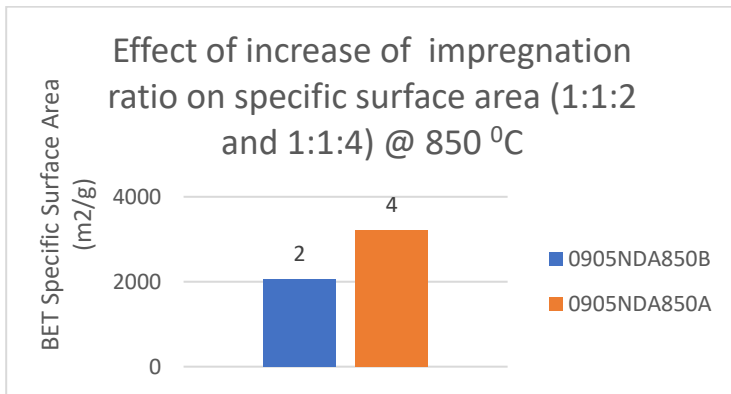
Figure 4. 22 Effect of increase of impregnation ratio at 850 ºC (Cu)

Samples 0905NDA850B and 0905NDA850A show an increase in the surface area as the impregnation ratio increases from 1:1:2 to 1:1:4. The surface area increased from 2056 m²/g to 3203 m²/g.
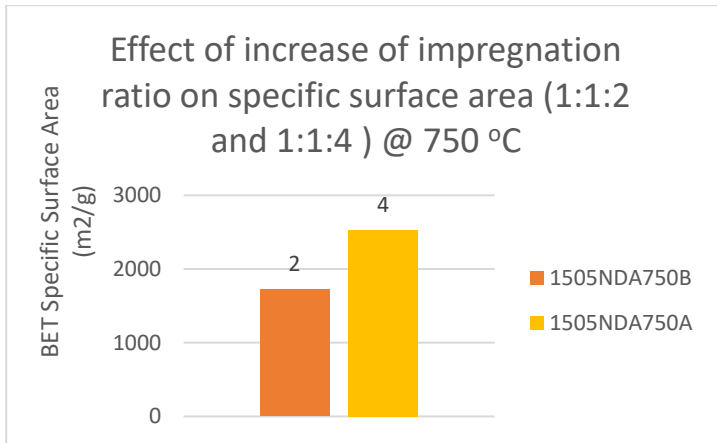
Figure 4. 23 Effect of increase in impregnation ratio at 750 ℃ (Cu)

Figure 4.23 shows samples 1505NDA750(B and 1505NDA750A with impregnation ratios of 1:1:2 and 1:1:4 produced at 750 ℃. The surface area increased from 1724 m²/g to 2523 m²/g as the impregnation ratio increased from 2 to 4

Figure 4. 24 Effect of increase in impregnation ratio at 850 ℃ (Cu) (additive ratio =2)

In samples 2105NDA850B and 2105NDA850A shown in Figure 4.24 having ratios of 1:2:2 and 1:2:4 respectively produced at 850 ℃, the specific surface increased from 1888 m²/g to 2295 m²/g as the impregnation ratio increased from 2 to 4.
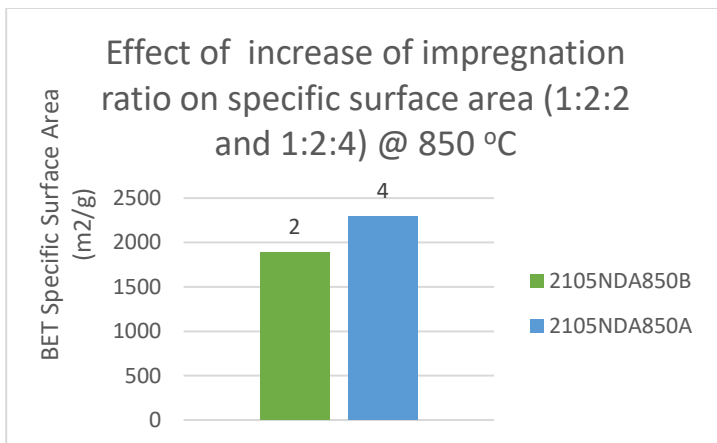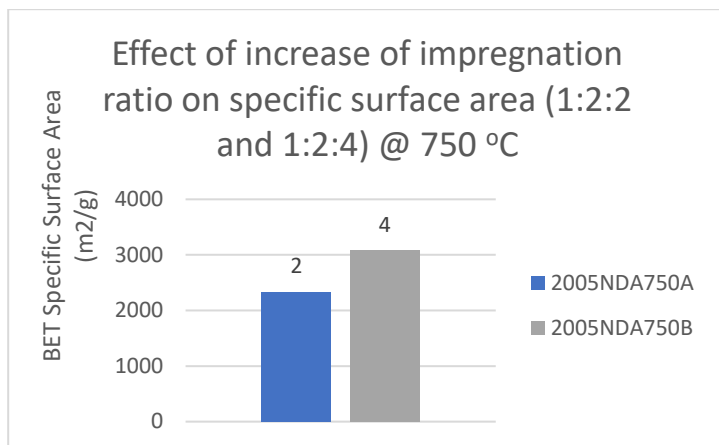
Figure 4. 25 Effect of increase in impregnation ratio at 750 °C (Cu) (additive ratio =2)

In Samples 2005NDA750A and 2005NDA750B shown in Figure 4.25 having ratios of 1:2:2 and 1:2:4 respectively produced at 750 °C, the specific surface area increased from 1050 m²/g to 1936 m²/g as the impregnation ratio increased from 2 to 4.

The samples highlighted above all displayed an increase in the surface area as the impregnation ratio increased. Samples activated using an impregnation ratio of 4 showed more extensive activation evidenced by the large increase in surface area in comparison to impregnation ratios of 2. Similar findings have been documented by a large variety of researchers[93, 95, 102]. Increase in the impregnation ratio was highlighted as the factor responsible for increased CO_2 formation leading to more gasification of the carbon atoms and dissolution of the ash by caustic digestion[112]. The reduced ash contented was reported to 'result in higher values of measured surface and pore volume since the ash which had negligible surface area and volume in comparison to the microporous carbon would be removed'[95].

4.3.5   Effect of Increase in Additive Intensity/Ratio on Specific Surface Area

The additive ratio was varied using intensities of 0.25, 0.5, 1 and 2. The four different ratios used were in combination with the different temperature levels and the different impregnation ratios. They are shown in Table 4.5a, b and illustrated in Figure 4.5a,b.

Temperature °C	Sample ID	AC:KOH ratio	BET Specific surface area (m²/g)
750	1303NDA750A	1:0.25:4	2692
	1303NDA750B	1:0.5:4	2415
	1104NDA750B	1:1:4	1299
	2811NDA750	1:2:4	866

72

Temperature °C	Sample ID	AC:KOH ratio	BET Specific surface area (m²/g)
850	1103NDA750A	1:0.25:4	2924
	1103NDA750B	1:0.5:4	2789
	1504NDA750B	1:1:4	1564
	2911NDA750	1:2:4	1237

Table 4. 17 (a-b) Effect of increase in additive ratio on surface area (Al) at different temperatures
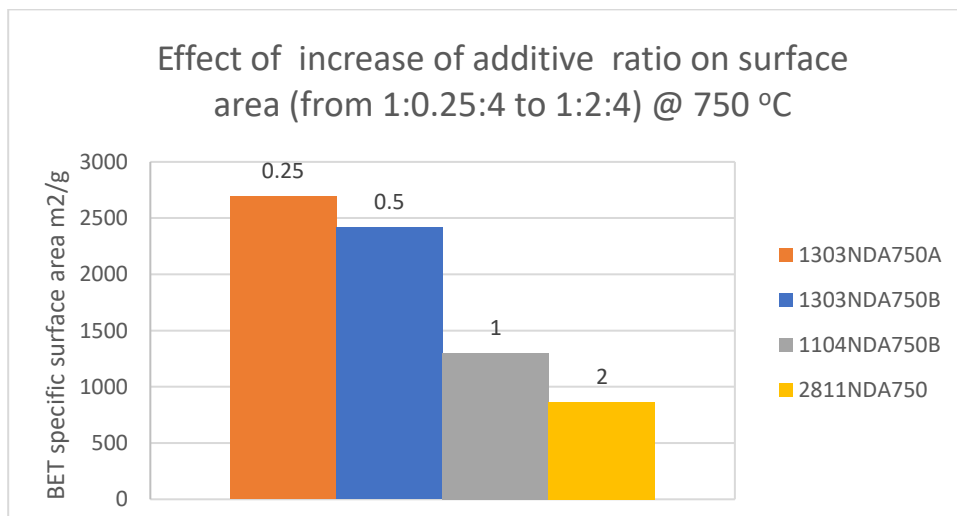
Figure 4. 26 Effect of increase in Al additive ratio at 750 ºC

Figure 4.26 shows the increase in additive ratio considering different samples with ratios of 1:0.25:4, 1:0.5:4, 1:1:4 and 1:2:4 as indicated in the chart. The surface area was seen to decrease from 2692 m²/g to 856 m²/g as the additive ratio increased from 0.25 to 2.
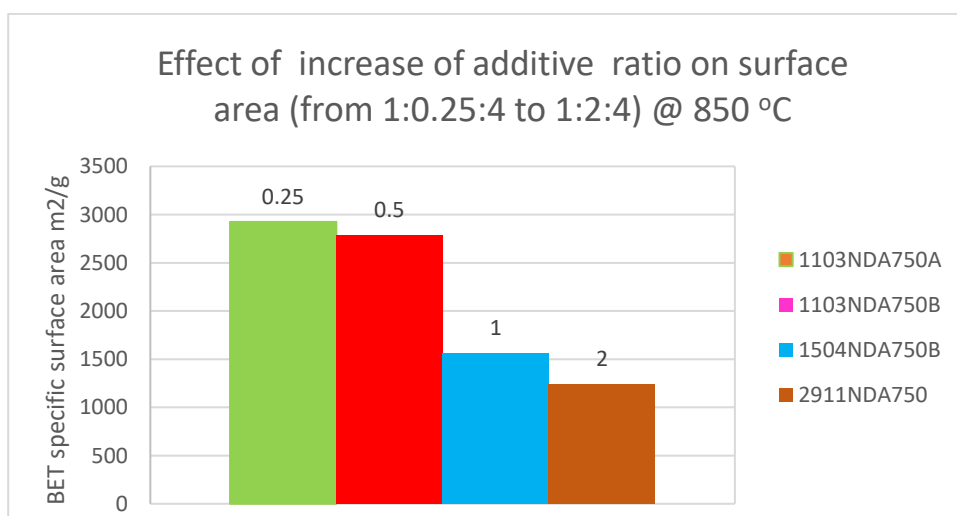
Figure 4. 27 Effect of increase in Al additive ratio at 850 °C

The decrease in specific surface area as additive ratio increases is also highlighted in Figure 4.27 with samples produced at 850 ºC. the specific surface area decreased from 2924 to 1237 m²/g as the impregnation ratio increased from 0.25 to 2.

From the above observations, it is evident that for NDA samples with the Al additive, increasing the additive ratio slightly hinders the activation of the wood char. A reason postulated for this would be the reduction of the surfaces of the carbon in contact with the KOH during the activation process. This additive present would cover some of the pore sites which would have been exposed to further activation especially during the heat treatment. The Al additive optimum amount would be the lowest concentration of 0.25 since higher amounts hindered the more extensive activation which would have occurred.

For the NDA with Cu samples

Temperature °C	Sample ID	AC:KOH ratio	BET Specific surface area (m²/g)
750	2504NDA750B	1:0.25:4	2636
	2504NDA750A	1:0.5:4	3350
	1504NDA750A	1:1:4	2524
	2005NDA750B	1:2:4	1936

Temperature °C	Sample ID	AC:KOH ratio	BET Specific surface area (m²/g)
850	2404NDA850B	1:0.25:4	2954
	2404NDA850A	1:0.5:4	2925
	0905NDA850A	1:1:4	3203
	2105NDA850A	1:2:4	2295

Table 4. 18 Effect of increase in Cu additive ratio on surface area at different temperatures
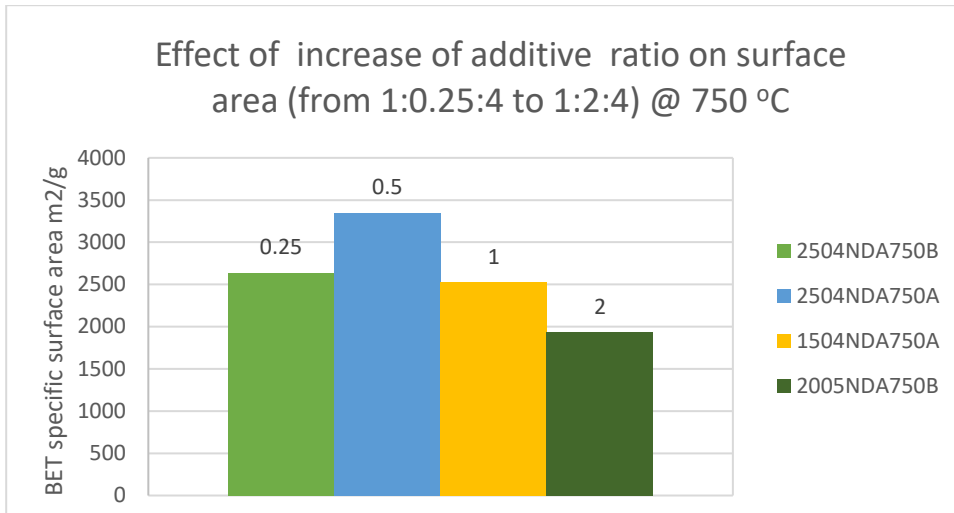
Figure 4. 28 Effect of increase in Cu additive ratio at 750 ºC

The effect of increase in Cu additive ratio from 1:0.25:4 to 1:2:4 at 750 ºC is shown in Figure 4.28. The specific surface area is seen to decrease from 2636 m²/g to 1936 m²/g as the additive ratio increased from 0.25 to 2. An exception was seen at 1:0.5:4 which showed the highest specific surface area of 3350 m²/g , a deviation from the trend observed. This highlighted the optimum additive intensity which would effectively catalyse the decomposition of the KOH into Potassium metal and extensively promote the further activation of the wood char at this temperature.
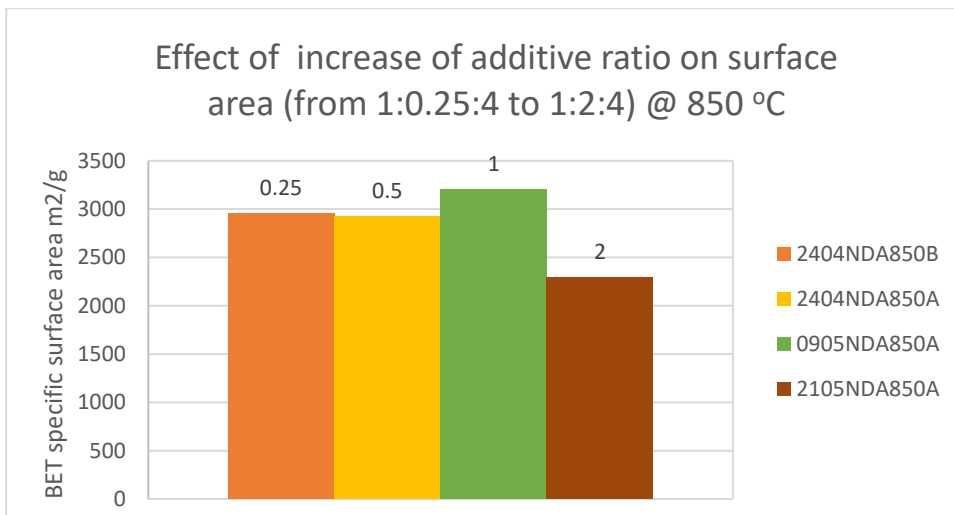
Figure 4. 29 Effect of increase in Cu additive ratio at 850 ºC

The effect of increase in Cu additive ratio from 1:0.25:4 to 1:2:4 at constant temperature of 850 ºC is shown in Figure 4.29. The surface area decreased from 2953 m²/g to 2295 m²/g as the additive ratio increased from 0.25 to 2 with an exception of sample 0905NDA850A (1:1:4) which had the highest specific surface area of 3203 m²/g. This also deviated from the pattern

and can be proposed as the optimum Cu additive intensity at 850 °C. The increase in surface area can also be explained by similar conclusions made in the previous section. A balance between the additive ratio, impregnation ratio and temperature are needed as extensive activation leading to collapse of pores and decrease in specific surface area would occur if any of these factors are not in the right proportion. The appropriate balance has been discovered by the above mentioned additive intensity seeing that at 750 °C, the additive intensity at 0.5 was sufficient to promote decomposition of the potassium hydroxide and increase or decrease beyond this would either results in lesser specific surface area generated via the exfoliation or collapse of the structures due to extensive activation. This can also be used in the explanation of the trend at 850 °C with an optimum additive intensity of 1.

4.3 XRD CHARACTERIZATION.

X-ray diffraction analysis was performed on the activated carbon samples to investigate the effectiveness of the washing and ensure that the surface area obtained was by the wood precursor alone not via contribution of the metal oxides which could be formed. Taking a case note of Alumina which could possess very high surface area. Figure 4.30 shows the results obtained from the XRD analysis of selected samples with high surface areas.
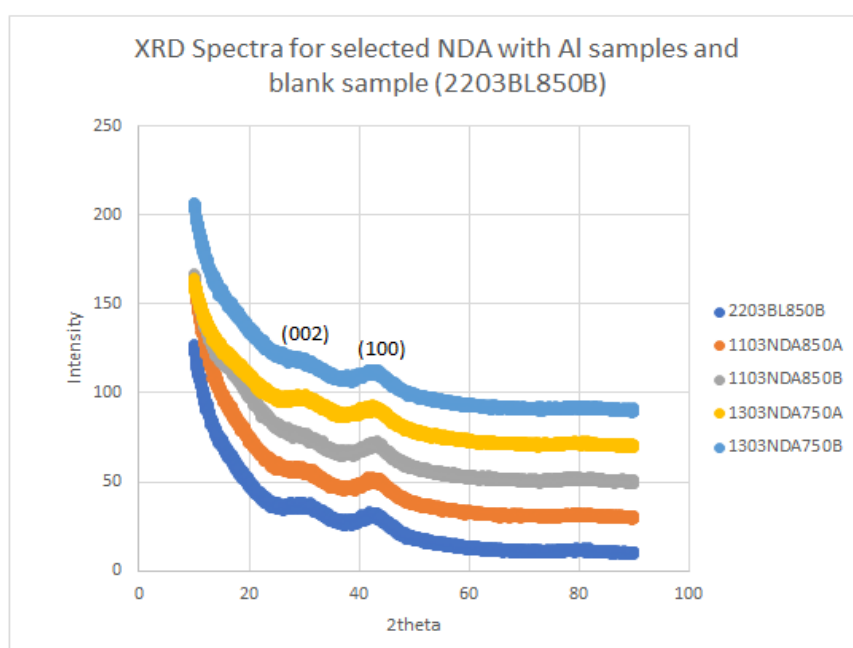
Figure 4. 30 XRD spectra for selected NDA with Al samples and blank Sample (2203BL850B)

XRD analysis was also conducted on the samples produced using copper additive. Figure 4.31 shows the spectra obtained for selected samples with very high specific surface area in order to confirm that the surface area generated was purely from the activated carbon and to confirm the efficiency of the washing step in the removal of the Copper additive from the samples after activation.
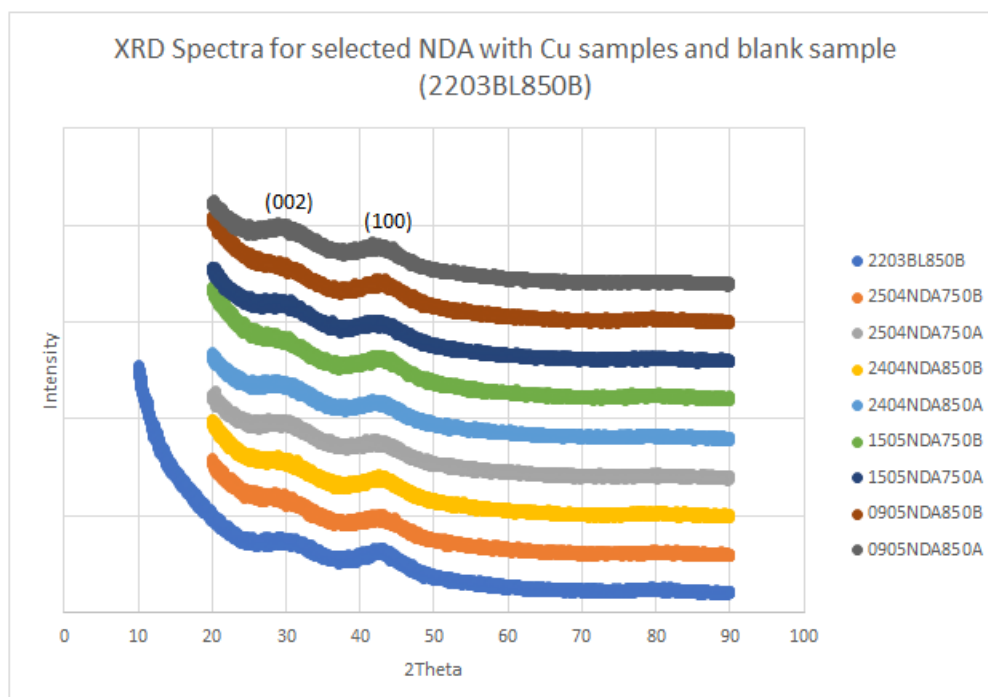
Figure 4. 31 XRD Spectra for selected NDA with Cu samples and blank sample (2203BL850B)

Identical peaks at theta values of 26^0 and 42^0 corresponding to carbon as reported in several literature[113, 114] were observed in the two different sets of experiment with the Al and Cu additive and also with the Blank sample 2203BL850B identified by the spectra starting from 10^0. Many authors have attributed the peaks present to the onset of graphitization which began at temperatures above 750 $^{\circ}$C and a mix between amorphous carbon and the onset on graphitization with low crystallinity[115]. Similar peaks were observed in the works of Sivachidambaram et al [113] with the peaks prominent at 26^0 and 42^0 corresponding to the (002) and (100) graphic plane [114, 115], and thus explaining why these samples with the intense peaks, would have excellent conductivity required for its application in supercapacitor fabrication (with this conductivities tagged by the authors as 'in plane conductivity required for

electrochemical application')[115]. According to Kalpana et al[109] ,the broad (002) peaks between 20° and 30° are an indication of possible 'small domains of coherent and parallel stacking of graphene sheets'. The XRD spectra obtained also confirms that the washing step was effective in the complete removal of the metal additive added during the non-destructive activation process. This was realized by comparing spectra of samples which had very low surface area due to high additive ratios of 2 as seen in sample 200NDA850B (Cu additive) and 1801NDA850 (Al additive) shown in Figure 4.32 with the spectra obtained for the blank sample without the additive 2203BL850B. The concentration of KOH used in the washing step had to be altered several times due to the initial XRD and ash content analysis indicating high presence of several peaks of Alumina and other unidentified complexes which were formed during the reaction. This challenge was solved via improvement of the washing step as explained in the earlier paragraphs.
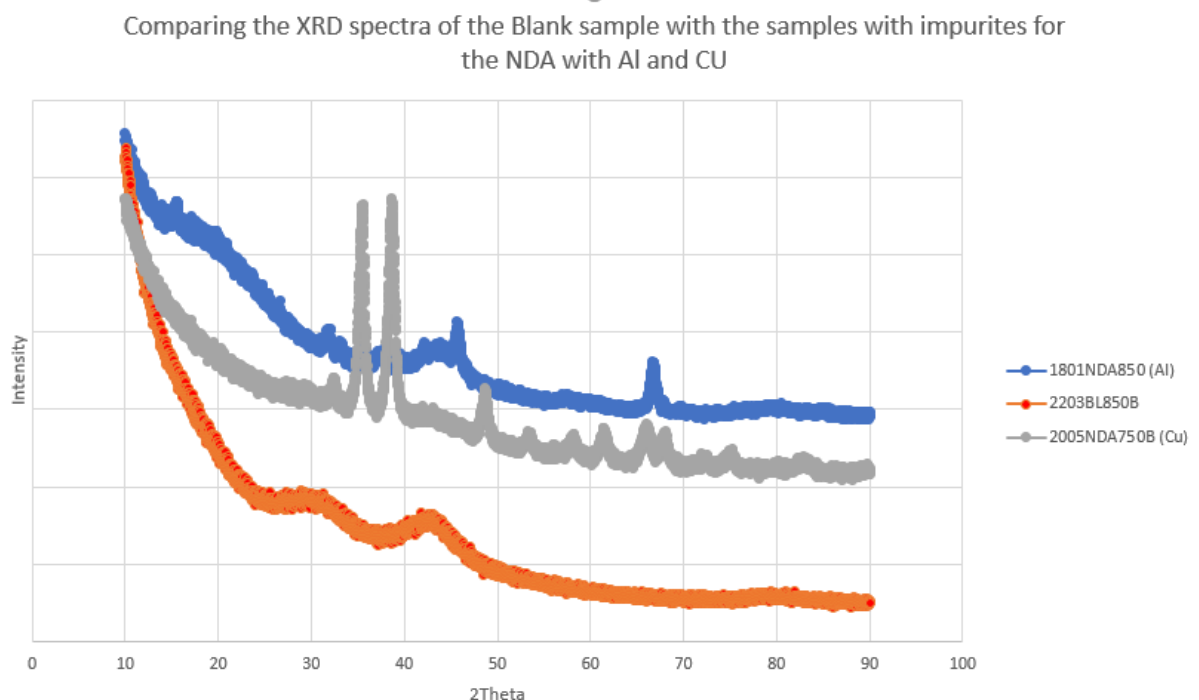
Figure 4. 32 Comparing the XRD spectra of the Blank sample with the samples with impurities for the NDA with Al and Cu

4.4   SEM/EDX CHARACTERIZATION

The large surface area of activated carbon has been widely reported in so many publications. SEM analysis was carried out in addition to EDX to view the surface morphology of the activated carbon and to see the effect of the additive on the surface of the activated carbon

samples. A characteristic honeycomb structure was prominent in all the samples analysed with Figure 4.33 displaying the SEM image obtained for the blank experiment 2203BL850B with no additive added. Similar honeycomb structures in activated carbon were obtained by Sivachidambaram et al[113] which can be said to be a visible evidence of activation which occurred on the carbon citing the extensive number of pores on the images. Dutta et al[116] also made similar findings of honeycomb structured activated carbon upon analysis of *Acacia auriculiformis* scrap wood.

2 Apr 2019	10 µm*	Mag = 1.09 K X	Brightness = 51.6 %	Aperture Size = 30.00 µm	Scan Speed = 6
11:00:16		Pixel Size = 338.00 nm	Contrast = 27.6 %	EHT = 10.00 kV	Signal A = SE2
2203_BL850A_003.tif				WD = 14.0 mm	
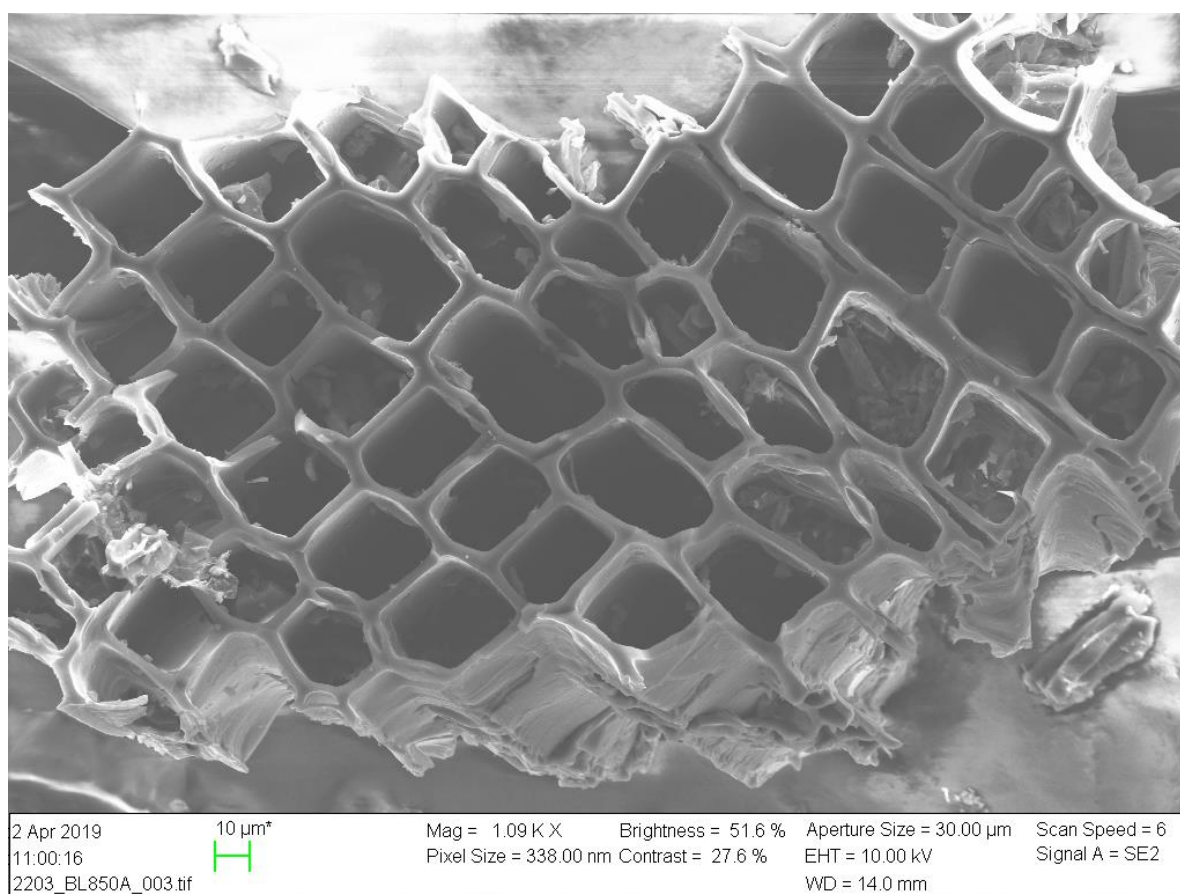
Figure 4. 33 SEM image of Blank experiment 2203BL850A with no additive

The SEM images shown in figure indicate the presence of honeycomb structure typical for activated carbon. The large pores and well developed pore network in some samples relate to the large surface area which was obtained during the BET analysis. The absence of aluminium was also clearly visible due to the absence of the characteristic shine caused by the presence of

aluminium when the incident electrons are beamed on particles containing this aluminium.
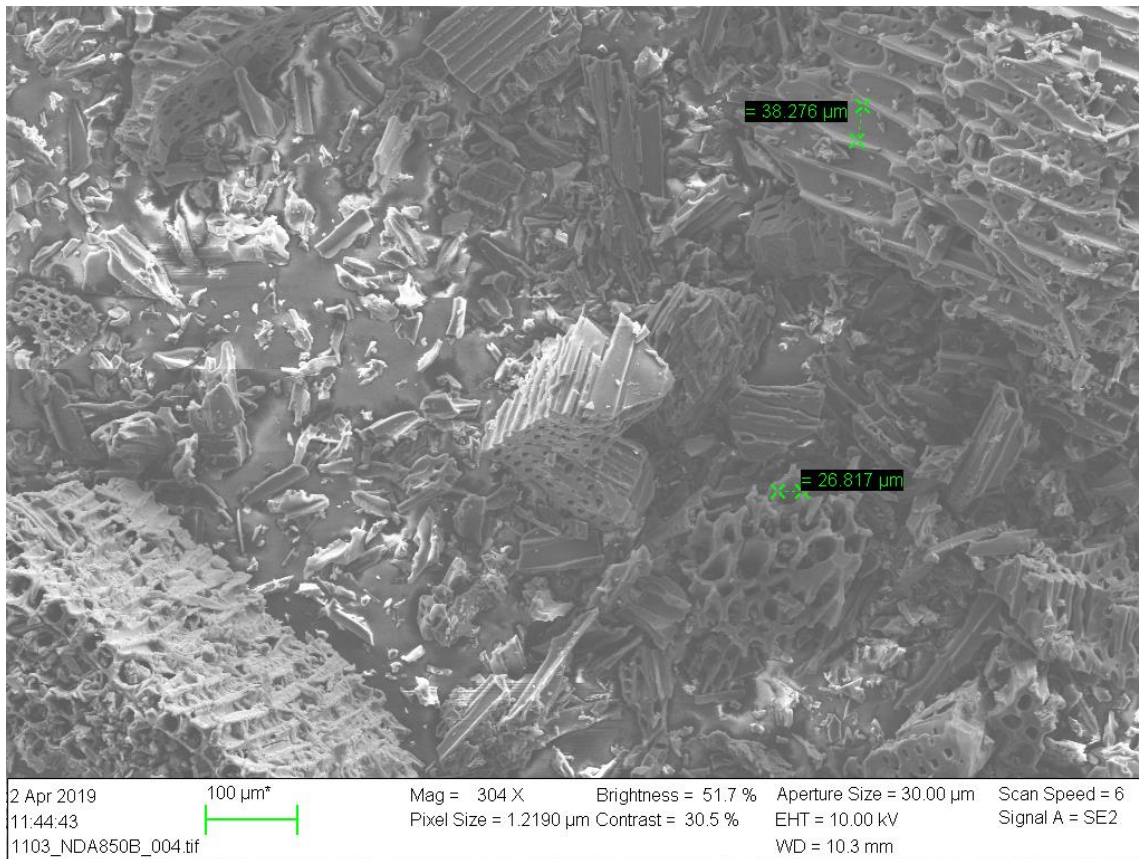
Figure 4. 34 SEM images of sample 1103NDA850B

A large distribution of wall thickness could be observed on both the blank samples and NDA samples. Similarities were also present with structures having thick walls present in both the blank samples and NDA samples shown in Figure 4.35
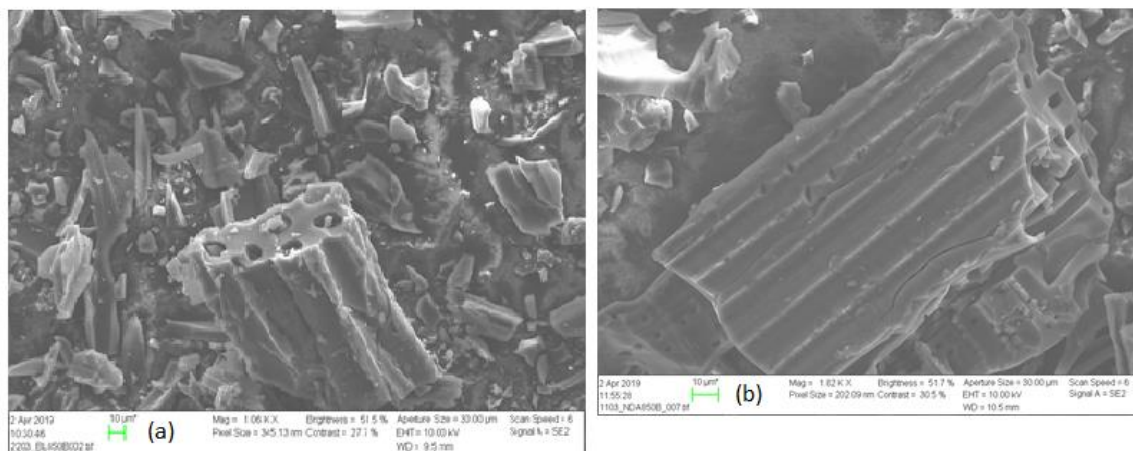
Figure 4. 35 Comparing the thickness of the walls between a blank sample (a) and an NDA sample (b) at identical conditions of 850 °C and impregnation ratio 1:4

No clear difference could be observed when comparing the images obtained from the Blank experiment and the non-destructive activated carbon. They both possessed varied structures with well-defined honeycomb structures and in some cases collapsed pores. Some other selected larger chunks also had thicker walls compared to cases with thinner walls and larger pores. This showed that there existed a wide distribution between mesopores and micropores .
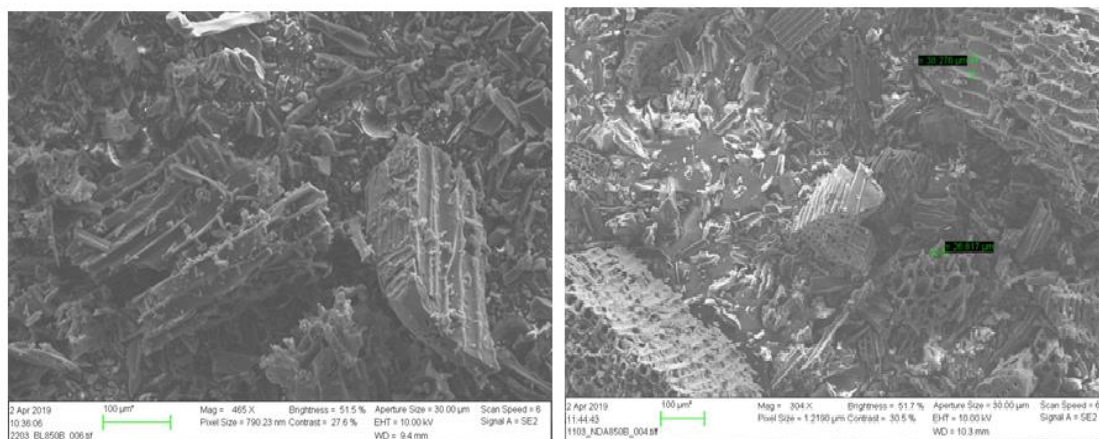
Figure 4. 36 Comparing a blank sample and an NDA sample

The decrease in surface area observed in samples which had higher ratios of Aluminium could be explained by the blockage of the pores of the activated carbon by the Aluminium cluster formed. The improper washing of the activated samples with such high ratios would lead to cases where the clusters is bonded unto the surface of the activated carbon shown in Figure 4.37. Electrochemical tests carried out on the samples with such clusters showed that they had very low electrochemical capabilities. This further led to the improvement of the washing step and selection of lower ratios of additive added in order to decrease the effect of the additive on the surface area of the Activated carbon.
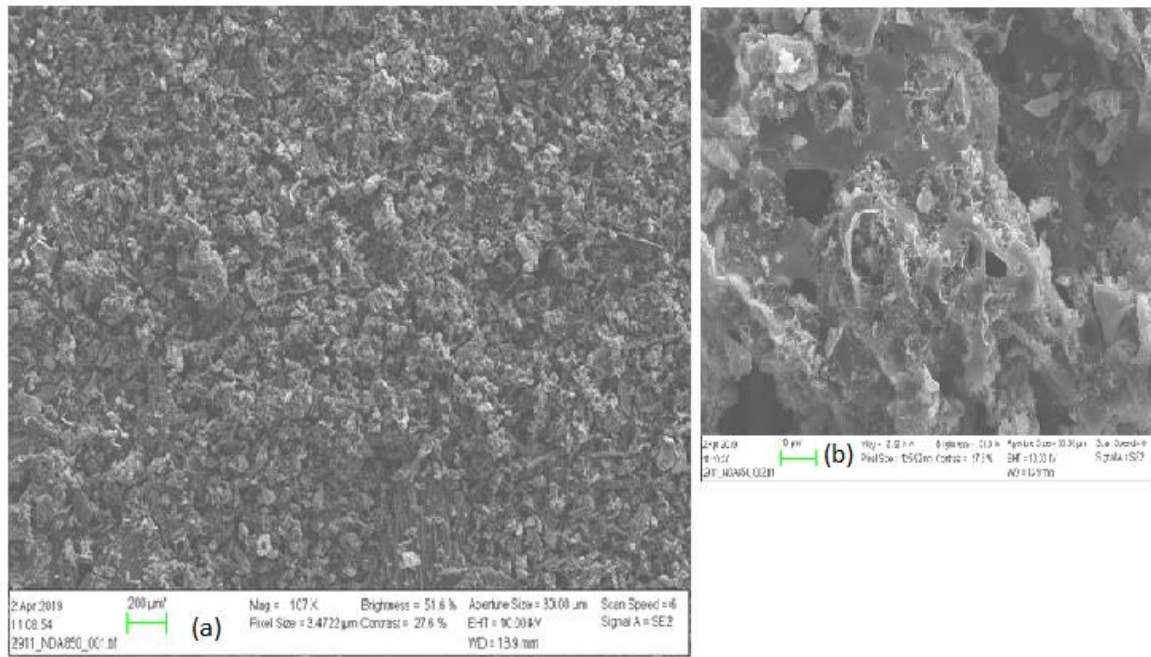
Figure 4. 37 Clusters present in an Improperly washed NDA sample with high Al ratio
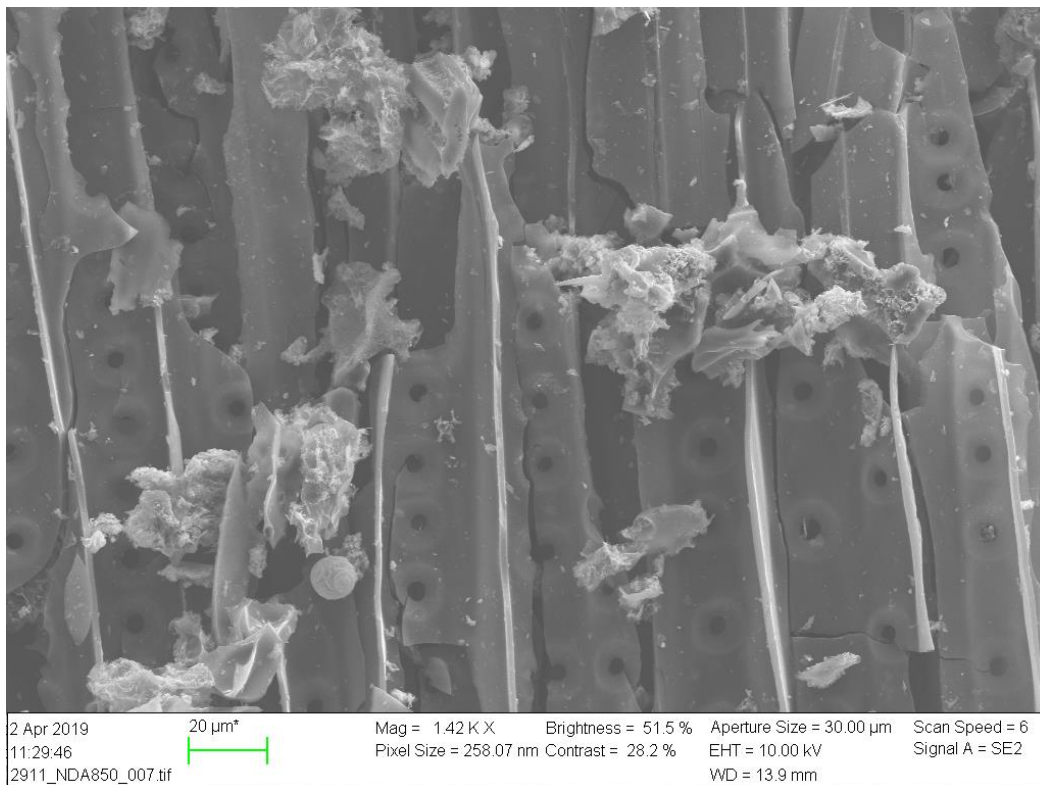
Figure 4. 38 Improperly washed samples with high Al additive ratio

Despite the fact that several beautiful structures were obtained from the SEM analysis, a lot of valuable information concerning morphology differences between the blank and non-destructively activated carbon couldn't be obtained from these images alone. A reason for this

would be the washing step which eliminated all traces of the Aluminium additive present thus rendering the samples in similar form. Crushing of the samples during the activation process while mixing the char and the KOH process would be responsible for some of the collapsed structures, this in addition to the vigorous washing step.

4.4.1 Elemental Analysis

Elemental analysis using EDS was conducted a number of samples with during the SEM analysis. The best results from the blank experiment 2203BL850B as well as Samples 1103NDA850B with the highest surface area for the NDA samples with Al is shown in Figure 4.39 and 4.40
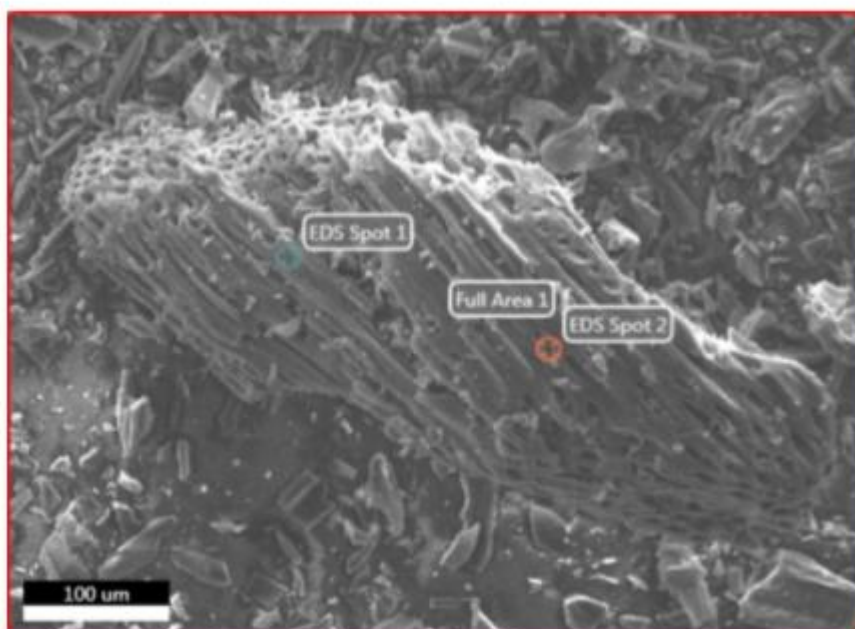
Figure 4. 39 Spots Analysed during EDS on blank experiment 2203BL850B

Element	Weight %	Atomic %	Net Int.	Error %	Kratio	Z	A	F
C K	99.65	99.74	830.57	2.27	0.9950	1.0002	0.9983	1.0000
O K	0.35	0.26	2.20	64.72	0.0010	0.9430	0.3058	1.0000

Element	Weight %	Atomic %	Net Int.	Error %	Kratio	Z	A	F
C K	99.54	99.66	988.21	2.24	0.9935	1.0003	0.9978	1.0000
O K	0.46	0.34	3.45	44.28	0.0013	0.9431	0.3061	1.0000

Element	Weight %	Atomic %	Net Int.	Error %	Kratio	Z	A	F
C K	94.95	96.16	542.32	2.65	0.9290	1.0028	0.9757	1.0000
O K	5.05	3.84	23.37	13.29	0.0152	0.9455	0.3188	1.0000

Table 4. 19 (a-c) Elemental composition of different Spots on 2203BL850B and total area

The Blank sample 2203BL850B as expected had no impurities present. Carbon and oxygen were the only Elements present. High percentage of carbon of about 94% and oxygen of 5.05% was observed. The large amount of oxygen could be from the washing process and adsorption of oxygen from the air during the drying and cooling.

1103NDA850B
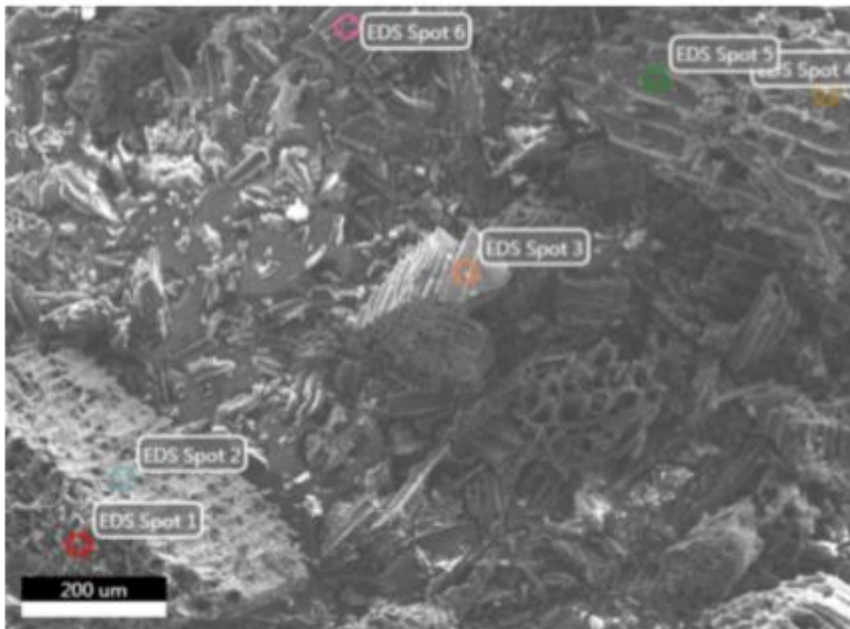
Figure 4. 40 Spots analysed on sample 1103NDA850B during EDS

Element	Weight %	Atomic %	Net Int.	Error %	Kratio	Z	A	F
C K	97.37	98.01	979.23	2.35	0.9617	1.0015	0.9862	1.0000
O K	2.63	1.99	19.51	14.87	0.0072	0.9442	0.2891	1.0000

Element	Weight %	Atomic %	Net Int.	Error %	Kratio	Z	A	F
C K	96.41	97.28	211.66	3.09	0.9479	1.0020	0.9812	1.0000
O K	3.59	2.72	5.89	23.70	0.0099	0.9447	0.2916	1.0000

Element	Weight %	Atomic %	Net Int.	Error %	Kratio	Z	A	F
C K	97.37	98.01	979.23	2.35	0.9617	1.0015	0.9862	1.0000
O K	2.63	1.99	19.51	14.87	0.0072	0.9442	0.2891	1.0000

Element	Weight %	Atomic %	Net Int.	Error %	Kratio	Z	A	F
C K	97.55	98.15	1201.79	2.30	0.9643	1.0014	0.9871	1.0000
O K	2.45	1.85	22.21	16.27	0.0067	0.9441	0.2886	1.0000

Element	Weight %	Atomic %	Net Int.	Error %	Kratio	Z	A	F
C K	96.68	97.48	795.18	2.46	0.9517	1.0019	0.9826	1.0000
O K	3.32	2.52	20.38	14.02	0.0091	0.9446	0.2909	1.0000

Element	Weight %	Atomic %	Net Int.	Error %	Kratio	Z	A	F
C K	97.61	98.19	1102.47	2.31	0.9651	1.0013	0.9874	1.0000
O K	2.39	1.81	19.89	16.49	0.0065	0.9441	0.2885	1.0000

Table 4. 20 (a-e) EDS for different spots on sample 1103NDA850B

The results showed that the sample was pure, and the additives were completely removed from the activated carbon. An average of 97% of Carbon and 3% of oxygen was found to be the constituent of most of the NDA samples produced with no metallic impurity present. This can also add to the conclusion that the washing step was effective in the removal of impurities from the activated carbon.

4.5 ELECTROCHEMICAL ANALYSIS

After the construction of the coin cells, a variety of tests were carried out to investigate properties such as specific capacitance, self-discharge as well as ohmic resistance. The result from the best samples of activated carbon was compared with those of the commercially available activated carbon. They are presented in Table 4.21.

Sample ID	Description	Specific capacitance @ 0.1mA	Specific capacitance @ 5mA	Self-discharge %
1103NDA850B	NDA with Al	129.88	165.08	96.14
YP80F20190424	Commercial AC	107.76	107.01	46.17
2203BL850B	Blank Experiment	164.58	177.34	70.57

Table 4. 21 Electrochemical testing of assembled coin cells

the activated carbon samples selected for electrochemical testing were the samples which had the highest surface area from the BET analysis. The blank samples as reported earlier had surface areas of about 3000 m²/g which the NDA samples with Aluminium had surface areas of about 2923 m²/g which. Initial assembly of the coin cells with the electrodes fabricated from this samples yielded very high specific capacitance of about 164.58 F/g for the blank samples and 130 F/g for the NDA samples with Aluminium. This value was very high compared to coin cells fabricated with commercial activated carbon available which was in a range of 91-107 F/g. although the values of specific capacitance were high, the self-discharge rates turned out to be very high compared which resulted in a new challenge. Investigating the efficiency of the washing step led to the examination of XRD results as well as EDS elemental analysis in addition to the ash content test conducted, all subsequently ruled out the effect of parasitic faradic reactions caused by the presence of metal impurities in the activated carbon. The assembly method and materials were considered but the outlined process has been quality checked severally with a large number of coin cells fabricated using similar technique while also recording a great deal of success and less instances of self-discharge. The only factor left to be explored was the existence of oxygen functional groups at the surface which has been reported as an agent responsible for high self-discharge in supercapacitors[46, 100]. Yoshida et al[45] and Pandolfo et al[46] documented that lower leakage currents are observed when the oxygen surface functionalities are removed by High temperature treatments in inert environments. Thus, the activated carbon samples were introduced into the furnace and thermal treated at 1000 °C for 1 hour which was a means of driving off oxygen functional groups which might have been present on the surface. The results are presented in the Table 4.22

Sample ID	Description	Specific capacitance @ 0.1mA	Specific capacitance @ 5mA	Ohmic resistance $\Omega.cm^2$	Self-discharge % @72hrs
1103NDA850B	NDA with Al	129.88	165.08	-	96.14
1103NDA850BHT	NDA with Al+ HT	148.79	150.21	0.135	25.72
YP80F20190410	Commercial AC	107.76	107.01	0.34	46.17
2203BL850B	Blank Experiment	164.58	177.34	-	70.57
2203BL850BHT	Blank Experiment +HT	156.37	161.61	0.21	13.5

Table 4. 22 Electrochemical testing of thermally treated samples

The samples with the term HT added are the thermally treated samples. The self-discharge was seen to be reduced by about 73% in the NDA activated samples with Al upon comparison between the discharge rate of the two samples. An almost similar reduction of about 80% occurred in those of the blank samples with the thermal treatment responsible for reducing the self-discharge rate to 13% after 72hours. Thus, effectively saying that the blank samples would self-discharge at a rate of about 5% each day compared to those of the commercially activated samples with a rate of about 15% each day. The NDA activated samples discharged at a rate of about 8% each day which was better than the performance of the commercial activated carbon.

CHAPTER 5

5.0 CONCLUSION AND RECOMMENDATIONS

5.1 CONCLUSION

Different sets of Activated carbon were prepared via chemical impregnation with KOH in addition to non-destructively activated samples with Cu and Al additive. The activation was carried out while varying the activation time, temperature and additive ratio.

High specific surface areas up to 3350 m^2/g were obtained following the Nitrogen Adsorption analysis carried out. 850 $^{\circ}$C and a KOH impregnation ratio of 4 was the optimum condition for high surface area activated carbon. Cu as an additive was more efficient following the relatively higher surface areas obtained especially with additive ratios of 0.5 and 1 at 750 $^{\circ}$C and 850 $^{\circ}$C respectively. The activated carbon samples produced had significant mesoporous content and narrow micropore size distribution in the range of 0.8911-1.165nm. The micropore volume was seen to increase with increasing additive concentration for the NDA with Al and Cu samples. The mesopore volume of the NDA with Al samples decreased with increasing additive concentration but the opposite occurred for the NDA with Cu. It was confirmed via XRD , EDS and ash content analysis that the high surface areas obtained from the NDA samples were not as a result of impurities in form of the additives present. This study buttresses the possibility of obtaining wide varieties of activated carbon with different microporous and mesoporous content. Based on nature of electrolyte and ion size, it is possible to match the pore size of the activated carbon to the required ion size of the electrolyte which would result in supercapacitors with excellent performances[3].

Coin cells were fabricated with selected activated carbon samples with the highest surface areas and compared with commercially available activated carbon YP80. The specific capacitance from the blank experiment were the highest with values of 156F/g @ 0.1mA and 161 F/g @ 5mA , followed by the NDA with Al samples (149 F/g @ 0.1mA and 150F/g @5mA) and they all performed better than the commercially available activated carbon samples in terms of self-discharge and ohmic resistance tests. The ohmic resistance of the NDA with Al sample was the lowest with a value of 0.13 $\Omega.cm^2$.

The potential of non-destructive activation of a wood precursor has been investigated but a lot more optimization and careful analytical study is needed to determine the effectiveness of the NDA samples in improving the specific capacitance and confirming the defect free nature of the synthesized activated carbon.

5.2   RECCOMENDATION

Work can be done on the optimization of the pore size and pore size distribution of the synthesized activated carbon through variation of activation time. The effectiveness of the non-destructive activation can also be further investigated through a variety of coin cells assembled and compared with those of the blank samples. A host of different additives such as Nickel , Magnesium could also be investigated to ascertain their effectiveness and appropriate intensity necessary to achieve activated carbons with reduced defects.

Following the results obtained from this experiment, it is possible to generate data based on the specific surface area of the activated carbon as it relates to the specific capacitance. This would be essential to document the effective pore size, pore size distribution and surface area with the matching specific capacitance and other electrochemical properties of the supercapacitor.

REFERENCES

1. Omer, A.M., Energy, environment and sustainable development. *Renewable and sustainable energy reviews*, 2008. **12**(9): p. 2265-2300.
2. Larcher, D. and J.-M. Tarascon, Towards greener and more sustainable batteries for electrical energy storage. *Nature chemistry*, 2015. **7**(1): p. 19.
3. Segalini, J., et al., Steric effects in adsorption of ions from mixed electrolytes into microporous carbon. *Electrochemistry Communications*, 2012. **15**(1): p. 63-65.
4. Nocera, D.G., Living healthy on a dying planet. *Chemical Society Reviews*, 2009. **38**(1): p. 13-15.
5. Chu, S., Y. Cui, and N. Liu, The path towards sustainable energy. *Nature materials*, 2017. **16**(1): p. 16.
6. Yan, J., et al., Recent advances in design and fabrication of electrochemical supercapacitors with high energy densities. *Advanced Energy Materials*, 2014. **4**(4).
7. Lukatskaya, M.R., B. Dunn, and Y. Gogotsi, Multidimensional materials and device architectures for future hybrid energy storage. *Nature Communications*, 2016. **7**: p. 12647.
8. Ahuja, D. and M. Tatsutani, Sustainable energy for developing countries. *SAPI EN. S. Surveys and Perspectives Integrating Environment and Society*, 2009(2.1).
9. Xie, J., et al., Puzzles and confusions in supercapacitor and battery: Theory and solutions. *Journal of Power Sources*, 2018. **401**: p. 213-223.
10. *Vision of the fjords: «Ship of the Year» kåres denne uken. Dette er favoritten.* . Available from https://www.tu.no/artikler/ship-of-the-year-kares-denne-uken-dette-er-favoritten/351088.
11. report, E.T., *The impact of international shipping on European air quality and climate forcing*. 2013: Luxembourg.
12. *Climate action tracker.* . Available from: http://climateactiontracker.org/countries/norway.html.
13. Ahmed, S., A. Ahmed, and M. Rafat, Supercapacitor performance of activated carbon derived from rotten carrot in aqueous, organic and ionic liquid based electrolytes. *Journal of Saudi Chemical Society*, 2018. **22**(8): p. 993-1002.
14. Khare, V., S. Nema, and P. Baredar, Solar–wind hybrid renewable energy system: A review. *Renewable and Sustainable Energy Reviews*, 2016. **58**: p. 23-33.
15. Cheng, X.-B., et al., Toward safe lithium metal anode in rechargeable batteries: a review. *Chemical reviews*, 2017. **117**(15): p. 10403-10473.

16. Simon, P., Y. Gogotsi, and B. Dunn, Where do batteries end and supercapacitors begin? *Science*, 2014. **343**(6176): p. 1210-1211.

17. Ciszewski, M., et al., Review of the Selected Carbon-Based Materials for Symmetric Supercapacitor Application. *Journal of Electronic Materials*, 2019. **48**(2): p. 717-744.

18. Béguin, F., et al., Carbons and electrolytes for advanced supercapacitors. *Advanced materials*, 2014. **26**(14): p. 2219-2251.

19. *National Forest Inventory*. Available from: https://www.ssb.no.

20. Bommier, C., et al., Self-activation of cellulose: A new preparation methodology for activated carbon electrodes in electrochemical capacitors. *Nano Energy*, 2015. **13**: p. 709-717.

21. *Supercapacitor electric boat : Ar Vag Tredan operates in France*. Available from: https://www.supercaptech.com/supercapacitor-electric-boat-ar-vag-tredan-operates-in-france.

22. Levine, I.N., *Physical chemistry, International student Edition*. 1995, McGraw-Hill International Book Company.

23. Kötz, R. and M. Carlen, Principles and applications of electrochemical capacitors. *Electrochimica acta*, 2000. **45**(15-16): p. 2483-2498.

24. Borchardt, L., et al., Ordered mesoporous carbide-derived carbons prepared by soft templating. *Carbon*, 2012. **50**(11): p. 3987-3994.

25. Gamby, J., et al., Studies and characterisations of various activated carbons used for carbon/carbon supercapacitors. *Journal of power sources*, 2001. **101**(1): p. 109-116.

26. Faraji, S. and F.N. Ani, The development supercapacitor from activated carbon by electroless plating—A review. *Renewable and Sustainable Energy Reviews*, 2015. **42**: p. 823-834.

27. Izadi-Najafabadi, A., et al., Extracting the full potential of single-walled carbon nanotubes as durable supercapacitor electrodes operable at 4 V with high power and energy density. *Advanced Materials*, 2010. **22**(35): p. E235-E241.

28. Wen, Z., et al., Crumpled nitrogen-doped graphene nanosheets with ultrahigh pore volume for high-performance supercapacitor. *Advanced materials*, 2012. **24**(41): p. 5610-5616.

29. Largeot, C., et al., Relation between the ion size and pore size for an electric double-layer capacitor. *Journal of the American Chemical Society*, 2008. **130**(9): p. 2730-2731.

30. Chmiola, J., et al., Effect of pore size and surface area of carbide derived carbons on specific capacitance. *Journal of Power Sources*, 2006. **158**(1): p. 765-772.

31. Snook, G.A., P. Kao, and A.S. Best, Conducting-polymer-based supercapacitor devices and electrodes. *Journal of power sources*, 2011. **196**(1): p. 1-12.

32. Du Pasquier, A., et al., A Nonaqueous Asymmetric Hybrid Li4Ti5 O 12/Poly (fluorophenylthiophene) Energy Storage Device. *Journal of the Electrochemical Society*, 2002. **149**(3): p. A302-A306.

33. Kandasamy, S.K. and K. Kandasamy, Recent advances in electrochemical performances of graphene composite (graphene-polyaniline/polypyrrole/activated carbon/carbon nanotube) electrode materials for supercapacitor: a review. *Journal of Inorganic and Organometallic Polymers and Materials*, 2018: p. 1-26.

34. Ardizzone, S., G. Fregonara, and S. Trasatti, "Inner" and "outer" active surface of RuO2 electrodes. *Electrochimica Acta*, 1990. **35**(1): p. 263-267.

35. Liu, T.C., et al., Behavior of molybdenum nitrides as materials for electrochemical capacitors comparison with ruthenium oxide. *Journal of the Electrochemical Society*, 1998. **145**(6): p. 1882-1888.

36. Laidler, K. and J. Meiser, *Physical Chemistry. 1999*. Houghton Mifflin.

37. Ruther, R.E., et al., Stable electrolyte for high voltage electrochemical double-layer capacitors. *Journal of The Electrochemical Society*, 2017. **164**(2): p. A277-A283.

38. Brousse, T., M. Toupin, and D. Belanger, A hybrid activated carbon-manganese dioxide capacitor using a mild aqueous electrolyte. *Journal of the Electrochemical Society*, 2004. **151**(4): p. A614-A622.

39. Kim, H. and B.N. Popov, Characterization of hydrous ruthenium oxide/carbon nanocomposite supercapacitors prepared by a colloidal method. *Journal of Power Sources*, 2002. **104**(1): p. 52-61.

40. Hu, C.-C. and T.-W. Tsou, Ideal capacitive behavior of hydrous manganese oxide prepared by anodic deposition. *Electrochemistry Communications*, 2002. **4**(2): p. 105-109.

41. Guo, Y., et al., Performance of electrical double layer capacitors with porous carbons derived from rice husk. *Materials Chemistry and Physics*, 2003. **80**(3): p. 704-709.

42. Wu, F.-C., et al., Physical and electrochemical characterization of activated carbons prepared from firwoods for supercapacitors. *Journal of Power Sources*, 2004. **138**(1-2): p. 351-359.

43. Subramanian, V., et al., Supercapacitors from activated carbon derived from banana fibers. *The Journal of Physical Chemistry C*, 2007. **111**(20): p. 7527-7531.

44. Pay, S. and Y. Baghzouz. *Effectiveness of battery-supercapacitor combination in electric vehicles*. in *Power Tech Conference Proceedings, 2003 IEEE Bologna*. 2003. Citeseer.

45. Yoshida, A., I. Tanahashi, and A. Nishino, Effect of concentration of surface acidic functional groups on electric double-layer properties of activated carbon fibers. *Carbon*, 1990. **28**(5): p. 611-615.

46. Pandolfo, A. and A. Hollenkamp, Carbon properties and their role in supercapacitors. *Journal of power sources*, 2006. **157**(1): p. 11-27.

47. Simon, P. and Y. Gogotsi, Materials for electrochemical capacitors. *Nature Materials*, 2008. **7**: p. 845.

48. Kinoshita, K., *Carbon: electrochemical and physicochemical properties*. 1988, United States.

49. Pollak, E., et al., The dependence of the electronic conductivity of carbon molecular sieve electrodes on their charging states. *The Journal of Physical Chemistry B*, 2006. **110**(14): p. 7443-7448.

50. Ma, R., et al., Study of electrochemical capacitors utilizing carbon nanotube electrodes. *Journal of Power Sources*, 1999. **84**(1): p. 126-129.

51. Noked, M., A. Soffer, and D. Aurbach, The electrochemistry of activated carbonaceous materials: past, present, and future. *Journal of Solid State Electrochemistry*, 2011. **15**(7-8): p. 1563.

52. Hernández-Montoya, V., J. García-Servin, and J.I. Bueno-López, *Thermal treatments and activation procedures used in the preparation of activated carbons*, in *Lignocellulosic Precursors Used in the Synthesis of Activated Carbon-Characterization Techniques and Applications in the Wastewater Treatment*. 2012, InTech.

53. Mohammadi, S.Z., et al., Removal of Pb (II) from aqueous solutions using activated carbon from Sea-buckthorn stones by chemical activation. *Desalination*, 2010. **262**(1-3): p. 86-93.

54. Mourão, P., et al., Influence of oxidation process on the adsorption capacity of activated carbons from lignocellulosic precursors. *Fuel Processing Technology*, 2011. **92**(2): p. 241-246.

55. Yavuz, R., et al., Influence of preparation conditions on porous structures of olive stone activated by H3PO4. *Fuel Processing Technology*, 2010. **91**(1): p. 80-87.

56. Gratuito, M., et al., Production of activated carbon from coconut shell: Optimization using response surface methodology. *Bioresource Technology*, 2008. **99**(11): p. 4887-4895.

57. Yakout, S. and G.S. El-Deen, Characterization of activated carbon prepared by phosphoric acid activation of olive stones. *Arabian Journal of Chemistry*, 2016. **9**: p. S1155-S1162.

58. Niaounakis, M. and C.P. Halvadakis, *Olive processing waste management: literature review and patent survey*. Vol. 5. 2006: Elsevier.

59. Mokgalaka, N., R. McCrindle, and B. Botha, Multielement analysis of tea leaves by inductively coupled plasma optical emission spectrometry using slurry nebulisation. *Journal of Analytical Atomic Spectrometry*, 2004. **19**(10): p. 1375-1378.

60. Mahmood, T., et al., Potential of used Camellia sinensis leaves as precursor for activated carbon preparation by chemical activation with H3PO4; optimization using response surface methodology. *Process Safety and Environmental Protection*, 2017. **109**: p. 548-563.

61. Malikov, I., et al., Granulated sorbents from wood waste. *Solid Fuel Chemistry*, 2007. **41**(2): p. 100-106.

62. Ngernyen, Y., C. Tangsathitkulchai, and M. Tangsathitkulchai, Porous properties of activated carbon produced from Eucalyptus and Wattle wood by carbon dioxide activation. *Korean Journal of Chemical Engineering*, 2006. **23**(6): p. 1046-1054.

63. Asakura, R., et al., Preparation of fibrous activated carbons from wood fiber. *Journal of materials science*, 2004. **39**(1): p. 201-206.

64. Rodriguez-Reinoso, F. and M. Molina-Sabio, Activated carbons from lignocellulosic materials by chemical and/or physical activation: an overview. *Carbon*, 1992. **30**(7): p. 1111-1118.

65. Danish, M. and T. Ahmad, A review on utilization of wood biomass as a sustainable precursor for activated carbon production and application. *Renewable and Sustainable Energy Reviews*, 2018. **87**: p. 1-21.

66. Mopoung, S., et al., Characterization and properties of activated carbon prepared from tamarind seeds by KOH activation for Fe (III) adsorption from aqueous solution. *The Scientific World Journal*, 2015. **2015**.

67. Zaini, M.A.A. and M.J. Kamaruddin, Critical issues in microwave-assisted activated carbon preparation. *Journal of analytical and applied pyrolysis*, 2013. **101**: p. 238-241.

68. Hui, T.S. and M.A.A. Zaini, Potassium hydroxide activation of activated carbon: a commentary. *Carbon letters*, 2015. **16**(4): p. 275-280.

69. Muniandy, L., et al., The synthesis and characterization of high purity mixed microporous/mesoporous activated carbon from rice husk using chemical activation with NaOH and KOH. *Microporous and Mesoporous Materials*, 2014. **197**: p. 316-323.

70. Yu, Q., et al., Preparation and phosphine adsorption of activated carbon prepared from walnut shells by KOH chemical activation. *Separation Science and Technology*, 2014. **49**(15): p. 2366-2375.

71. Caturla, F., M. Molina-Sabio, and F. Rodriguez-Reinoso, Preparation of activated carbon by chemical activation with ZnCl2. *Carbon*, 1991. **29**(7): p. 999-1007.

72. Hu, Z., M. Srinivasan, and Y. Ni, Novel activation process for preparing highly microporous and mesoporous activated carbons. *Carbon*, 2001. **39**(6): p. 877-886.

73. Li, X.F., et al., Preparation and characterization of activated carbon from Kraft lignin via KOH activation. *Environmental Progress and Sustainable Energy*, 2014. **33**(2): p. 519-526.

74. Zuo, S., et al., Significance of the carbonization of volatile pyrolytic products on the properties of activated carbons from phosphoric acid activation of lignocellulosic material. *Fuel Processing Technology*, 2009. **90**(7-8): p. 994-1001.

75.   Kouotou, D., et al., Optimization of activated carbons prepared by and steam activation of oil palm shells. *Journal of Chemistry*, 2012. **2013**.

76.   Budinova, T., et al., Characterization and application of activated carbon produced by H3PO4 and water vapor activation. *Fuel processing technology*, 2006. **87**(10): p. 899-905.

77.   Nahil, M.A. and P.T. Williams, Pore characteristics of activated carbons from the phosphoric acid chemical activation of cotton stalks. *Biomass and Bioenergy*, 2012. **37**: p. 142-149.

78.   Lee, H.-M., et al., A Study on Pore Development Mechanism of Activated Carbons from Polymeric Precursor: Effects of Carbonization Temperature and Nano Crystallite Formation. *Chemical Engineering Journal*, 2019.

79.   Minkova, V., et al., Thermochemical treatment of biomass in a flow of steam or in a mixture of steam and carbon dioxide. *Fuel Processing Technology*, 2000. **62**(1): p. 45-52.

80.   Savova, D., et al., Biomass conversion to carbon adsorbents and gas. *Biomass and Bioenergy*, 2001. **21**(2): p. 133-142.

81.   Petrov, N., et al. *Preparation of activated carbons from cherry stones, apricot stones and grape seeds for removal of metal ions from water*. in *Proceedings of the 2nd OlleIndstorm Symposium on Renewable Energy-Bioenergy*. 1999.

82.   Webb, P.A. and C. Orr, *Analytical methods in fine particle technology*. 1997: Micromeritics Instrument Corp.

83.   Sing, K.S., Reporting physisorption data for gas/solid systems with special reference to the determination of surface area and porosity (Recommendations 1984). *Pure and applied chemistry*, 1985. **57**(4): p. 603-619.

84.   Barrett, E.P., L.G. Joyner, and P.P. Halenda, The determination of pore volume and area distributions in porous substances. I. Computations from nitrogen isotherms. *Journal of the American Chemical society*, 1951. **73**(1): p. 373-380.

85.   Kaufmann, E.N., Characterization of Materials, 2 Volume Set. *Characterization of Materials, 2 Volume Set, by Elton N. Kaufmann (Editor), pp. 1392. ISBN 0-471-26882-8. Wiley-VCH, January 2003.*, 2003: p. 1392.

86.   Cullity, B., Diffraction I: The directions of diffracted beams. *Elements of X-ray Diffraction*, 1956. **1**: p. 84.

87.   Cullity, B.D., Elements of X-ray Diffraction. 2001.

88.   Holzwarth, U. and N. Gibson, The Scherrer equation versus the'Debye-Scherrer equation'. *Nature nanotechnology*, 2011. **6**(9): p. 534.

89.   Chauhan, A. and P. Chauhan, Powder XRD technique and its applications in science and technology. *Journal of Analytical & Bioanalytical Techniques*, 2014. **5**(5): p. 1.

90. Inagaki, M., H. Konno, and O. Tanaike, Carbon materials for electrochemical capacitors. *Journal of power sources*, 2010. **195**(24): p. 7880-7903.

91. Mitani, S., et al., Contrast structure and EDLC performances of activated spherical carbons with medium and large surface areas. *Electrochimica Acta*, 2006. **51**(25): p. 5487-5493.

92. Kiseleva, E., et al. *Influence of carbon conductive additives on electrochemical double-layer supercapacitor parameters*. in *Journal of Physics: Conference Series*. 2018. IOP Publishing.

93. Sevilla, M. and R. Mokaya, Energy storage applications of activated carbons: supercapacitors and hydrogen storage. *Energy & Environmental Science*, 2014. **7**(4): p. 1250-1280.

94. Lillo-Ródenas, M., et al., About reactions occurring during chemical activation with hydroxides. *Carbon*, 2004. **42**(7): p. 1371-1375.

95. Teng, H. and L.-Y. Hsu, High-porosity carbons prepared from bituminous coal with potassium hydroxide activation. *Industrial & engineering chemistry research*, 1999. **38**(8): p. 2947-2953.

96. Sonia, T., et al., Composite supercapacitor electrodes made of activated carbon/PEDOT: PSS and activated carbon/doped PEDOT. *Bulletin of Materials Science*, 2013. **36**(4): p. 547-551.

97. Andreas, H.A., Self-discharge in electrochemical capacitors: a perspective article. *Journal of The Electrochemical Society*, 2015. **162**(5): p. A5047-A5053.

98. Ricketts, B. and C. Ton-That, Self-discharge of carbon-based supercapacitors with organic electrolytes. *Journal of Power Sources*, 2000. **89**(1): p. 64-69.

99. Burke, A., Ultracapacitors: why, how, and where is the technology. *Journal of power sources*, 2000. **91**(1): p. 37-50.

100. Conway, B.E., *Electrochemical supercapacitors: scientific fundamentals and technological applications*. 2013: Springer Science & Business Media.

101. Gualous, H., et al., Experimental study of supercapacitor serial resistance and capacitance variations with temperature. *Journal of power sources*, 2003. **123**(1): p. 86-93.

102. Marsh, H. and F.R. Reinoso, *Activated carbon*. 2006: Elsevier.

103. Yorgun, S. and D. Yıldız, Preparation and characterization of activated carbons from Paulownia wood by chemical activation with H3PO4. *Journal of the Taiwan Institute of Chemical Engineers*, 2015. **53**: p. 122-131.

104. Gomez-Serrano, V.d., et al., Preparation of activated carbons from chestnut wood by phosphoric acid-chemical activation. Study of microporosity and fractal dimension. *Materials Letters*, 2005. **59**(7): p. 846-853.

105. Rahman, M., M. Adil, and A. Yusof, Porosity development in activated carbon from palm kernel and coconut shell by chemical activation method. *Research Journal of Chemistry and Environment*, 2012. **16**(4): p. 189-191.

106. Wu, F.-C., et al., Effects of pore structure and electrolyte on the capacitive characteristics of steam-and KOH-activated carbons for supercapacitors. *Journal of Power Sources*, 2005. **144**(1): p. 302-309.

107. Tseng, R.-L., F.-C. Wu, and R.-S. Juang, Liquid-phase adsorption of dyes and phenols using pinewood-based activated carbons. *Carbon*, 2003. **41**(3): p. 487-495.

108. Kissinger, P. and W.R. Heineman, *Laboratory Techniques in Electroanalytical Chemistry, revised and expanded*. 1996: CRC press.

109. Kalpana, D. and Y. Lee, Effects of Temperature and Pore Structure on High Surface Area-Activated Carbon Obtained from Peanut Shells. *Journal of nanoscience and nanotechnology*, 2016. **16**(3): p. 2950-2955.

110. Ahmadpour, A. and D. Do, The preparation of activated carbon from macadamia nutshell by chemical activation. *Carbon*, 1997. **35**(12): p. 1723-1732.

111. Tromp, P. and E. Cordfunke, A thermochemical study of the reactive intermediate in the alkali-catalyzed carbon gasification. I. X-ray diffraction results on the alkali-carbon interaction. *Thermochimica acta*, 1984. **77**(1-3): p. 49-58.

112. Illán-Gómez, M., et al., Activated carbons from Spanish coals. 2. Chemical activation. *Energy & Fuels*, 1996. **10**(5): p. 1108-1114.

113. Sivachidambaram, M., et al., Preparation and characterization of activated carbon derived from the Borassus flabellifer flower as an electrode material for supercapacitor applications. *New Journal of Chemistry*, 2017. **41**(10): p. 3939-3949.

114. Wang, Y., et al., Graphene-based solid-phase extraction combined with flame atomic absorption spectrometry for a sensitive determination of trace amounts of lead in environmental water and vegetable samples. *Analytica Chimica Acta*, 2012. **716**: p. 112-118.

115. Bhattacharjya, D. and J.-S. Yu, Activated carbon made from cow dung as electrode material for electrochemical double layer capacitor. *Journal of Power Sources*, 2014. **262**: p. 224-231.

116. Dutta, M., et al., Application of various activated carbons in the adsorptive removal of methylene blue from aqueous solution. *Res. J. Environ. Sci*, 2011. **5**: p. 741-751.